STATIC PERFORMANCE AND NOISE TESTS ON A THRUST REVERSER FOR AN AUGMENTOR WING AIRCRAFT

by D. L. Harkonen, C. C. Marrs, and J. V. O'Keefe

July 1974

D6-41926

Prepared under contract NAS2-7641

BOEING COMMERCIAL AIRPLANE COMPANY
P.O. Box 3707
Seattle, Washington 98124

for

AMES RESEARCH CENTER
NATIONAL AERONAUTICS AND SPACE ADMINISTRATION

1. Report No.	2. Government Accession No.	3. Recipient's Catalog No.

4. Title and Subtitle	5. Report Date
STATIC PERFORMANCE AND NOISE TESTS ON A THRUST REVERSER FOR AN AUGMENTOR WING AIRCRAFT	July 1974
	6. Performing Organization Code
7. Author(s)	8. Performing Organization Report No.
D. L. Harkonen, C. C. Marrs, and J. V. O'Keefe	D6-41926
	10. Work Unit No.
9. Performing Organization Name and Address	11. Contract or Grant No.
Boeing Commercial Airplane Company P.O. Box 3707 Seattle, Washington 98124	NAS2-7641
	13. Type of Report and Period Covered
12. Sponsoring Agency Name and Address	Contractor Report
National Aeronautics and Space Administration Washington, D.C. 20546	14. Sponsoring Agency Code

15. Supplementary Notes

16. Abstract

A 1/3 scale model static test program was conducted to measure the noise levels and reverse thrust performance characteristics of a wing-mounted thrust reverser that could be used on an advanced augmentor wing airplane. The configuration tested represents only the most fundamental designs where installation and packaging restraints are not considered. The thrust reverser performance is presented in terms of horizontal, vertical, and resultant effectiveness ratios and the reverser noise is compared on the basis of peak perceived noise level (PNL) and one-third octave band data (OASPL). From an analysis of the model force and acoustic data, an assessment is made on the stopping distance versus noise for a 90 900 kg (200 000 lb) airplane using this type of thrust reverser.

17. Key Words (Suggested by Author(s))	18. Distribution Statement
Augmentor wing Thrust reverser Noise STOL	Unclassified–Unlimited

19. Security Classif. (of this report)	20. Security Classif. (of this page)	21. No. of Pages	22. Price*
Unclassified	Unclassified	84	

*For sale by the National Technical Information Service, Springfield, Virginia 22151

CONTENTS

STATIC PERFORMANCE AND NOISE TESTS ON A THRUST REVERSER FOR AN AUGMENTOR WING AIRCRAFT

By D. L. Harkonen, C. C. Marrs, and J. V. O'Keefe

SUMMARY

Static performance and acoustic tests were conducted on a 1/3 scale two-dimensional model of a wing-mounted fan air thrust reverser applicable to an advanced augmentor wing aircraft. In concept, the thrust reverser would be deployed from the augmentor flap on landing and would turn and deflect the augmentor nozzle air up and forward above the wing. The reverser models consisted of two curved deflectors of different radii and were tested with various exit lip lengths and angles as shown in figure 1. A lobe nozzle (corrugated splitter, ref. 1) was selected for the test because of its excellent noise suppression and high thrust augmentation characteristics.

Typical levels of measured reverser effectiveness in terms of the ratio of the reverse thrust components to the measured nozzle thrust versus lip angle are presented in figure 1. This curve is for the smallest deflector radius tested (r_D = 1.0 nozzle height), which produces high reverse thrust levels and a high degree of thrust vector control. Resultant reverse thrust effectiveness levels (reverse fan thrust/nozzle thrust) of over 0.7 are attained, and by use of a flow deflector lip, vertical component effectiveness ratios varying 0.5 to negative values are available.

The noise levels were measured for several of the high performance configurations with a polar array of microphones. The noise data was scaled and extrapolated to different sideline distances for the various power settings. The reverser noise levels are compared to the bare nozzle noise and not with the levels produced by a lined augmentor.

In summary, the thrust reverser configurations increased the noise levels, particularly in the low and mid frequency bands (3-4 PNdB above the nozzle noise level), and redirected the noise toward the forward quadrant. The typical increase in the peak PNL noise levels and the change in noise directivity due to the reverser are presented in figure 2. It should be noted that the test configuration did not permit evaluation of a full wing chord on sideline far-field noise levels.

The static reverse thrust performance levels developed by the configuration with a 70° lip angle were applied to a stopping performance analysis for a 90 900 kg (200 000 lb) TOGW augmentor wing airplane. Reversal of only the fan air was considered here, with primary (hot) thrust spoiled. The noise levels measured at nozzle pressure ratios that correspond to engine fan thrust levels were scaled and extrapolated to a 152 m (500 ft) sideline. The peak PNL noise levels produced by the

reverser are plotted versus airplane stopping distance for dry, wet, and icy runways in figure 3. As indicated in this figure, use of high reverse thrust with attendant high noise levels is useful only in reducing stopping distance where the runway is considered slick, i.e., flooded or icy with μ factors near 0.05. Under these conditions, the reverser would allow the airplane to stop in 457 m (1500 ft) with 50% power with moderate noise levels, whereas use of brakes-only results in a stopping distance near 914 m (3000 ft). Where runways with high traction are available (μ = 0.3 to 0.4), the brakes provide most of the stopping force, minimizing the usefulness of the thrust reverser.

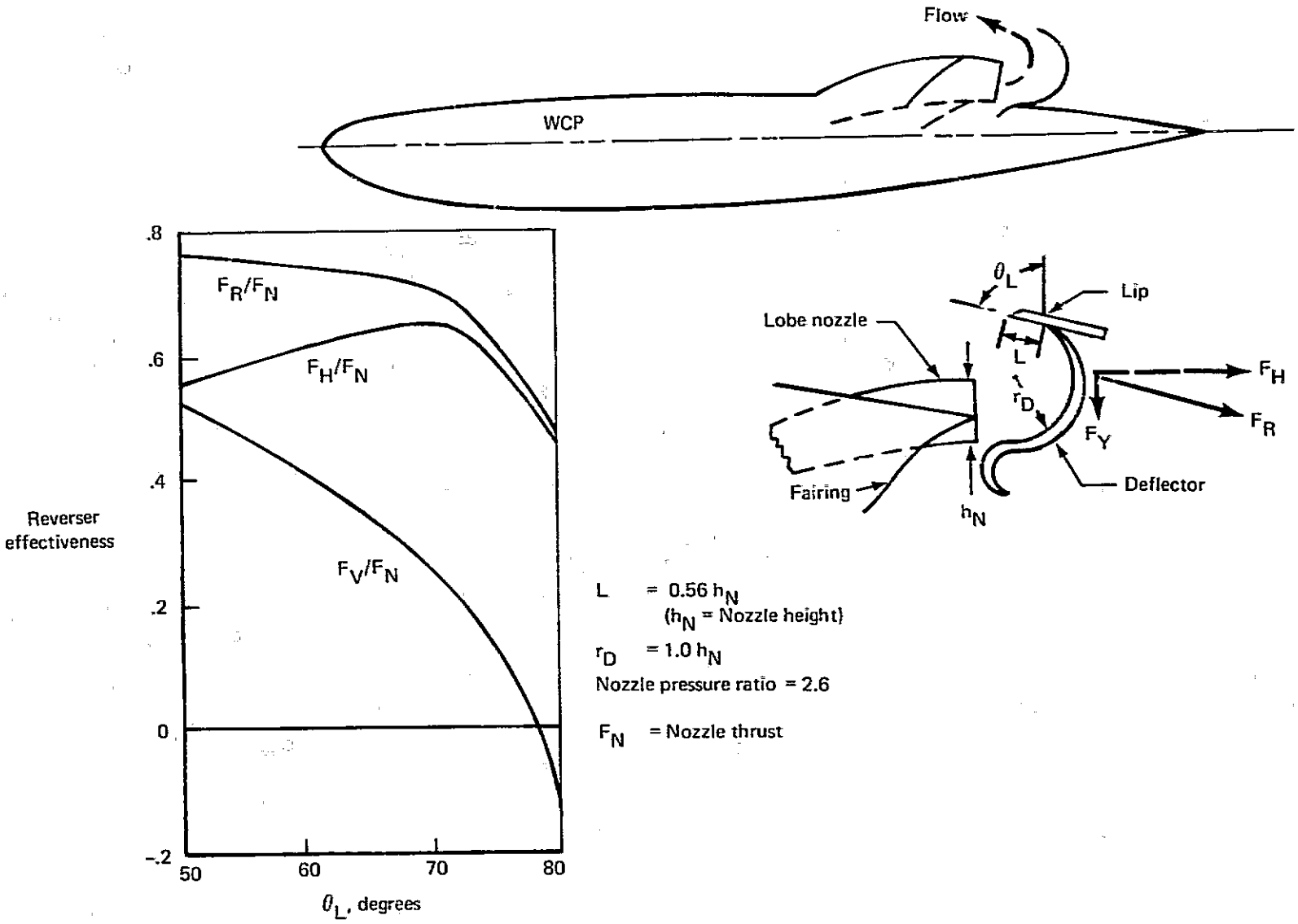

FIGURE 1.—EFFECTS OF DEFLECTOR LIP ANGLE AND LIP EXTENSION LENGTH ON STATIC REVERSER EFFECTIVENESS

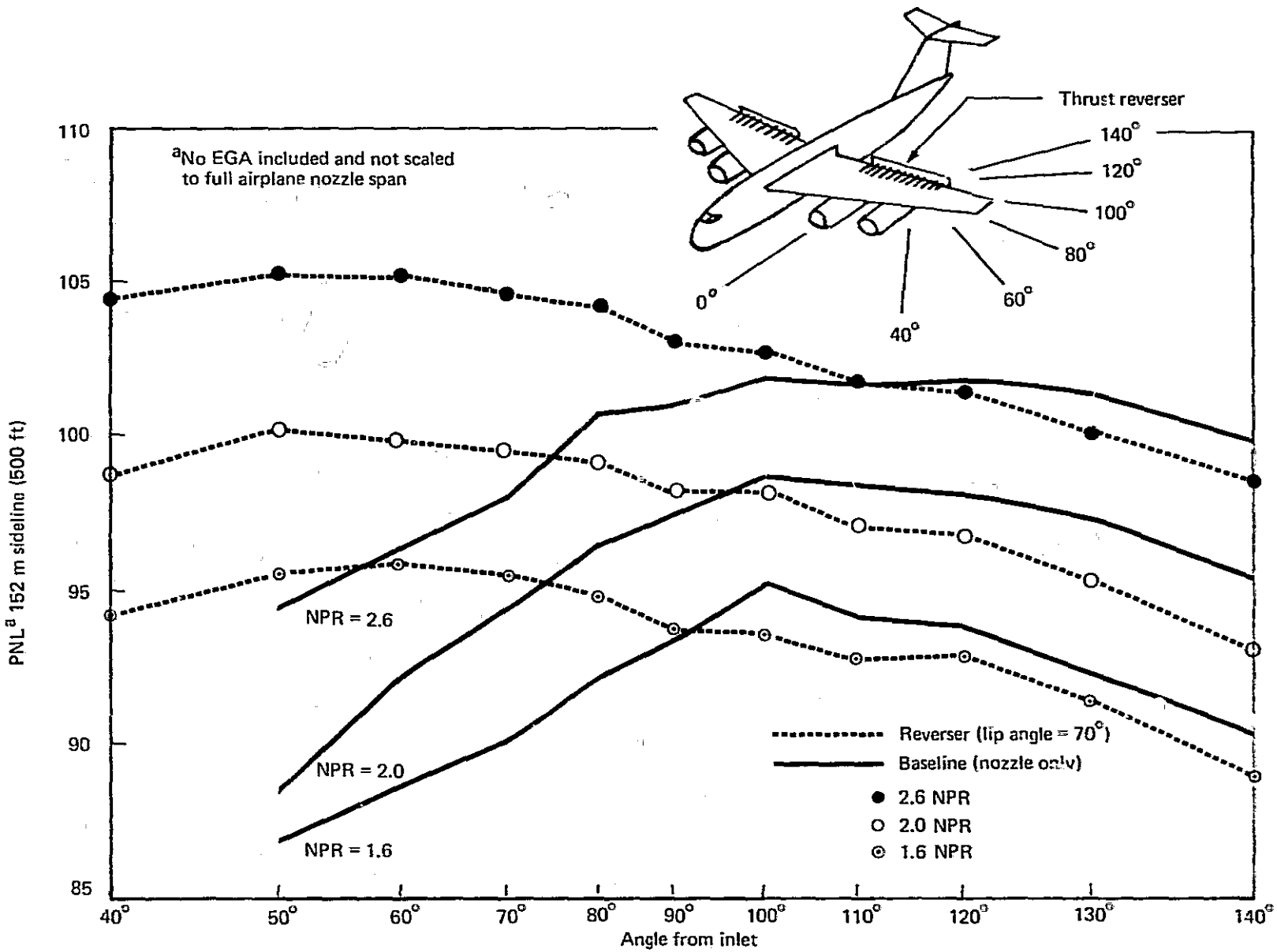

FIGURE 2.–EFFECTS OF A WING-MOUNTED THRUST REVERSER ON NOISE DIRECTIVITY

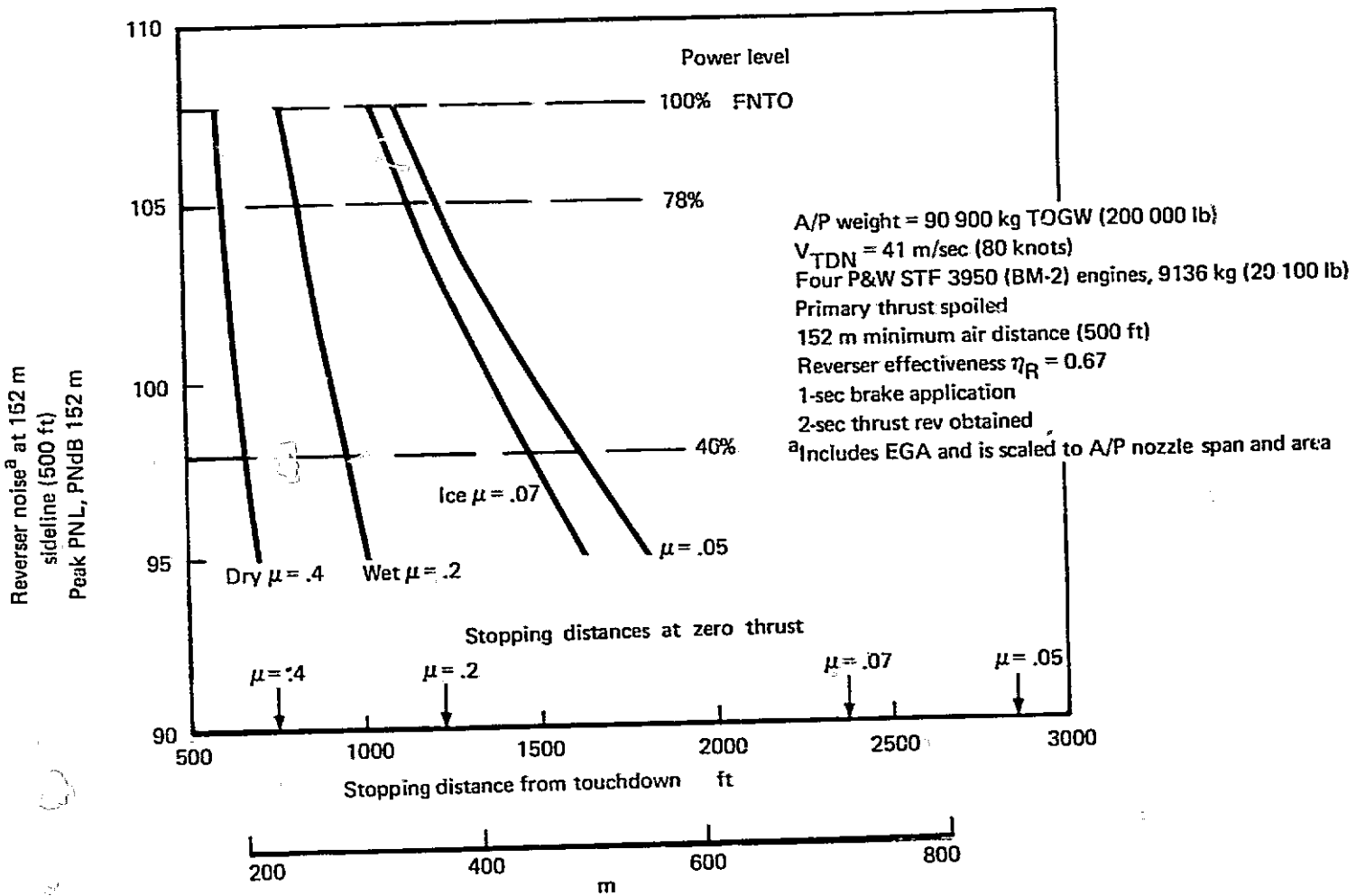

FIGURE 3.—RELATION OF ENGINE POWER AND REVERSER NOISE TO AIRPLANE STOPPING DISTANCE

INTRODUCTION

The distributed-flow augmentor wing system (also jet flap or USB distributed-flow systems) has the potential of superior thrust reversing characteristics. The concept of a turning vane deployed along the wing span to reverse the nozzle flow offers the following potential advantages:

1) Complete avoidance of reingestion.

2) Operation down to zero airplane speed.

3) Fast deployment.

4) Lower noise than a single nozzle, resulting from use of high breakup nozzles.

5) Spoiling of wing lift.

It has been demonstrated by static performance and acoustic tests (refs. 1 and 2) that high noise suppression and static thrust augmentation can be obtained by use of large-array-height lobe nozzles and relatively short-length augmentors ($C_F \approx 26\%$). Incorporating a fan air thrust reverser on an advanced augmentor wing airplane would most likely require deployment of the thrust reverser from within the augmentor flap envelope with the augmentor in the landing mode. Reverser stowage (space limitation) and actuation simplicity will be important considerations in the final design.

The noise levels and spectral characteristics produced by lobe nozzles with and without the augmentor flaps installed are well established. With the augmentor thrust reverser deployed after touchdown, the forward sideline noise is of main concern during reverser operation. The deflector reverser will tend to shield the nozzle high frequency noise from the aft arc, but it was speculated that the deflector itself will increase the noise levels in the low and mid frequency bands.

This static model test program examined the flow turning and noise characteristics of a curved deflector reverser and measured the static thrust reverser effectiveness.

It should be recognized that the test program described herein was exploratory, investigating only the most fundamental characteristics of a wing-mounted thrust reverser. A final installation design would require consideration of packaging restraints and deployment methods that would most likely result in changes to the reverser design. However, the test data acquired should provide valuable information for the direction of succeeding programs that must consider the installation requirements.

SYMBOLS AND ABBREVIATIONS

A	area, sq cm or sq in.
AR	nozzle aspect ratio
AAR	nozzle array area ratio (ratio of the area bounded by the primary nozzle exits to the measured nozzle exit area)
b	augmentor span, cm or in.
C	noise correction factor or wing chord, cm or in.
C_D	nozzle discharge coefficient
C_F	flap chord, cm or in. or % wing chord
C_V	nozzle velocity coefficient
F_H	reverser horizontal thrust component, kg or lb
F_N	augmentor nozzle thrust, kg or lb
F_R	reverser resultant thrust, kg or lb
F_V	reverser vertical thrust component, kg or lb
f	frequency, Hz
g	gravitational constant, m/sec^2 or ft/sec^2
h_N	augmentor nozzle height, cm or in.
L	reverser model exit lip length, cm or in.
m	mass airflow, slugs/sec (measured)
N	noy level, noys

NPR	augmentor nozzle pressure ratio
OASPL	overall sound pressure level, dB
PNdB	unit of perceived noise level, dB
PNL	perceived noise level, PNdB
r_D	reverser deflector radius, cm or in.
SLS	sea level static
S_N	Strouhal number (frequency x length)/velocity
SPL	sound pressure level
SR	slant range, m or ft
STOL	short takeoff and landing
T	temperature, °C or °F
T.O.	takeoff power setting
TOGW	takeoff gross weight, kg or lb
V	airplane velocity, m/sec or knots
WCP	wing chord plane
X	fore and aft position of the reverser deflector relative to the nozzle, cm or in.
Y	vertical position of the reverser deflector relative to the nozzle, cm or in.
α	air absorption (as a function of frequency), dB/305m or dB/1000 ft
β	model rotation with respect to the microphone orientation, deg
θ_E	effective resultant thrust angle with respect to the vertical, deg

θ_L	exit lip angle with respect to the vertical, deg
η_R	static reverser efficiency or effectiveness (F_R/F_N)
μ	braking coefficient

DISCUSSION

TEST FACILITY AND MODEL DESCRIPTION

In the paragraphs that follow, details of the test facility, test procedures, and instrumentation are discussed, as well as the accuracy and repeatability of performance and acoustic measurements.

Facility

The Boeing North Field Mechanical Laboratories in Seattle, Washington, were chosen for the test location. The laboratories have a facility especially suitable for large-scale combined acoustic and thrust performance test programs. Thrust is measured with a six-component, platform balance bridged with high-pressure air; the noise can be measured in a 180° arc in an acoustic arena as shown in figures 4, 5, and 6. The thrust stand accurately measures model forces using either heated air at 149°C (300°F) or ambient-temperature nozzle air. Nozzle flow rates are determined with precision using ASME venturi flow meters calibrated against a Boeing standard nozzle. An acoustically treated baffler plenum, located on the balance platform upstream of the test nozzle plenum, prevents noise generated by the air supply lines and control valves from reaching the test nozzles.

To acquire acoustic data of the highest quality, data were recorded only during a limited range of atmospheric conditions. Because of the precision desired for acoustic measurements, each component of the instrumentation system for noise measurement was carefully chosen and integrated. The basic noise-measuring system consists of microphones, a tape recorder, and one-third octave band analysis instrumentation calibrated and operated over a frequency range of 200 to 40 000 Hz. The output is punched cards, which are used to make computer plots of one-third octave band level versus frequency and other calculations used in the analysis.

Data Repeatability and Accuracy

Before beginning the tests on the thrust reverser models, a 100/1 A_R slot nozzle, used as a reference nozzle in previous tests, was installed and tested to check the facility thrust and airflow measuring systems after a long period of inactivity. The slot nozzle performance data (velocity and discharge coefficients), measured just prior to beginning the thrust reverser tests, are shown plotted with data recorded during the Task VII Design Integration and Noise Studies (ref. 3) on figure 7.

The reference slot nozzle performance data (runs 5-8), recorded prior to the reversed tests, shows good agreement with the performance levels measured nearly a year earlier. The discharge coefficient levels at or near 1.0 are not of concern, as some uncertainty exists in knowledge of the precise nozzle exit area.

The data from these four runs indicate a repeatability of test results of approximately ±0.5%. The balance lift axis (reverser vertical vector) was not used in the reference nozzle check runs but was calibrated by use of calibration weights.

Model Description

The nozzle selected for the augmentor thrust reverser tests was the existing corrugated splitter lobe nozzle array (fig. 8) which consists of 20 lobe nozzles equally spaced along a 111.7 cm span (44 in.). The design of an individual nozzle is shown in figure 9. The nozzle was selected for the reverser tests because its high noise suppression and high thrust augmentation characteristics had been demonstrated statically with an augmentor flap (ref. CR-114534). The lobe nozzles were fitted with a sheet metal aerodynamic fairing as shown in figure 10.

The thrust reverser is basically a curved deflector with a radiused inlet (bellmouth) on the lower side and an adjustable lip (flow deflector) on the top side (see fig. 11). Two deflector radii were tested, one of 1.0 nozzle height (1.0 h_N) and the other of 1.25 h_N. The curved deflectors were enclosed on the ends by end plates in order to provide two-dimensional flow characteristics (see fig. 12). The flow deflector exit lip (L) was designed to provide a considerable range of adjustment in both angle and extension length as shown in figure 11. The reverser assembly was supported on a lattice framework (fig. 13) fitted with adjustment capabilities that allowed movement of the reverser with respect to the nozzle in the X and Y directions.

Test Procedures

The effects of the many test variables on reverse thrust performance and noise were unknown for this type of thrust reverser. It was decided that noise data would only be recorded for configurations producing high reverse thrust performance. The reverser was initially set with minimum lip deflection ($\theta_L = 50°$) and the optimum position (X and Y) of the reverser with respect to the nozzle was first determined. Initial runs operating over the full range of pressure ratios (1.6 to 3.0) showed that the reverser performance was not particularly sensitive to pressure ratio. So, performance data was only recorded at nozzle pressure ratios of 2.3 and 2.6 while optimizing the different variables.

After the optimum X and Y positions were determined, the lip extension angle θ_L and length L were varied. Two lip angles for each deflector radius (1.0 h_N and 1.25 h_N) were tested for acoustics and final performance by heating the nozzle air to 149°C (300°F) and recording data at nozzle pressure ratios of 1.6, 2.0, 2.3, 2.6, and 3.0. All tests were made with the model oriented at beta = 90° (sideline).

Performance Definitions

Nozzle Performance

Velocity coefficient, $C_V = F_N/mV_I = F_N/C_D m_I V_I$

Discharge coefficient, $C_D = m/m_I$

Reverser Performance

Resultant effectiveness = F_R/F_N

Horizontal effectiveness = F_H/F_N

Vertical effectiveness = F_V/F_N

Effective thrust angle θ_E = arc cos F_V/F_R, degrees

where

F_N = measured nozzle thrust, kg or lb

m = measured nozzle mass flow, slugs/sec

V_I = isentropic velocity, m/sec or ft/sec

m_I = ideal nozzle mass flow, slugs/sec

F_R = resultant reverser thrust, kg or lb

F_H = horizontal reverser thrust component, kg or lb

F_V = vertical reverser thrust component, kg or lb

Acoustic Scaling and Extrapolation of Jet Noise

Acoustic scale-model testing follows Lighthill's theory that the total acoustic power radiated from a jet is proportional to the density of the jet, the eighth power of the velocity of the jet, and the second power of a characteristic dimension. To simplify scaling, both the density and jet

velocity of the model are left identical to the full-scale prototype; only the characteristic dimension is scaled. For linear arrays, this characteristic dimension is the height and span of the array. For the data shown in this report, the scale is 1/3.

The steps used to scale and extrapolate the jet noise measured from the scale models to a full-scale augmentor wing airplane installation are given in figure 14. In the first step, the acoustic signature is reduced to 23 one-third octave band sound pressure levels in the frequency range indicated. The spectra are obtained at a number of positions on a 15.25-m (50-ft) radius. These positions are chosen to include all probable directions from the airplane to the sideline. (See fig. 15.)

Corrections are needed to adjust the measured spectra (at 15.25 m or 50 ft) for air absorbtion, so the adjusted spectra are as observed on a standard day. A different correction is required for each frequency band. This correction is made as the second step in the procedure.

Scaling is performed as the third step. It consists of multiplying all linear dimensions by the scale factor. Using a scale factor of 3, the 15.25-m (50-ft) radius becomes a 45.75-m (150-ft) radius, the nozzle height becomes 27 cm (10.65 in.), the span of the test section becomes 328 cm (129 in.), and the frequency range becomes 63 Hz to 10 kHz.

Steps 4 and 5 are the final processing of the data to the appropriate sidelines and to PNL.

Since the data was scaled up by a factor of 3 when processed, leaving the effective length of the model span at 3.28 m (129 in.), step 6 was used to bring this dimension to full-scale semispan, 12.70 m (500 in.). Using the equation 10 log full-scale/model-scale span resulted in a span correction of +5.7 PNdB. This amount would be additive to the baseline and reverser data, increasing the sideline PNL values but not changing the delta values.

Another factor not included in the regular data processing is the effect of extra ground attenuation (EGA). This can be important because the noise source and transmission path of the sound are close to the ground plane for the entire distance to the sideline.

An EGA factor was calculated (step 7) for a typical spectrum from the test and resulted in a correction factor of approximately -5.4 PNdB per 305 m (1000 ft).

RESULTS

Thrust Reverser Static Performance

The largest deflector radius (1.25 h_N) was tested first with the exit lip set at the minimum deflection angle θ_L = 50° and extension length L equal to 0.99 h_N. The reverser was tested at several fore and aft (X) and vertical positions (Y) with respect to the lobe nozzle exit. As indicated in figure 16, the optimum fore and aft position is between X = 0.42 h_N and X = 0.70 h_N. At X = 0.70 h_N, the reverser assembly was moved in the -Y direction until the nozzle splitter screech shields interfered with the inlet bellmouth. The highest reverse thrust effectiveness was achieved with the nozzle flow impinging on the inlet bellmouth (Y = -0.14 h_N) as indicated in figure 17.

It appears that the additional friction losses resulting from the flow impingement that occurs in the negative Y position are offset by the higher turning efficiency produced by the lower position of the lobe nozzles.

With the reverser model set at the optimum X and Y positions with respect to the nozzle, the exit lip angle θ_L and the extension length L were varied. Three lip lengths were tested at lip angles varying from 50° to 80°. The reverser effectiveness parameters (F_R/F_N, F_N/F_N, and F_V/F_N) are plotted vs θ_L for lip extensions of 0.56 h_N, 0.99 h_N, and 1.41 h_N on figures 18, 19, and 20, respectively. As indicated in the three figures, the effectiveness parameters are quite sensitive to lip deflection angle but are not strongly affected by lip extension length. As the lip angle is increased from 50°, the horizontal reverse thrust component (F_H/F_N) increases to maximum effectiveness of about 0.70 at a 70° lip angle while the vertical thrust component (F_V/F_N) decreases steadily and finally reverses sign ($-F_V/F_N$) at a lip angle of 80°. The resultant thrust effectiveness (F_R/F_N) does not fall sharply until lip angles greater than 70° are reached. The resultant thrust effectiveness drops from a maximum of 0.80 at a 50° lip angle to approximately 0.45 at 80° lip angle.

Using the deflector radius of 1.25 h_N, two configurations (θ_L = 50° and 70°) were selected for acoustic evaluation through the full range of nozzle pressure ratios with the nozzle air heated to 149°C (300°F). The thrust reverser effectiveness parameters are plotted vs nozzle pressure ratio for lip angles of 70° and 50° on figures 21 and 22, respectively. The data shows that the effectiveness ratios are not very sensitive to nozzle pressure ratio or thrust level.

The effective reverse thrust angle θ_E was computed from the measured thrust components and compared with the lip angle θ_L in figure 23. This data indicates that flow overturning is occurring, particularly with the lip angle set at 70°. Flow visualization tests were conducted with the smaller deflector radius (r_D = 1.0 h_N) using a splitter plate.

The smallest deflector radius (1.0 h_N) was installed using the same inlet bellmouth and adjustable exit lip that were used with the preceding deflector. This reverser was also positioned at the optimum settings determined for the deflector radius of 1.25 h_N. Three lip extension lengths were tested (L = 0.99 h_N, 0.56 h_N, and 0.28 h_N) at lip angles varying from 50° to 80°.* Figures 24, 25, and 26 show the reverser effectiveness versus lip angle at a nozzle pressure ratio of 2.6 for the three lip lengths tested. As with the larger radius deflector, the reverser effectiveness parameters are quite sensitive to lip angle. The maximum horizontal thrust component is achieved with the lip angle at 70° for lip extension lengths equal to 0.99 h_N and 0.56 h_N, but for the shortest lip tested (L = 0.28 h_N), the peak horizontal thrust was produced at a lip angle of 80°. The resultant effectiveness parameter varies from a maximum of about 0.75 to approximately 0.45 at the largest lip angle tested. In general, as the lip length decreases, the sensitivity in trading horizontal thrust for vertical thrust diminishes.

At lip angles of 70° and 50°, acoustic and performance data were recorded with this deflector radius through the full range of pressure ratios, using heated air at T = 149°C (300°F).

The reverser effectiveness is shown versus nozzle pressure ratio for the two lip angles in figures 27 and 28. Again, the thrust effectiveness ratios are not very sensitive to pressure ratio or thrust level. The highest level of horizontal thrust and largest spread between the horizontal and vertical components is achieved with the 70° lip angle with the horizontal thrust effectiveness at about 0.65.

The effective resultant thrust angles, θ_E, are shown vs nozzle pressure ratio in figure 29 for the 70° and 50° lip angle configurations. Some overturning is evident with the 70° lip angle, particularly at the lower pressure ratios. Tests with the lip angle increased to 80° indicated that the flow was overturning to the point where the vertical thrust component, F_V, reversed sign as shown in figure 25. The effective thrust angle for this configuration is shown in figure 30 for two pressure ratios. More than 20° of overturning is realized.

In an effort to understand the nature of the flow overturning with the high lip angles, a few tests were conducted with a splitter plate installed as shown in figure 31. The splitter plate was coated with a mixture of lampblack and oil prior to turning on the air and photographed after shutdown.

As indicated in figures 32 and 33, some streamlines of the exit flow are greater than the lip angle of 70°. The procedure was repeated with the lip angle set at 80° and the nozzle pressure ratio set at 2.3. The lampblack pattern shown in figure 34 indicates a large amount of flow overturning as the streamlines are deflected well beyond the lip angle. It appears that the large amount of flow overturning is the result of the flow separating from the steeply deflected lip.

*A lip angle of 90 was tested with the shortest lip.

Thrust Reverser Installed Performance

This type of wing-mounted thrust reverser offers several advantages as described in the "Introduction" section. The static tests described above demonstrated that high reverser thrust effectiveness is available with this type of reverser. Two reverser configurations, for which noise data was measured, were selected as candidates for installed performance analysis on the augmentor wing airplane described in reference 4. These configurations were the 50° and the 70° lip angles for the smallest deflector radius tested ($r_D = 1.0\ h_N$). Their static performance levels are shown in figures 27 and 28. A preliminary analysis revealed that owing to the reverser being located aft of the main landing gear, the 50° lip angle would aggrevate the airplane pitch-up problem and also has a lower horizontal (retarding) force than the 70° lip angle. Only the 70° lip angle was therefore selected for the airplane stopping performance analysis.

A minimum nose gear load of 1818 kg (4000 lb) during reverser operation was selected as the criterion for establishing the maximum usable reverse thrust and the main landing gear location. The main landing gear was located 12% MAC aft of the airplane cg in order to maintain the minimum nose gear load with the four 9136 kg (20 100 lb) SLS engines at full power and the reverser operating at 70% effectiveness.

A breakdown of the available thrust levels for the P&W STF 395D (BM-2) engine is presented in figure 35. The total engine gross thrust, the thrust available at the fan offtake, the augmentor nozzle thrust, and the reverser resultant thrust are plotted against augmentor nozzle pressure ratio. Three engine power settings are identified (40%, 78%, and 100%) along with their appropriate augmentor nozzle pressure ratios used in the airplane stopping distance/noise analysis.

The airplane stopping distances were computed for three reverse thrust levels applied on an airplane velocity schedule as shown in figure 36. The effective resultant thrust angle was determined from the static performance data and applied at the wing location as shown in the sketch in figure 36. The throttle cutback point was chosen at 10.29 m/sec (20 knots) which assumes that reingestion would not be a problem with this type of reverser installation.

The airplane stopping distances were computed for the three engine power settings for a dry, wet, and icy runway and are shown in figure 37. The airplane selected for the analysis is the configuration described in reference 4 with a landing weight of 81 818 kg (180 000 lb). The assumptions for brake application time and time to attain reverse thrust are also given in figure 37. It is evident from this figure that for dry runway conditions, the reverser has little effect on stopping distance and is only effective for icy conditions.

In order to evaluate the tradeoffs in engine power, stopping distance, and sideline noise levels produced by the fan air thrust reverser, the noise levels are plotted versus stopping distance for the different runway conditions in figure 38. The 152 m (500 ft) sideline noise levels were selected from figure 39 at nozzle pressure ratios that correspond with the three engine power settings. The noise levels are scaled to the airplane nozzle areas and span dimensions and include EGA as described in the section "Acoustic Scaling and Extrapolation of Jet Noise."

Under dry runway conditions, figure 38 indicates that from a noise standpoint, it is not advantageous to apply high reverser thrust levels, as the stopping distance is hardly affected. High thrust levels with the attendant high noise levels should only be considered under icy conditions or partial brake applications where brake life and maintenance are considerations. The design of this thrust reverser for low maintenance is simplified by the relatively low gas temperature environment (149°C or 300°F). The reverser could then be considered for frequent use to reduce brake maintenance.

Acoustic Analysis

Peak Perceived Noise Level

Figures 39, 40, and 41 show the result of plotting the peak sideline PNL at 152 m (500 ft), 305 m (1000 ft), and 610 m (2000 ft) for the four reverser configurations and the baseline (nozzle only). These figures have been corrected for the full span and EGA factor. The remaining data plots in the report are for a 27-cm (10.65-in.) lobe height with a 328-cm (129-in.) nozzle span without EGA. Relative velocity effects have not been applied to the noise data.

All reverser noise comparisons are made with the bare nozzle (baseline) and not with an acoustically lined augmentor. As can be seen from figures 39, 40, and 41, the peak PNL of all the reverser configurations are within a plus or minus 1 dB range. Therefore, on a peak PNL basis, the differences in reverser radius and lip position do not have a great effect.

Figures 42, 43, and 44 are a plot of the data shown in figures 39, 40, and 41, but without the EGA and full nozzle span correction. Table I is a tabulation of the nozzle span and EGA correction factors and shows the net result of the two corrections at all angles and sideline distances. Since the one-third octave spectrum shapes are similar at all power settings, the values in table I are reasonably accurate for all nozzle pressure ratios.

Perceived Noise Level vs Sideline Angle

Although the peak value of PNL is used for the final analysis, the peak value does not fully define what is taking place along a given sideline. For better definition of the acoustic directivity

changes along the three pertinent sidelines, the data in figures 45 through 56 are included. The result of reversing the gas stream on the acoustic directivity is clearly shown in these figures. As would be expected, the acoustic level in the forward quadrant goes up as much as 10 dB when the gas stream is deflected forward. The aft quadrant acoustic levels drop (relative to a nonreversed stream) in the aft quadrant, but only by 2 to 5 dB. It is also noteworthy that the difference of reverser lip angle of 50° to 70° can change the acoustic directivity, but with a very slight total effect.

One-Third Octave Band Analysis

The one-third octave band spectra for the reverser configurations and baseline nozzle at pressure ratios of 1.6, 2.0, 2.3, 2.6, and 3.0 are compared in figures 57 through 62. The one-third octave spectra are selected at the location of the peak PNL for the given sideline and nozzle pressure ratio. Acoustic data for the 50° and 70° lip angles with the deflector radius of 1.25 h_N at the five nozzle pressure ratios are shown in figures 57, 58, and 59. The same type of data for the deflector radius of 1.0 h_N is shown in figures 60, 61, and 62. As indicated in these figures, the increase in PNL at the peak angle is caused by an increase in low and mid frequencies resulting from the flow scrubbing on the deflector reverser. The increase in noise level is brought about by the high turbulence during reverse operations.

CONCLUSIONS AND RECOMMENDATIONS

- High reverse thrust is available with a simple curved deflector operating with a lobe-type suppressor nozzle.

- Reversing the augmentor nozzle flow (fan air) above the wing results in increasing the noise level 3-4 PNdB above the basic nozzle-alone noise and redirects the noise forward of the airplane.

- The stopping distance for a 90 909 kg (200 000 lb) TOGW augmentor wing airplane with a touchdown velocity of 41 m/sec (80 knots) is significantly reduced only for icy runways by use of the augmentor nozzle thrust reverser.

- Further studies of this type of thrust reverser should consider airplane installation and packaging constraints.

Boeing Commercial Airplane Company
P.O. Box 3707
Seattle, Washington 98124, July 31, 1974

REFERENCES

1. Campbell, J.; Harkonen, D. L.; Lawrence, R.; and O'Keefe, J. V.: Task V–Noise Suppression of Improved Augmentors for Jet STOL Aircraft. Final Report, D6-60174, The Boeing Company, January 1973 (NASA CR-114534).

2. Campbell, J.; Lawrence, R.; and O'Keefe, J.: Design Integration and Noise Studies for Jet STOL Aircraft. Final Report, Volume III–Static Test Program, D6-40552-3, The Boeing Company, May 1972 (NASA CR-114285).

3. Campbell, J.; Harkonen, D. L.; and O'Keefe, J. V.: Task VIIC Augmentor Wing Cruise Blowing Valveless System. Volume I. Static Test Program, D6-41216, The Boeing Company, November 1973 (NASA CR-114623).

4. Roepcke, F. A.; and Nickson, T. B.: Task VIIA, Augmentor Wing Cruise Blowing Valveless System. Volume I. System Design and Test Integration, D6-40950, The Boeing Company, April 1973 (NASA CR-114621).

TABLE 1.—NOISE ADJUSTMENTS FOR AIRPLANE SEMISPAN NOZZLE AREA AND EGA

Noise Adjustment, PNdB (refer to fig. 14)

152 m sideline (500 ft)

Angle from inlet	40°	50°	60°	70°	80°	90°	100°	110°	120°	130°	140°
Nozzle span factor	+5.7	←								→	+5.7
EGA	-4.2	-3.5	-3.1	-2.9	-2.7	-2.7	-2.7	-2.9	-3.1	-3.5	-4.2
Net	+1.5	+2.2	+2.6	+2.8	+3.0	+3.0	+3.0	+2.8	+2.6	+2.2	+1.5

305 m sideline (1000 ft)

Nozzle span factor	+5.7	←								→	+5.7
EGA	-8.4	-7.1	-6.2	-5.7	-5.5	-5.4	-5.5	-5.7	-6.2	-7.1	-8.4
Net	-2.7	-1.4	-.5	0	+.2	+.3	+.2	0	-.5	-1.4	-2.7

610 m sideline (2000 ft)

Nozzle span factor	+5.7	←								→	+5.7
EGA	-16.8	-14.0	-12.5	-11.5	-10.9	-10.8	-10.9	-11.5	-12.5	-14.0	-16.8
Net	-11.1	-8.3	-6.8	-5.8	-5.2	-5.1	-5.2	-5.8	-6.8	-8.3	-11.1

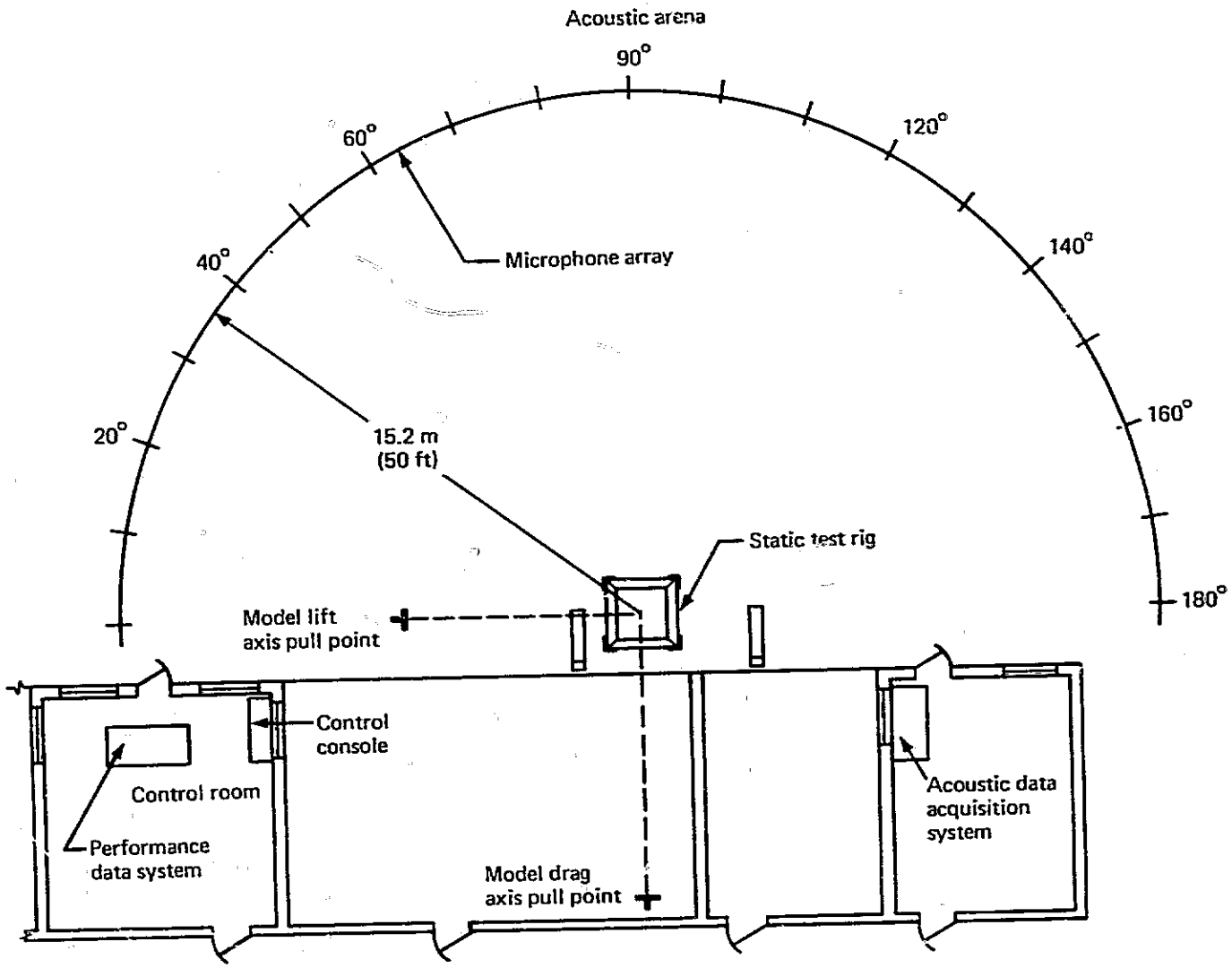

FIGURE 4.–STATIC TEST INSTALLATION

FIGURE 5.—THRUST STAND AND ACOUSTIC ARENA

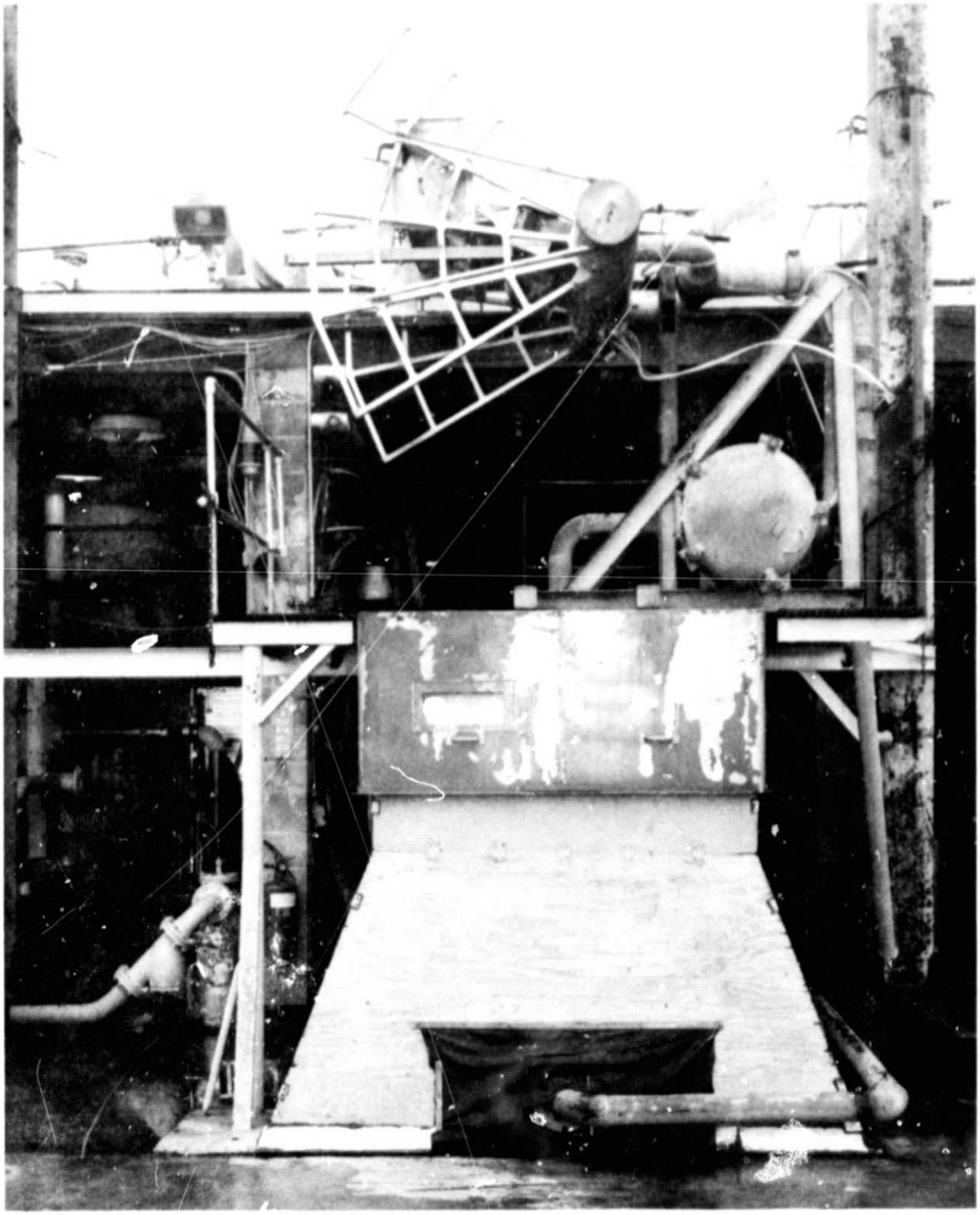

FIGURE 6.—THRUST REVERSER TEST MODEL INSTALLATION

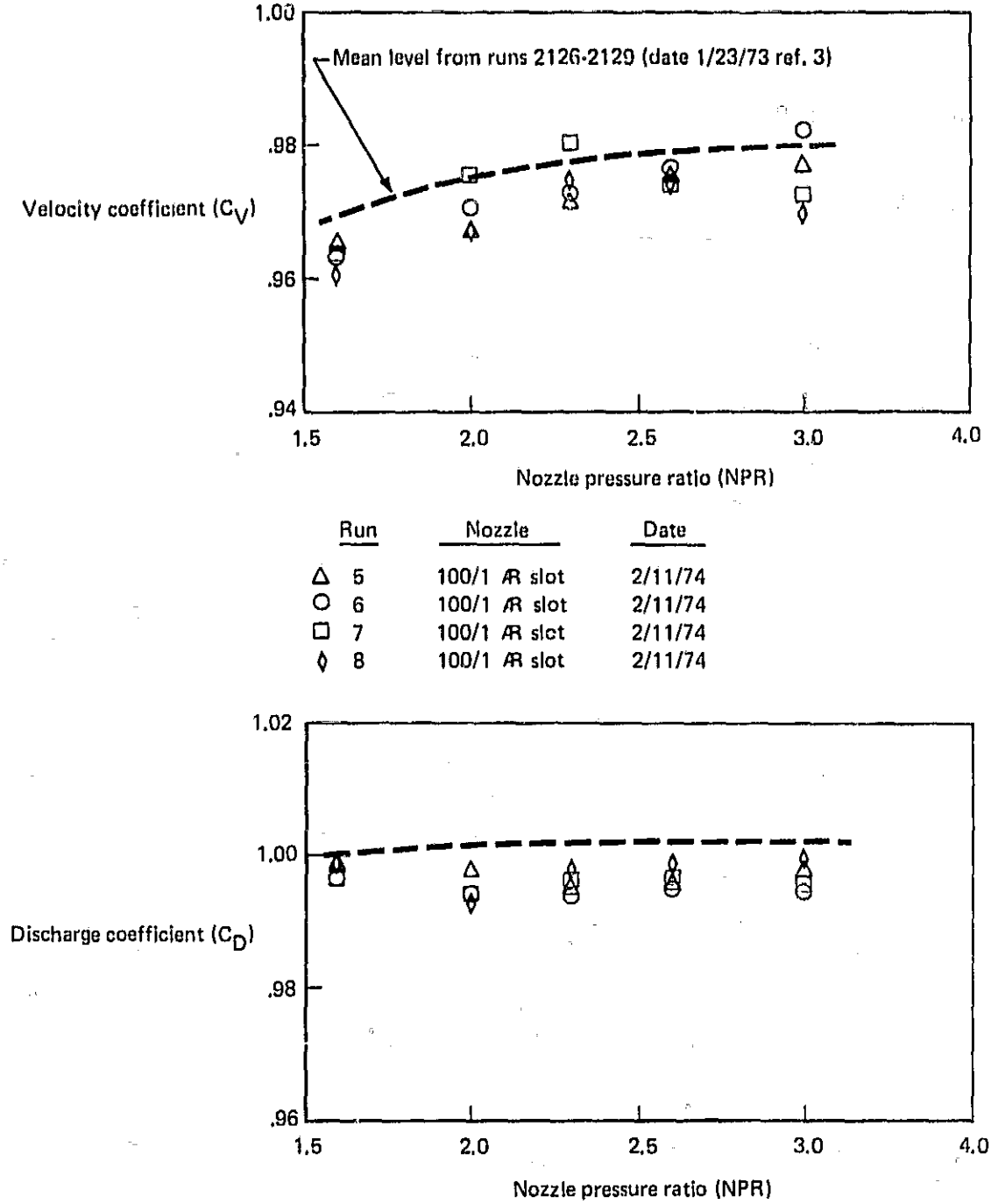

FIGURE 7.—REFERENCE NOZZLE (SLOT) PERFORMANCE LEVELS AND DATA REPEATABILITY

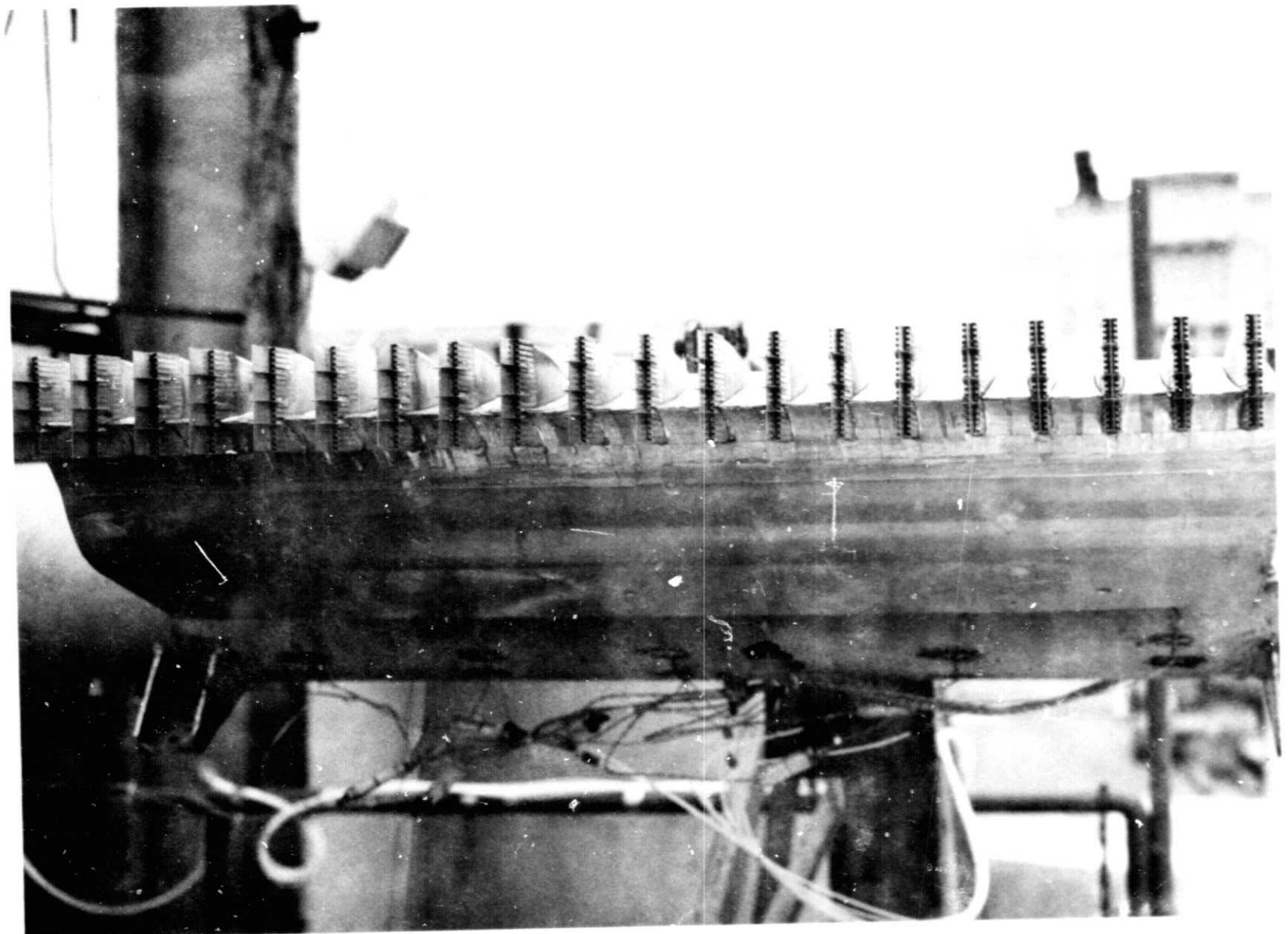

FIGURE 8.—ONE-THIRD SCALE CORRUGATED SPLITTER LOBE NOZZLE ARRAY

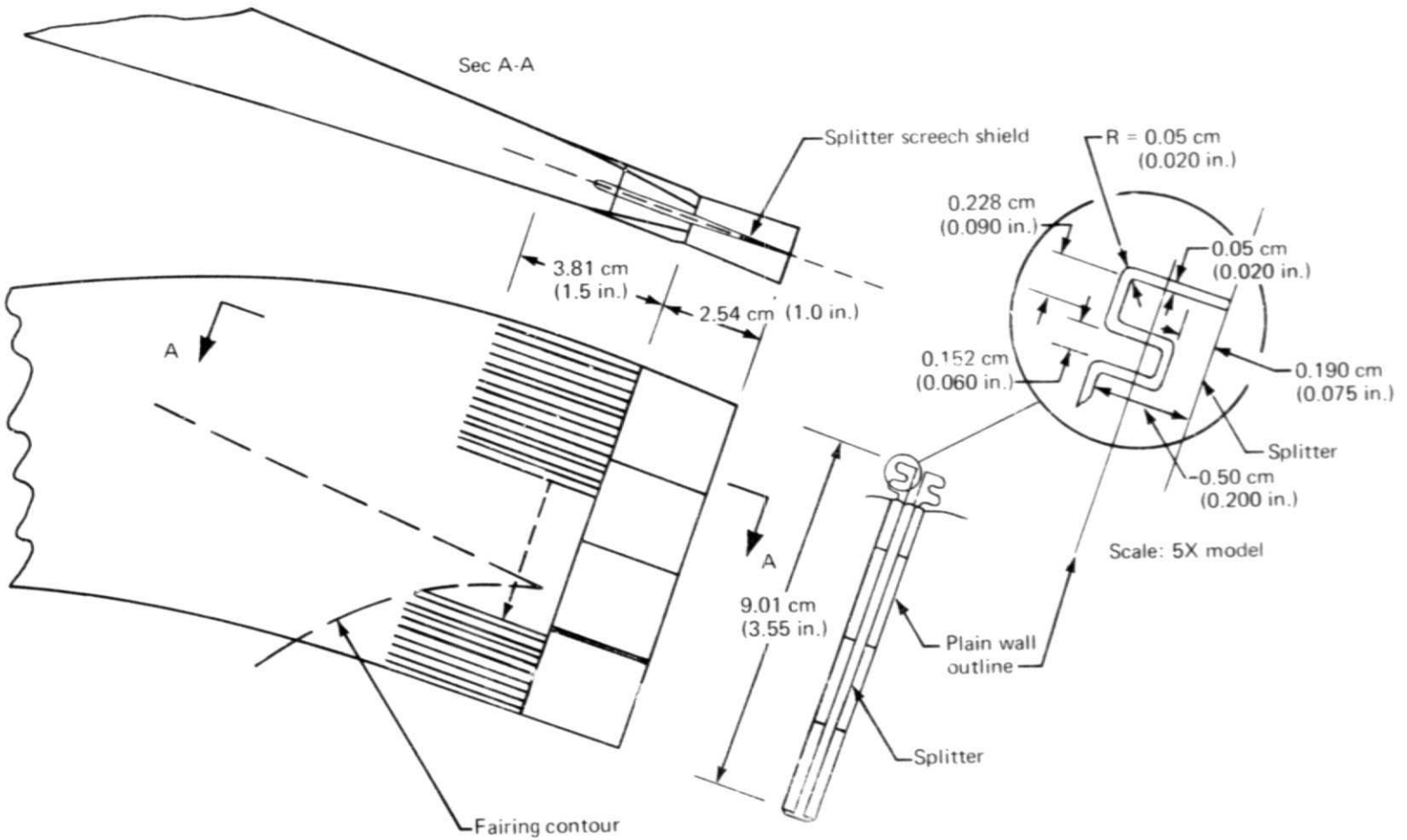

FIGURE 9.–DESIGN FEATURES OF A SINGLE CORRUGATED SPLITTER LOBE NOZZLE

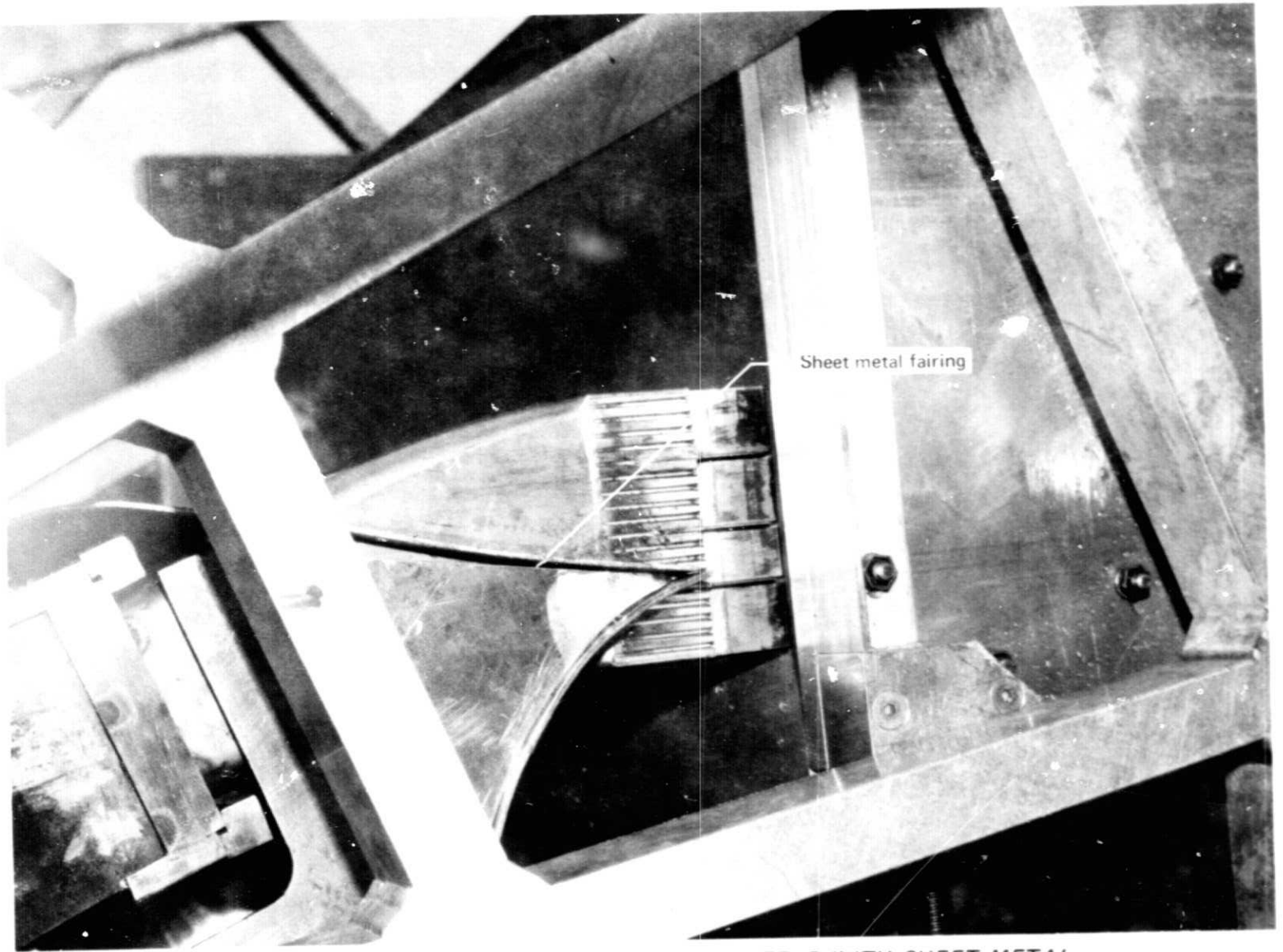

FIGURE 10.–CORRUGATED SPLITTER LOBE NOZZLE WITH SHEET METAL AERODYNAMIC FAIRING

AUGMENTOR NOZZLE–REVERSER ASSEMBLY
SIDE VIEW

Scale = 1/5

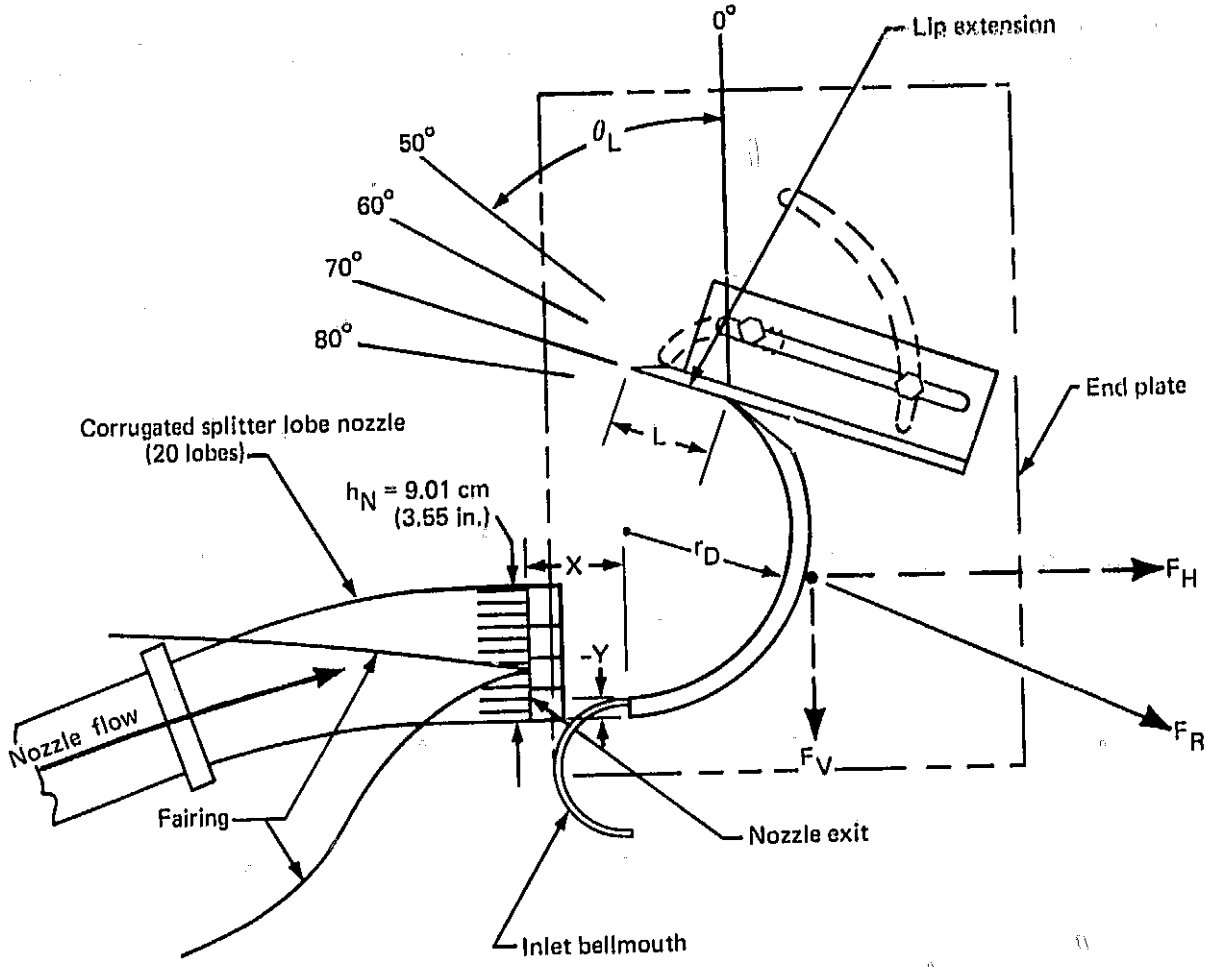

Variables and ranges tested–

r_D – 1.0 h_N, 1.25 h_N
θ_L – 50° to 140°
L – 0 to 1.4 h_N
X – 0.42 h_N to 1.26 h_N
Y – -0.14 h_N to +0.14 h_N

FIGURE 11.–THRUST REVERSER TEST HARDWARE ASSEMBLY AND TEST VARIABLES

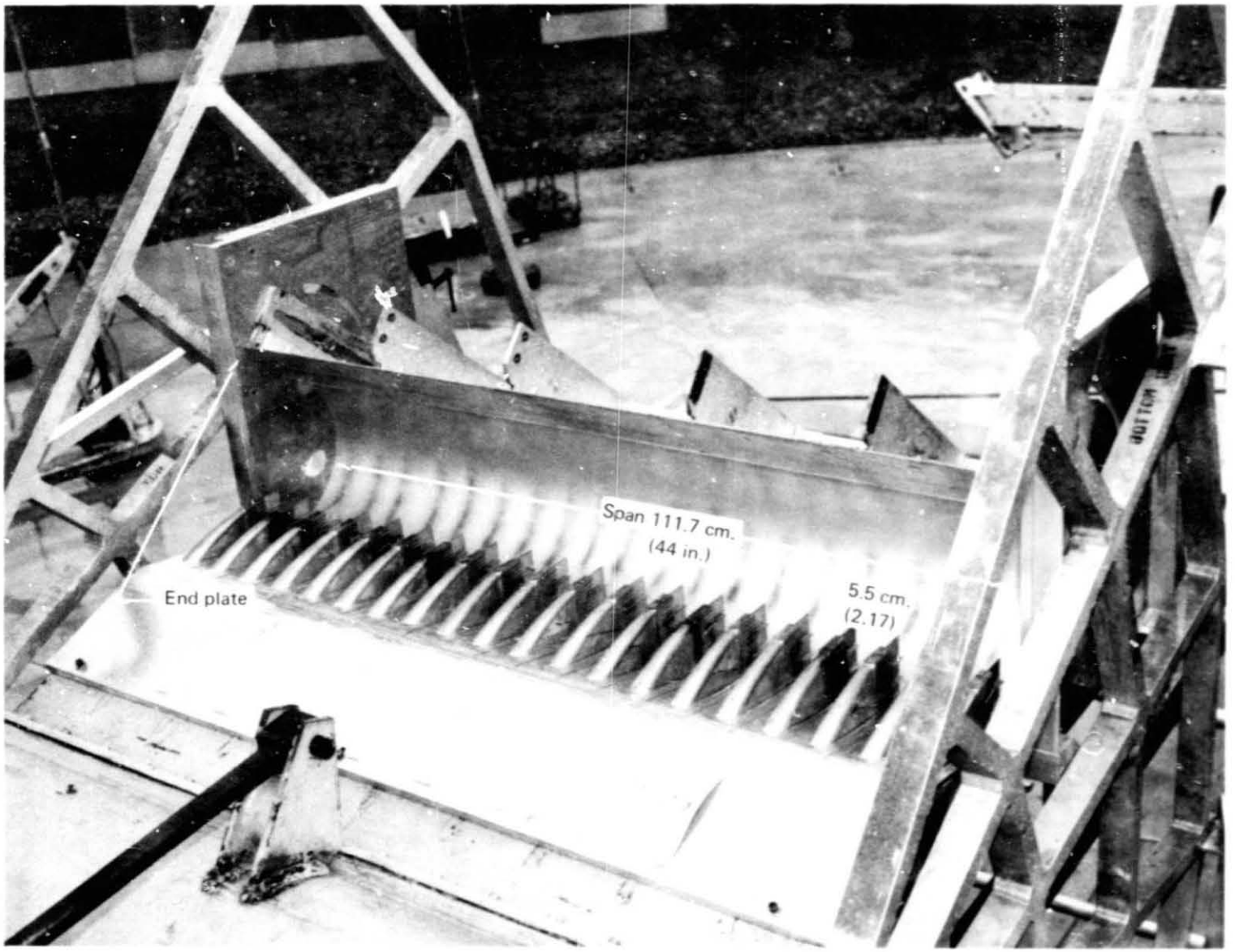

FIGURE 12.–LOBE NOZZLE, REVERSER, AND END PLATE INSTALLATION

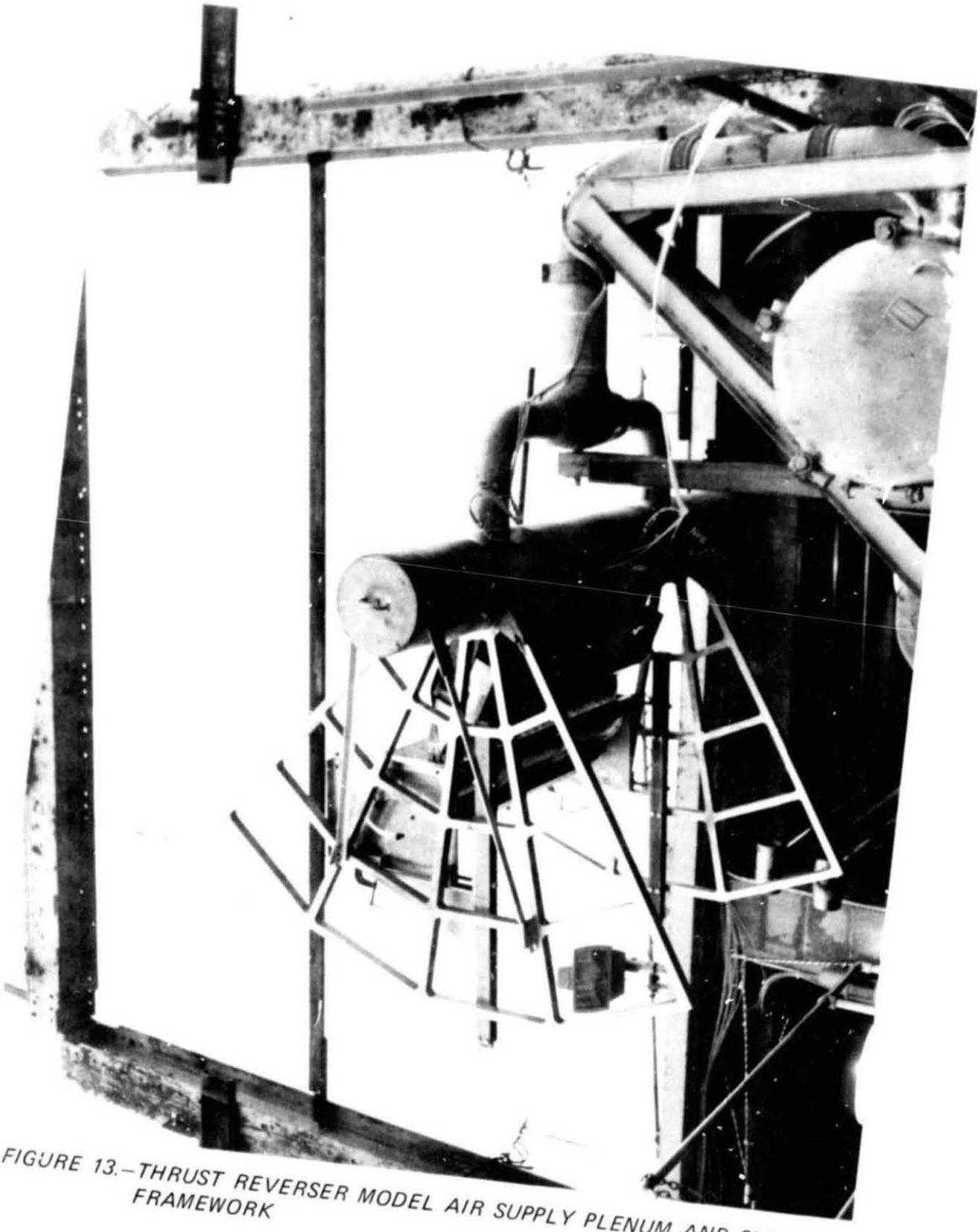

FIGURE 13.–THRUST REVERSER MODEL AIR SUPPLY PLENUM AND SUPPORT FRAMEWORK

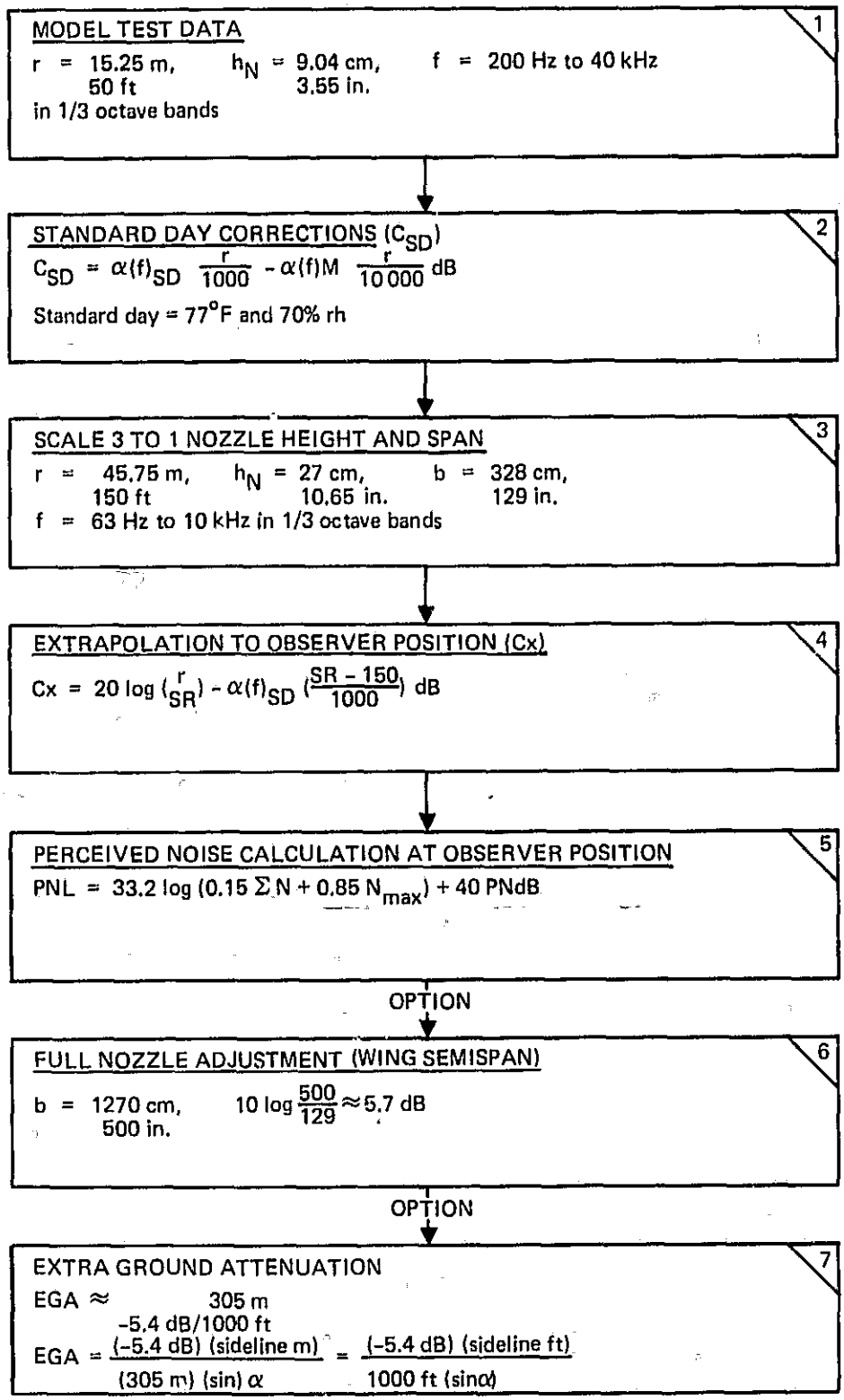

FIGURE 14.—JET NOISE SCALING AND EXTRAPOLATION PROCEDURES

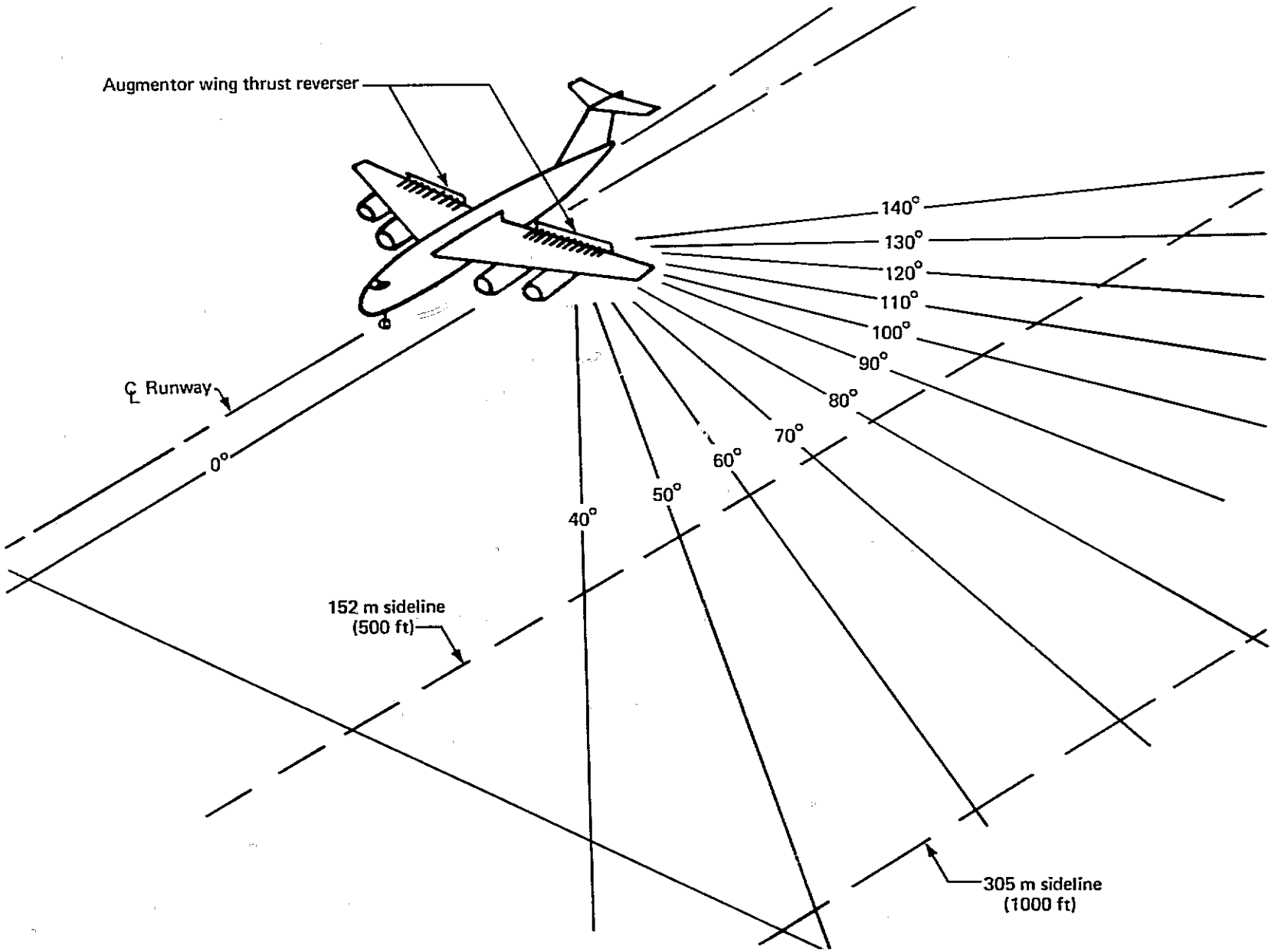

FIGURE 15.–AUGMENTOR WING AIRPLANE AND MICROPHONE ORIENTATION

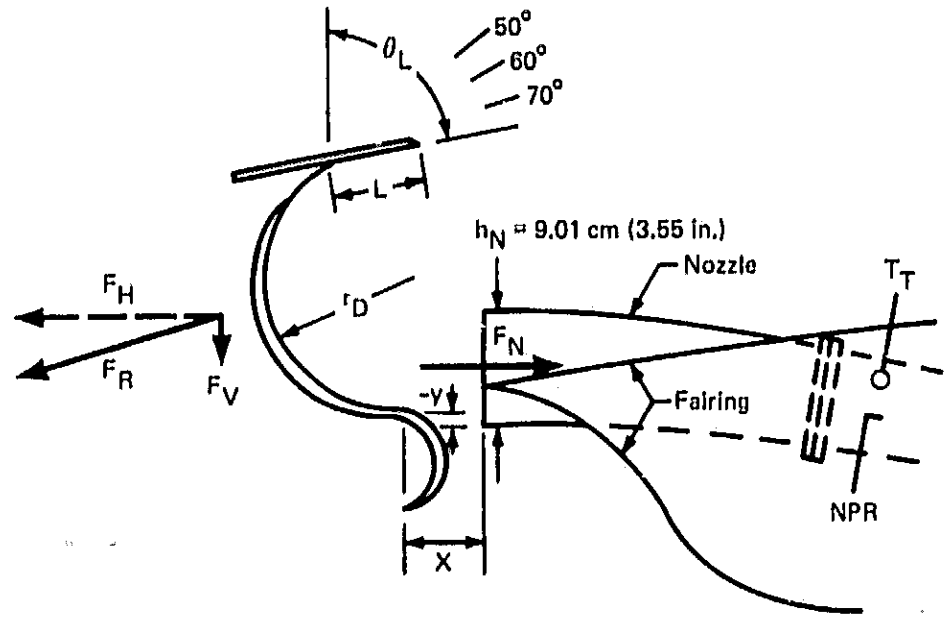

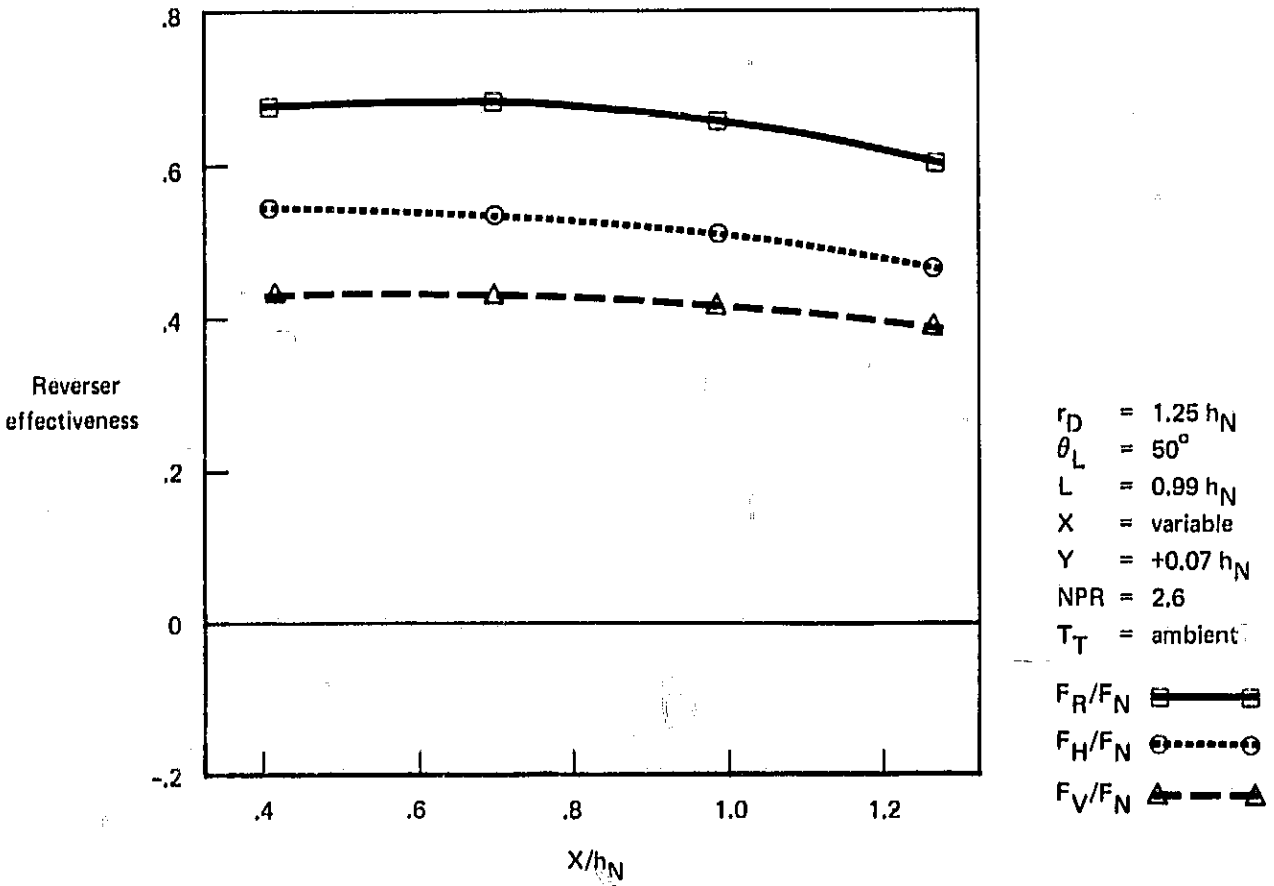

FIGURE 16.—SENSITIVITY OF REVERSER FORE AND AFT (X) POSITION ON STATIC REVERSER EFFECTIVENESS (r_D = 1.25 h_N)

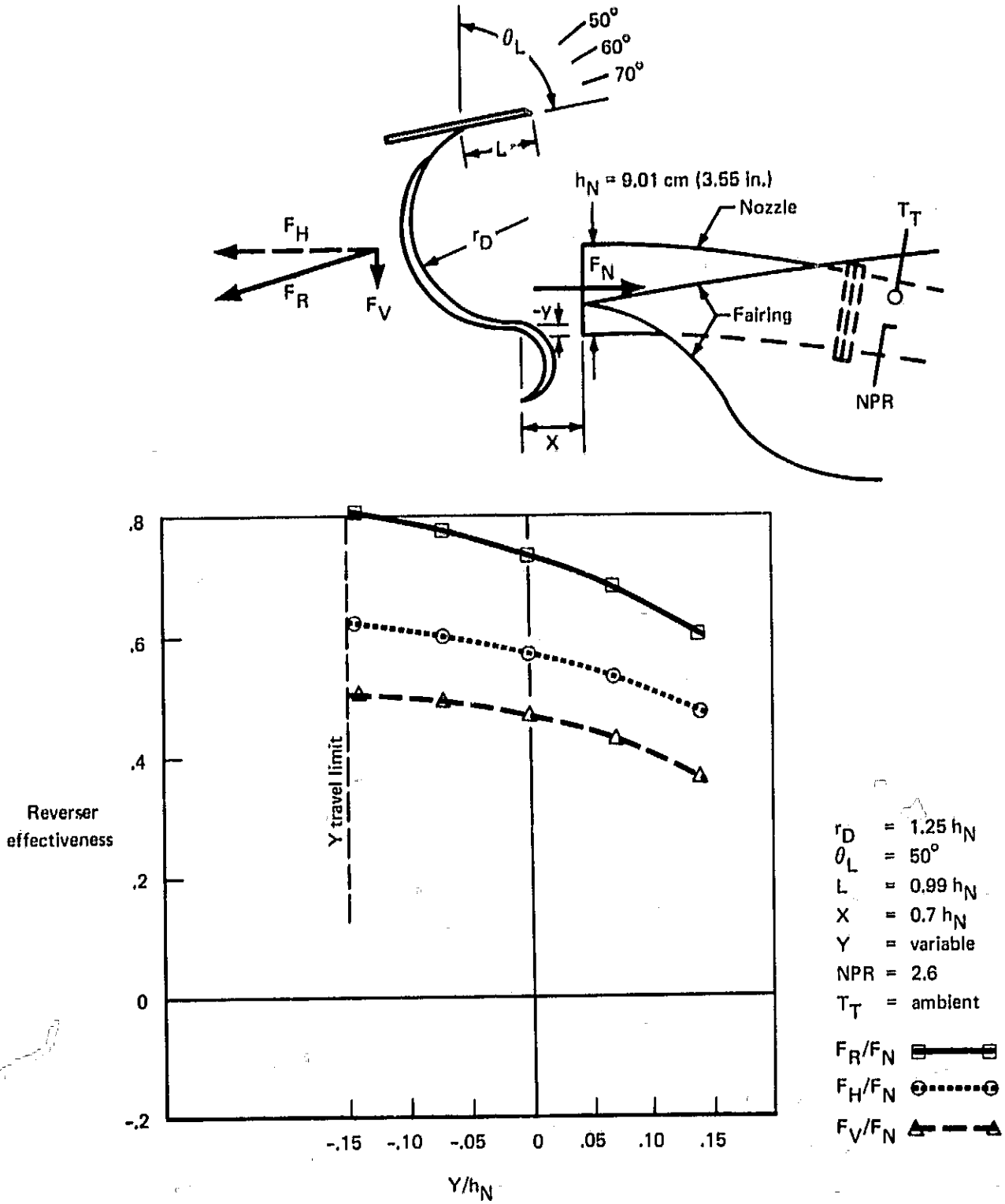

FIGURE 17.–SENSITIVITY OF REVERSER VERTICAL (Y) POSITION ON STATIC REVERSER EFFECTIVENESS (r_D = 1.25 h_N).

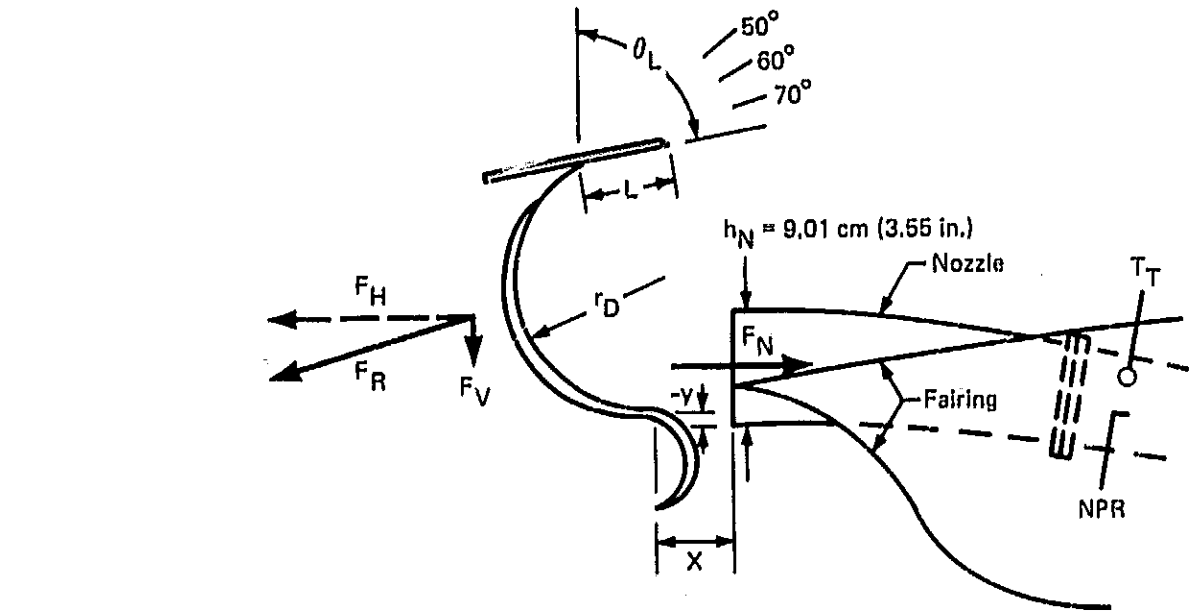

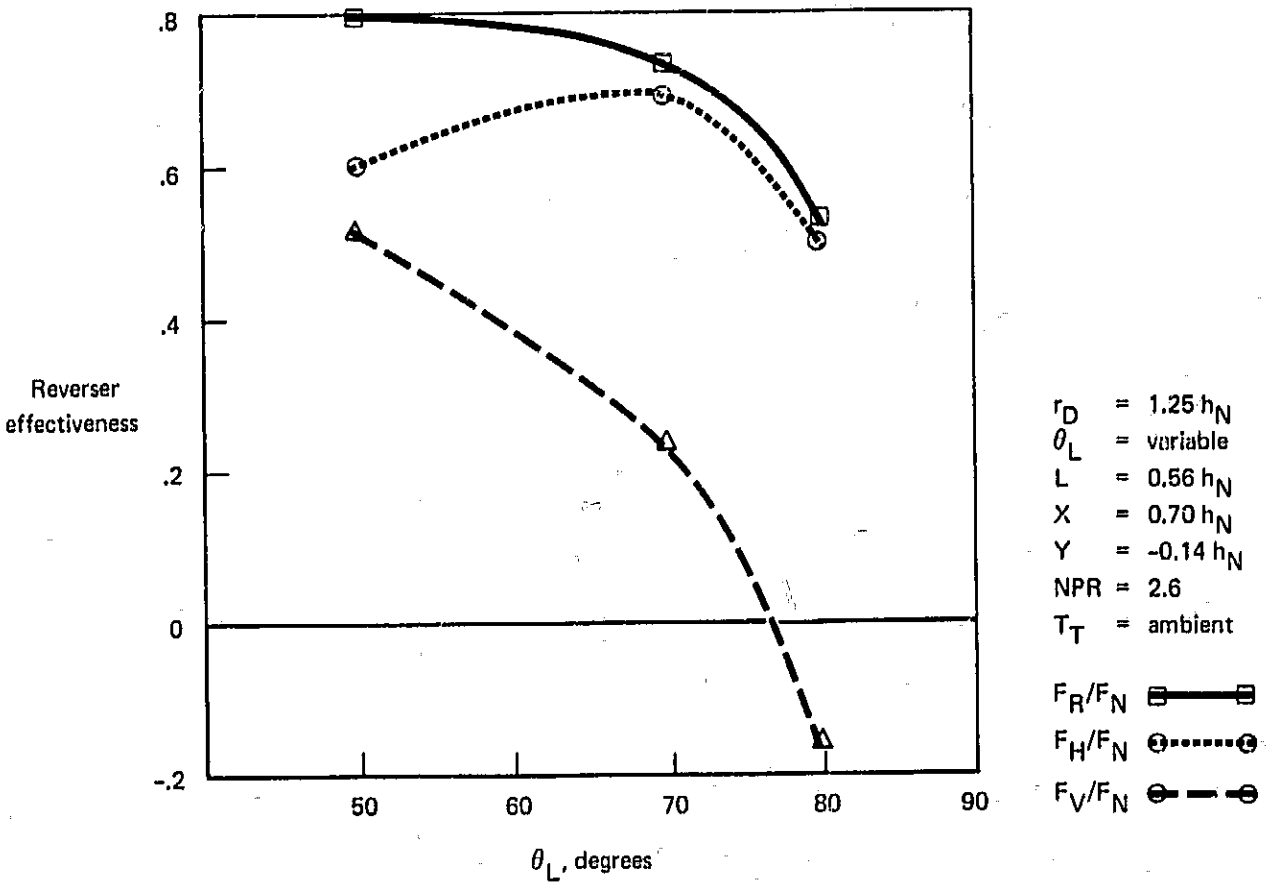

FIGURE 18.—EFFECTS OF DEFLECTOR LIP ANGLE (θ_L) ON REVERSER EFFECTIVENESS FOR A LIP LENGTH EQUAL TO 0.56 h_N (r_D = 1.25 h_N)

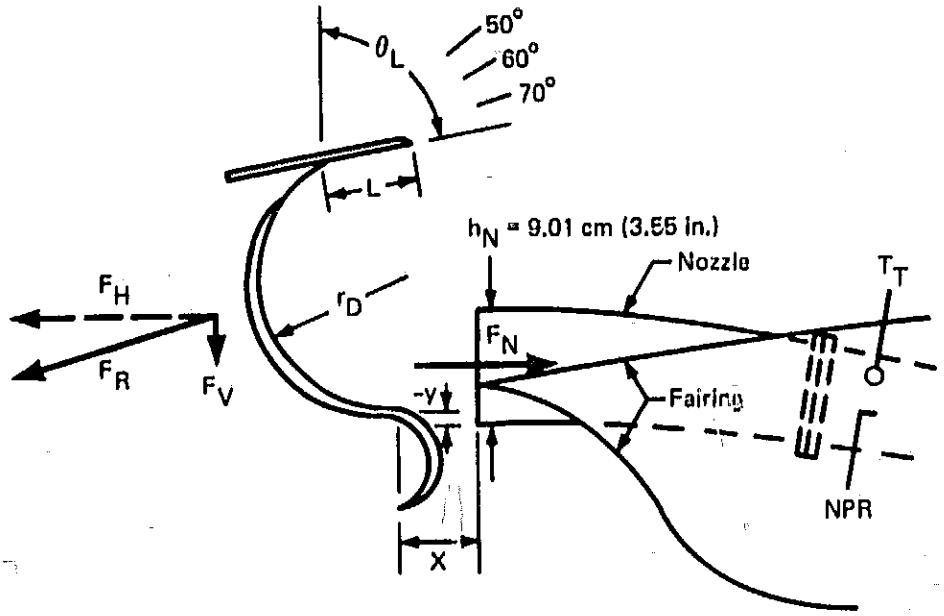

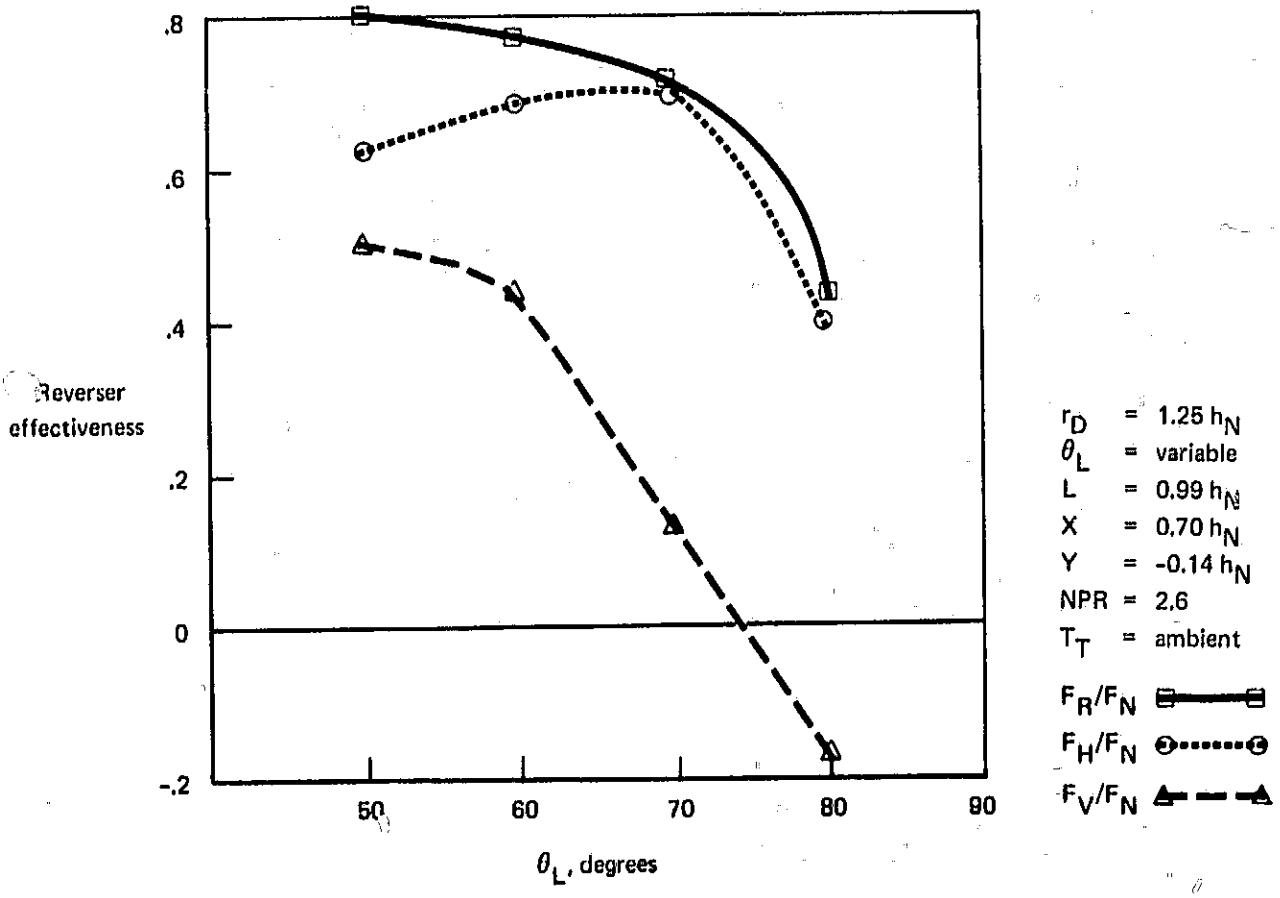

FIGURE 19.–EFFECTS OF DEFLECTOR LIP ANGLE (θ_L) ON REVERSER EFFECTIVENESS FOR A LIP LENGTH EQUAL TO 0.99 h_N (r_D = 1.25 h_N)

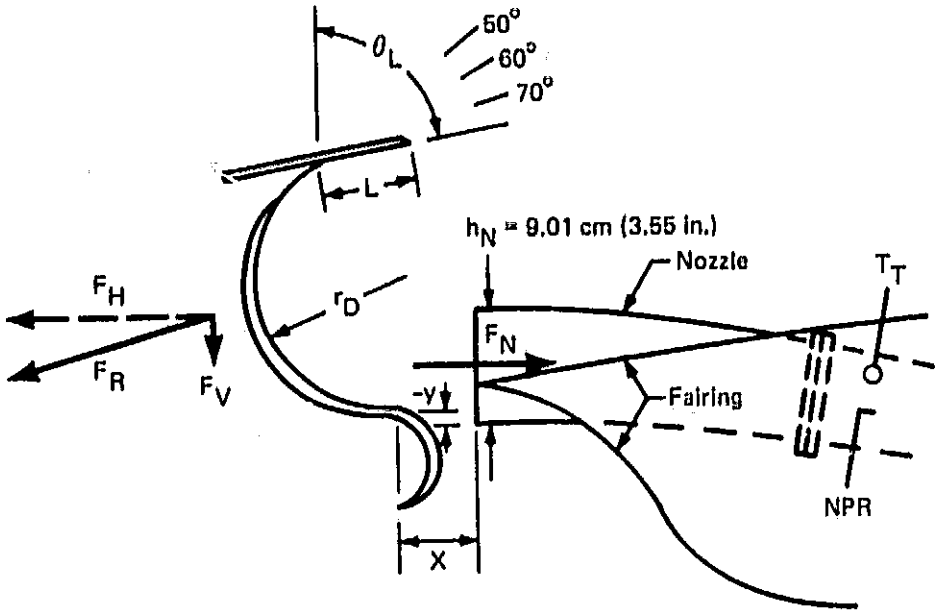

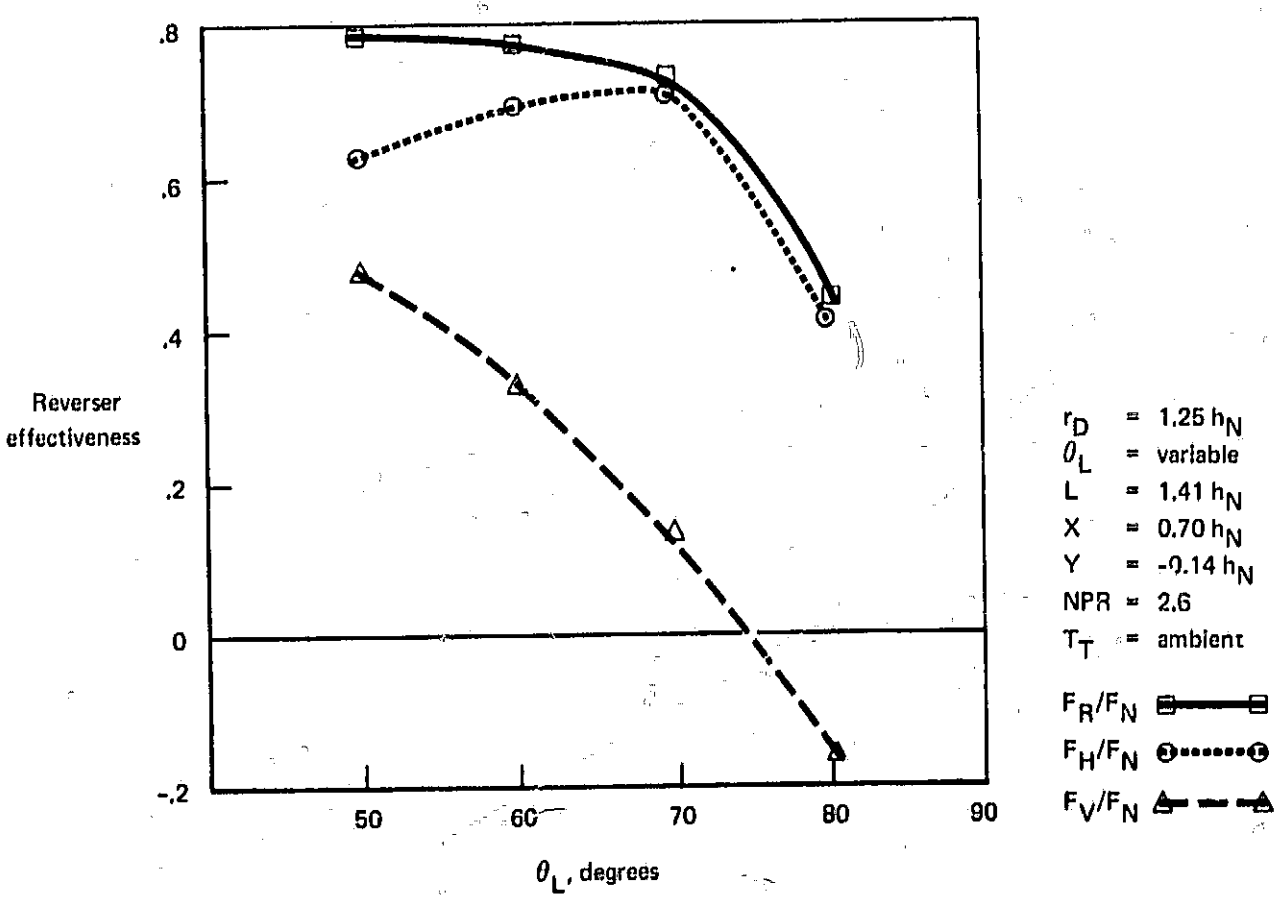

FIGURE 20.–EFFECTS OF DEFLECTOR LIP ANGLE (θ_L) ON REVERSER EFFECTIVENESS FOR A LIP LENGTH EQUAL TO 1.41 h_N (r_D = 1.25 h_N)

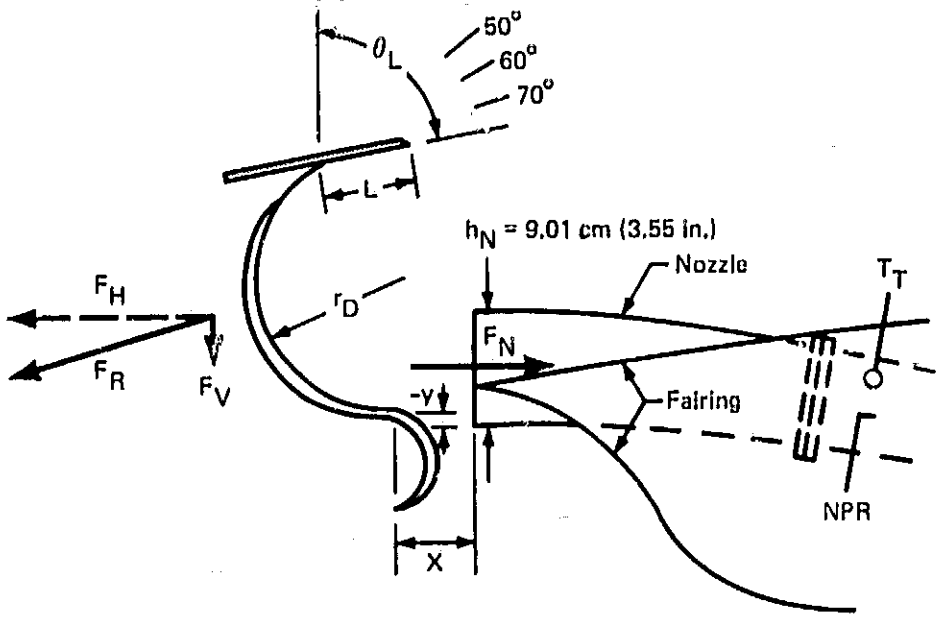

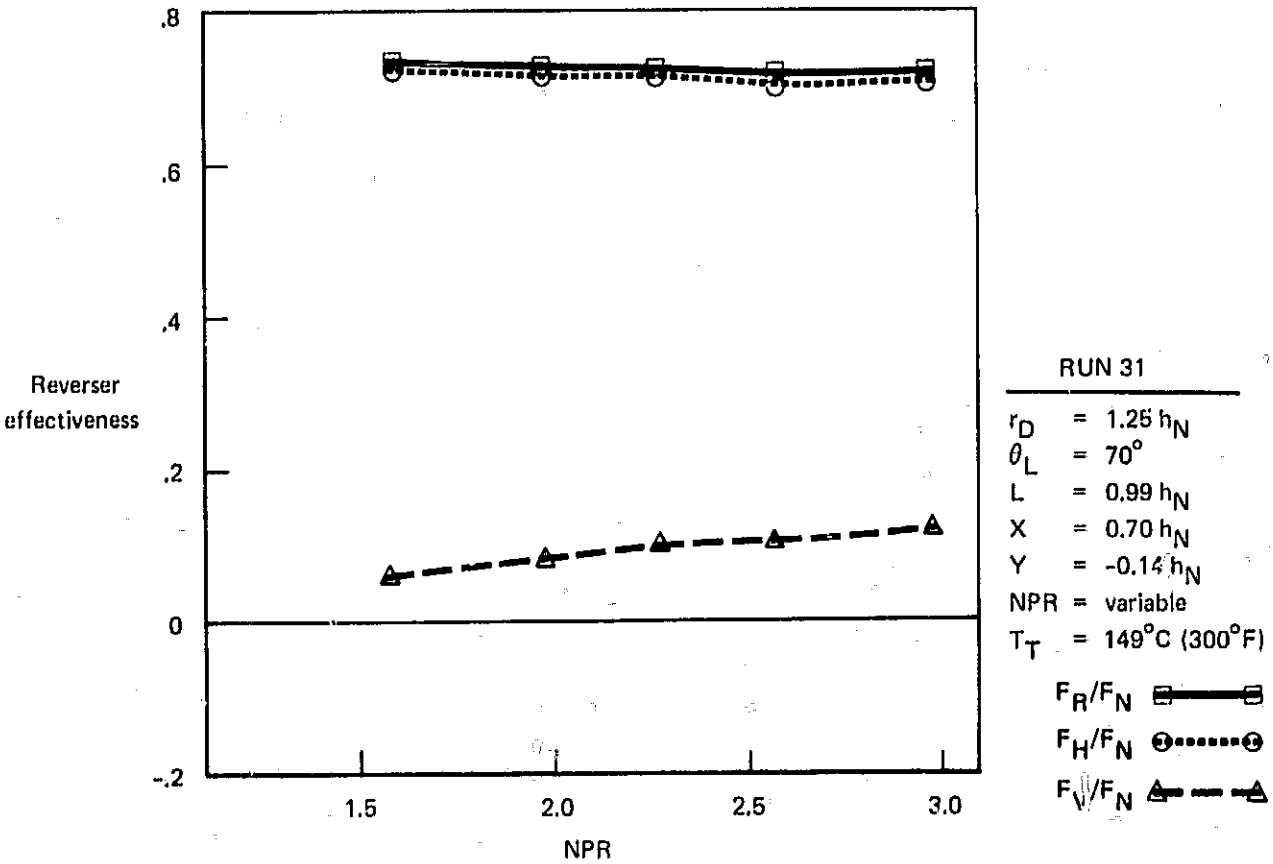

FIGURE 21.–SENSITIVITY OF NOZZLE PRESSURE RATIO ON REVERSER EFFECTIVENESS WITH LIP ANGLE (θ_L) OF 70° (r_D = 1.25 h_N)

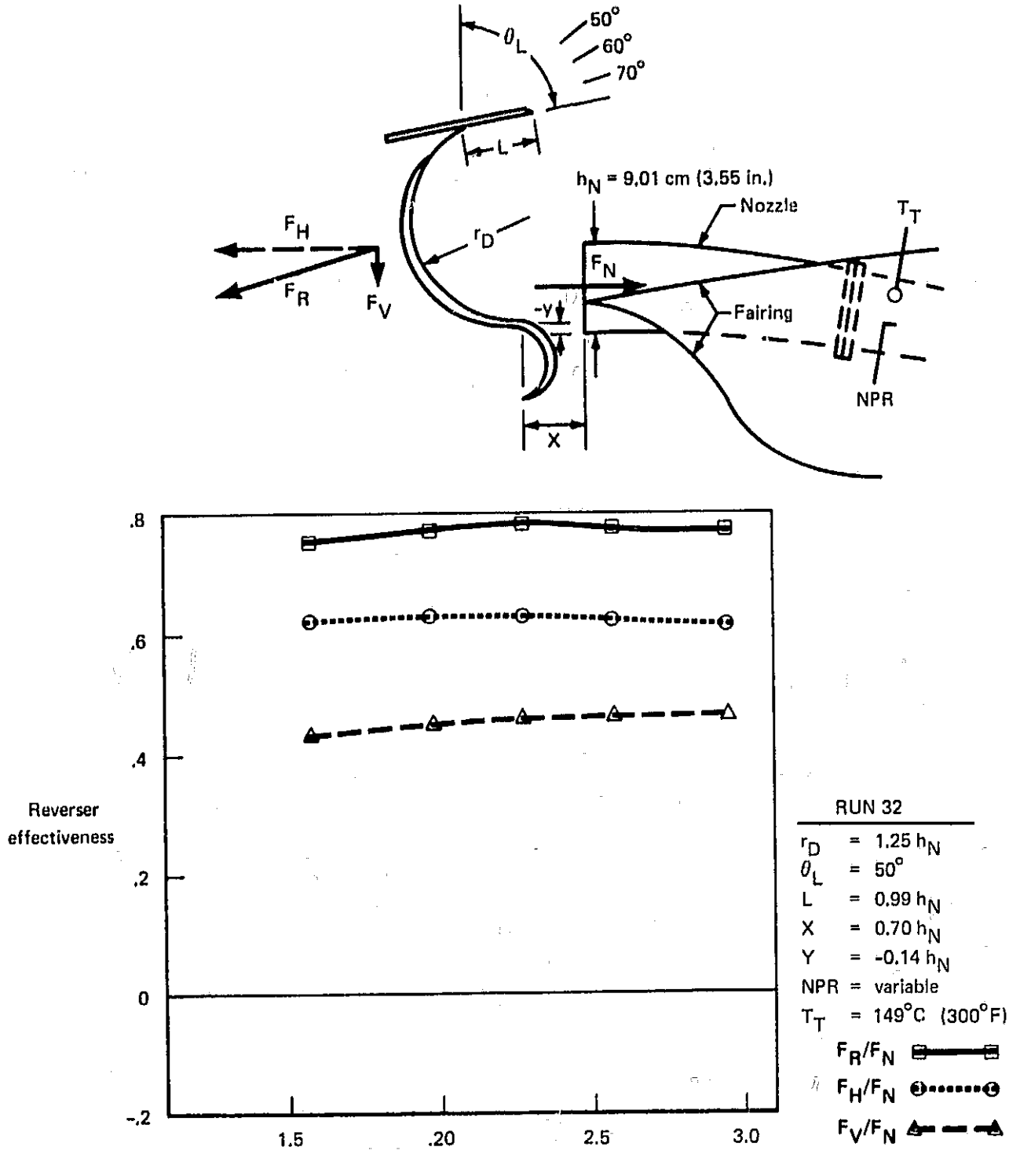

FIGURE 22.–SENSITIVITY OF NOZZLE PRESSURE RATIO ON REVERSER EFFECTIVENESS WITH LIP ANGLE (θ_L) of 50° ($r_D = 1.25\ h_N$).

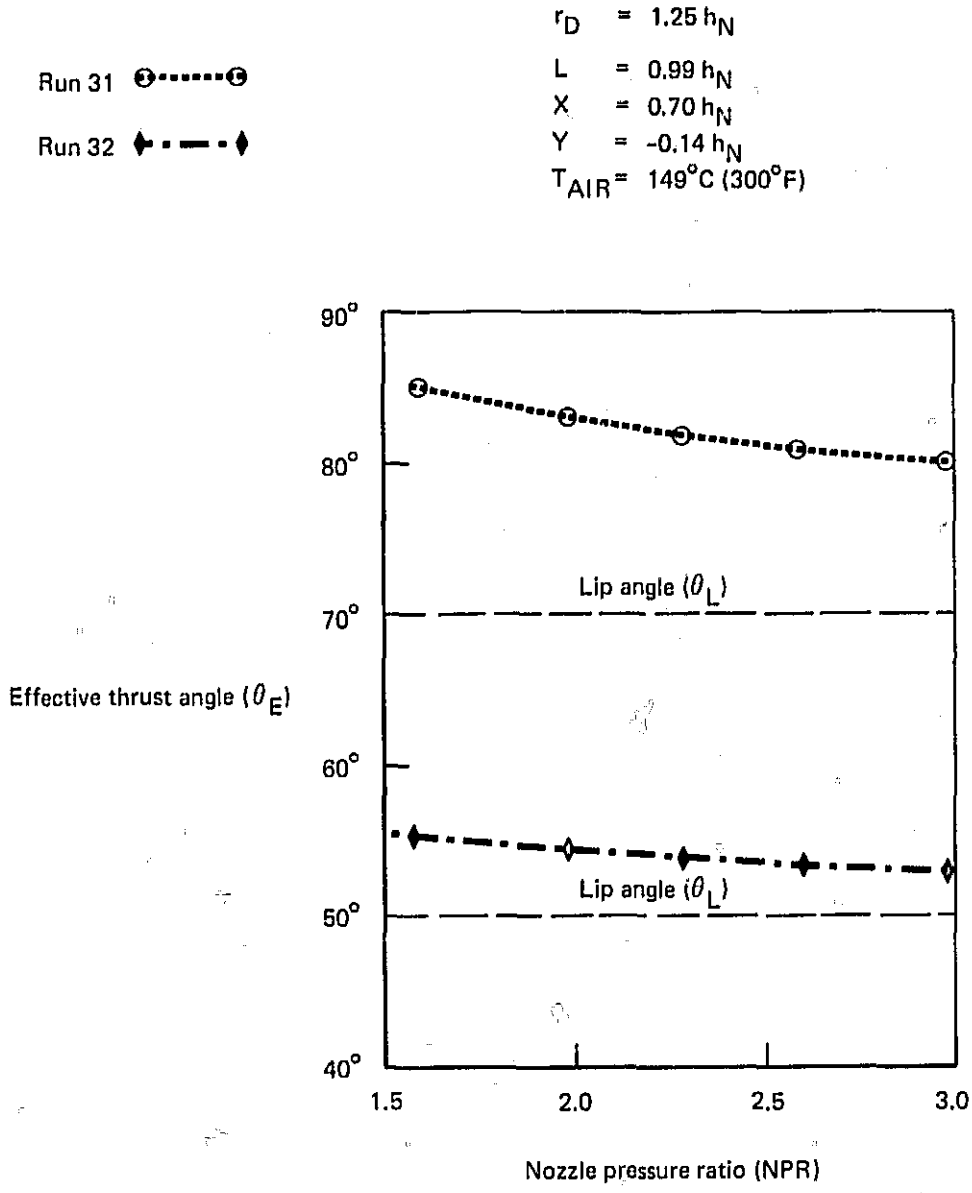

FIGURE 23.—EFFECTIVE REVERSER THRUST ANGLE (θ_E) COMPARED WITH THE GEOMETRIC LIP ANGLE (θ_L) OF 70°, 50° ($r_D = 1.25\ h_N$)

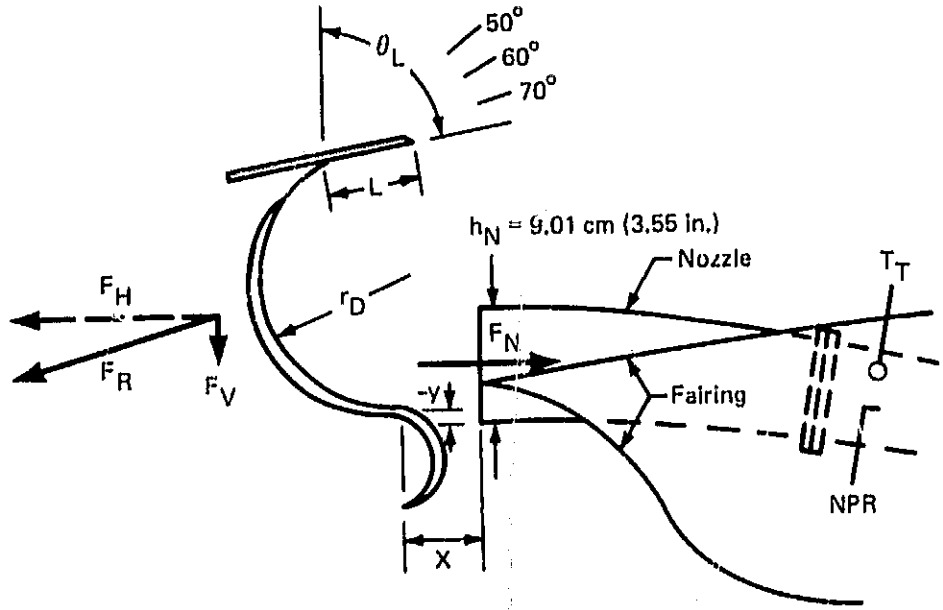

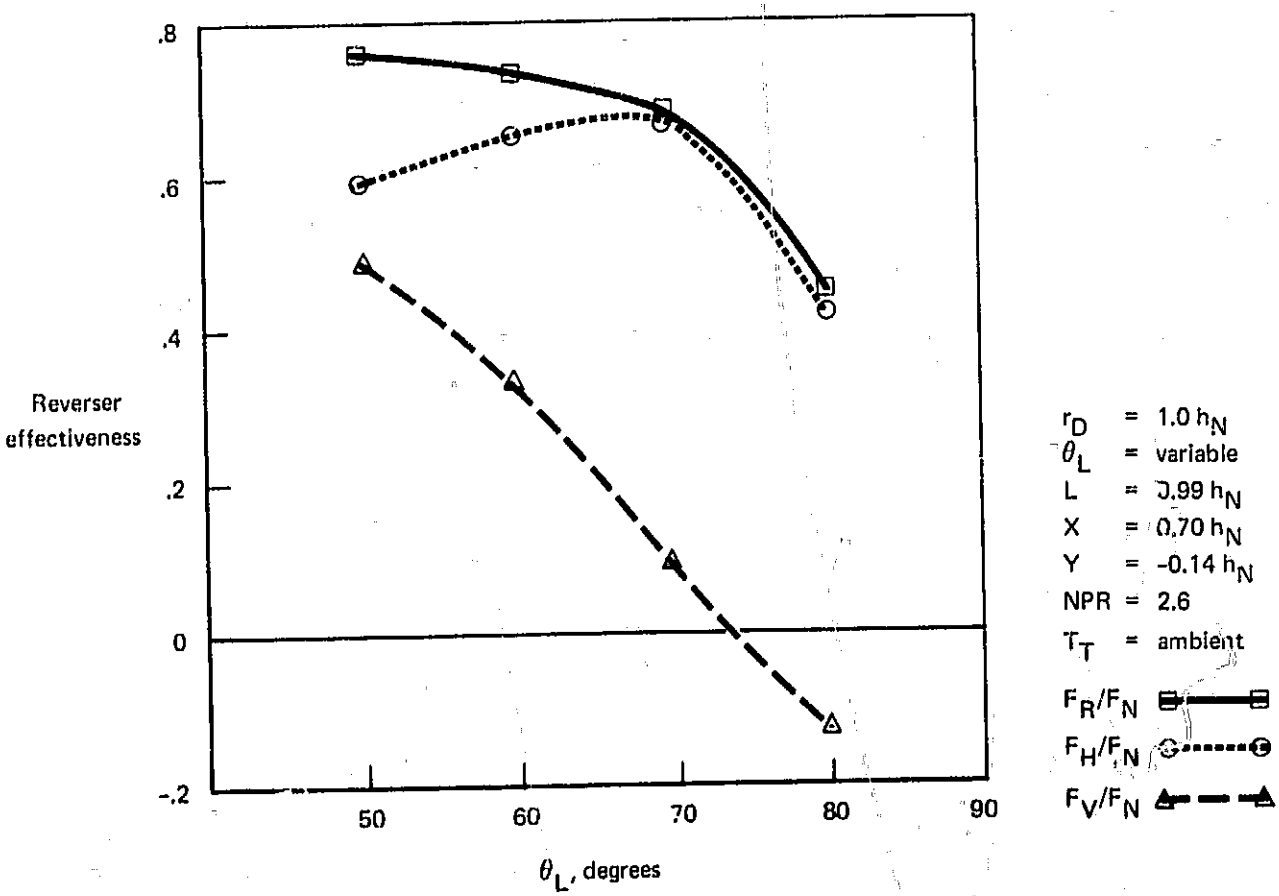

FIGURE 24.–EFFECTS OF DEFLECTOR LIP ANGLE (θ_L) ON REVERSER EFFECTIVENESS FOR A LIP LENGTH EQUAL TO 0.99 h_N (r_D = 1.0 h_N)

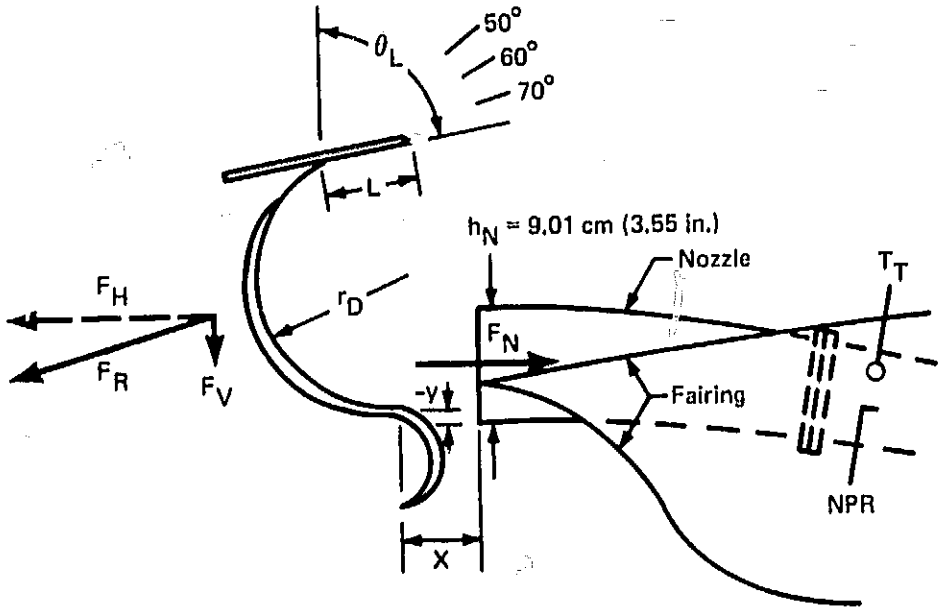

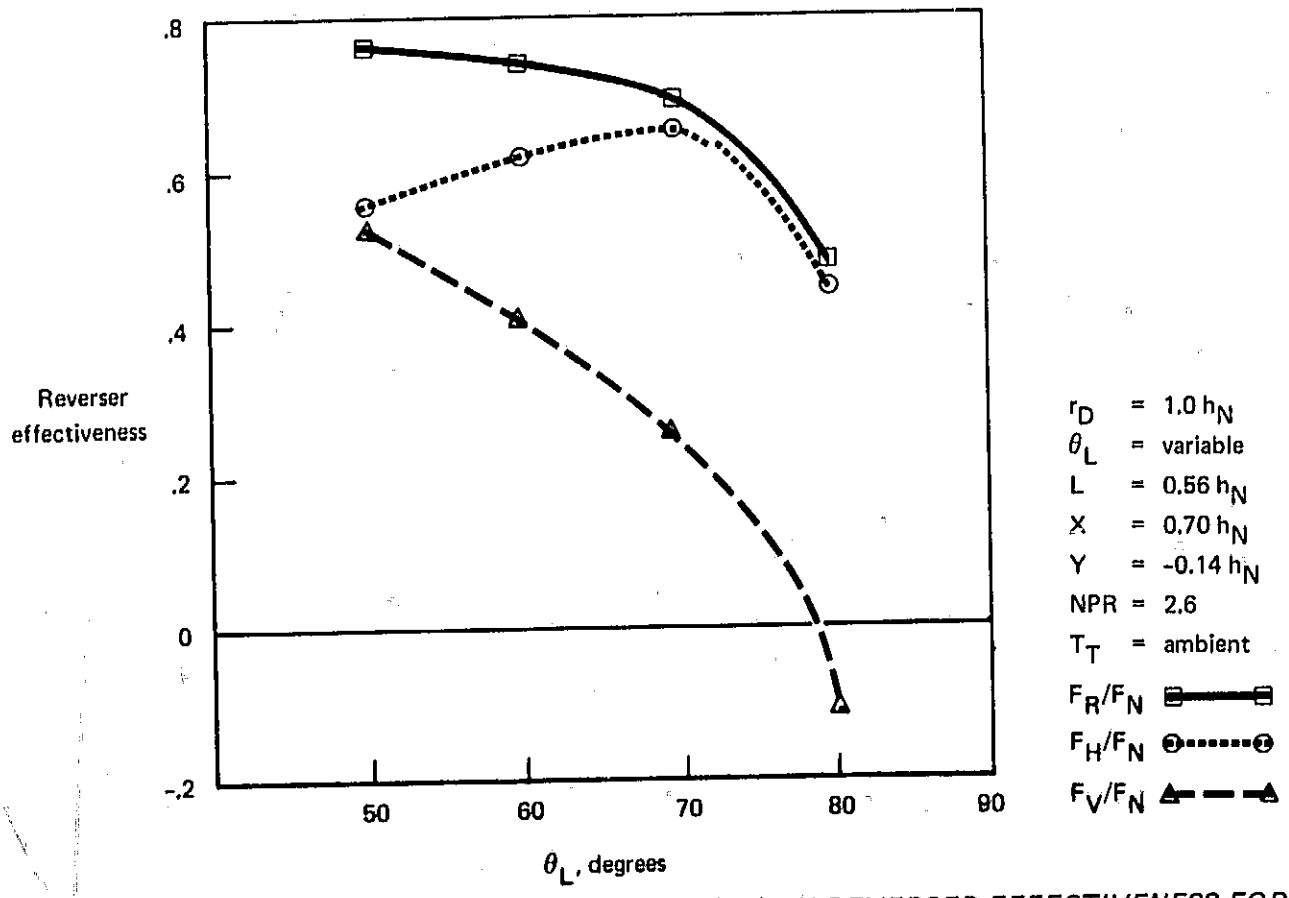

FIGURE 25.–EFFECT OF DEFLECTOR LIP ANGLE (θ_L) ON REVERSER EFFECTIVENESS FOR A LIP LENGTH EQUAL TO 0.56 h_N (r_D = 1.0 h_N)

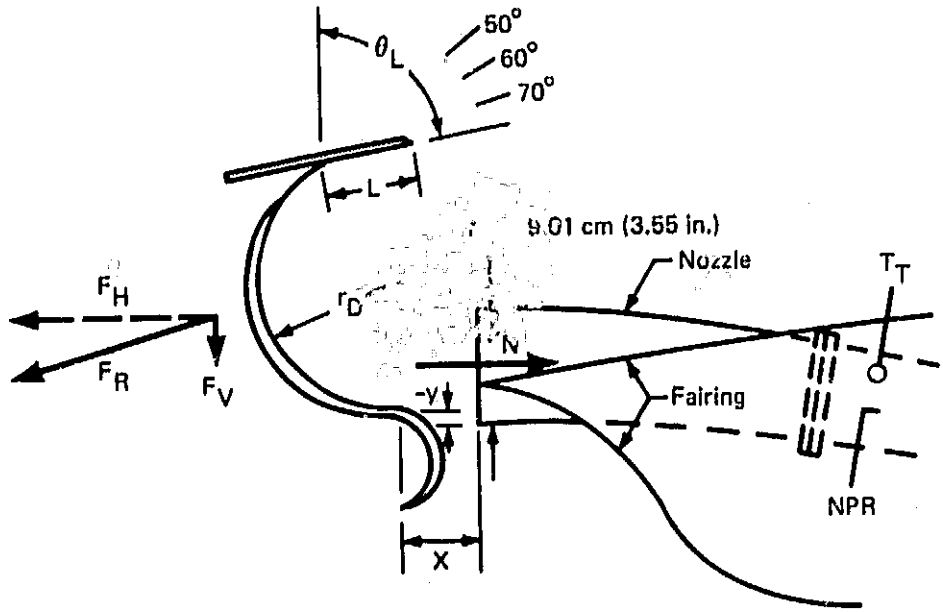

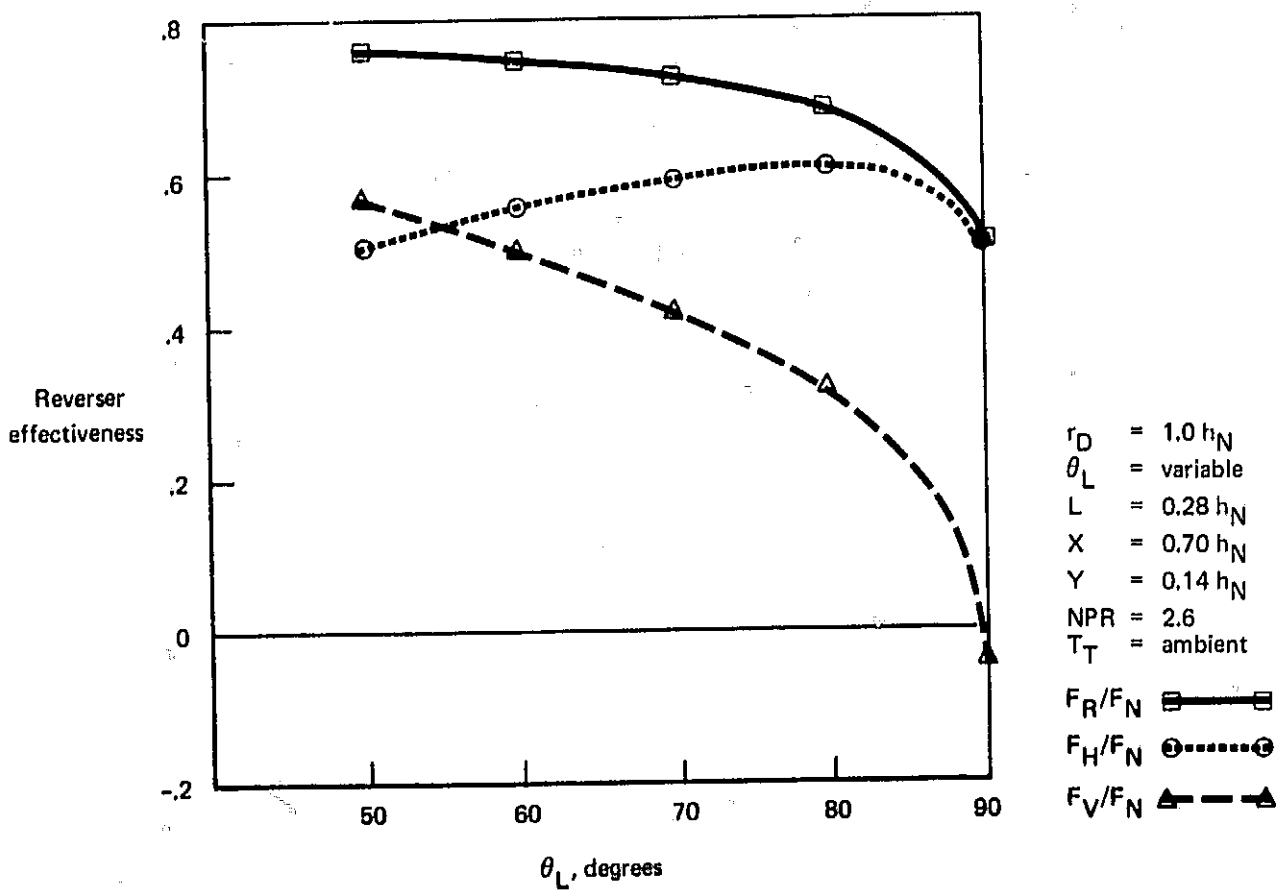

FIGURE 26.–EFFECTS OF DEFLECTOR LIP ANGLE (θ_L) ON REVERSER EFFECTIVENESS FOR A LIP LENGTH EQUAL TO 0.28 h_N (r_D = 1.0 h_N)

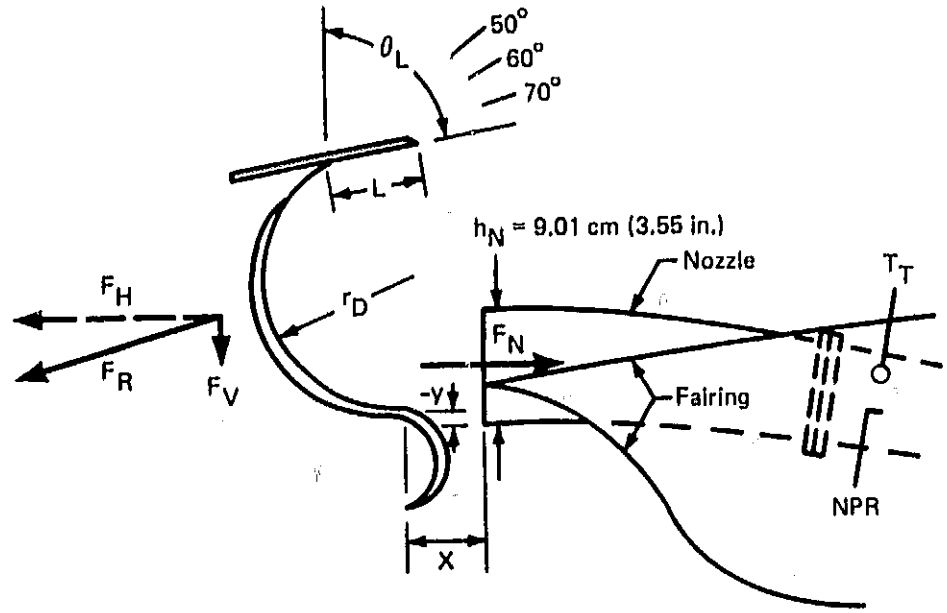

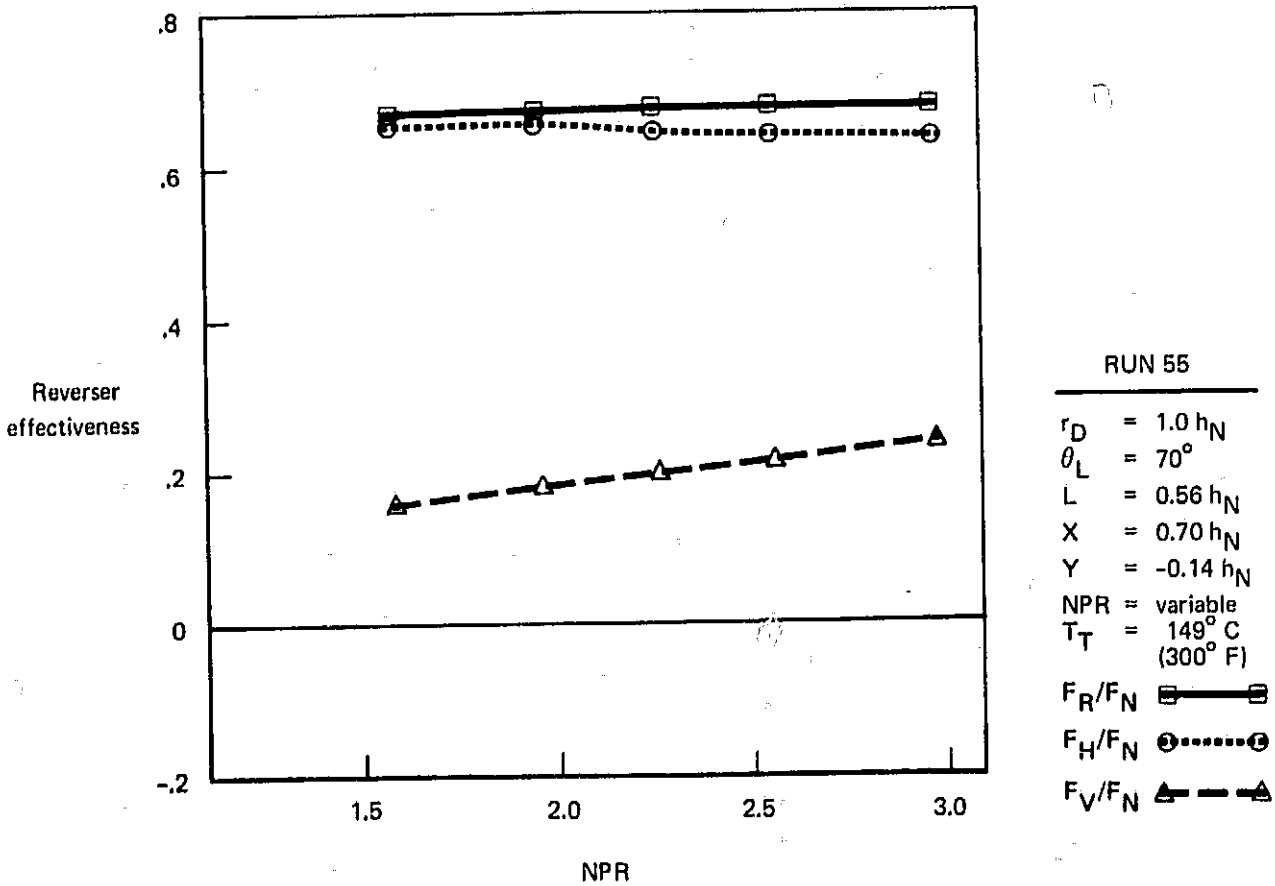

FIGURE 27.–SENSITIVITY OF NOZZLE PRESSURE RATIO ON REVERSER EFFECTIVENESS FOR A LIP ANGLE (θ_L) OF 70° ($r_D = 1.0\ h_N$)

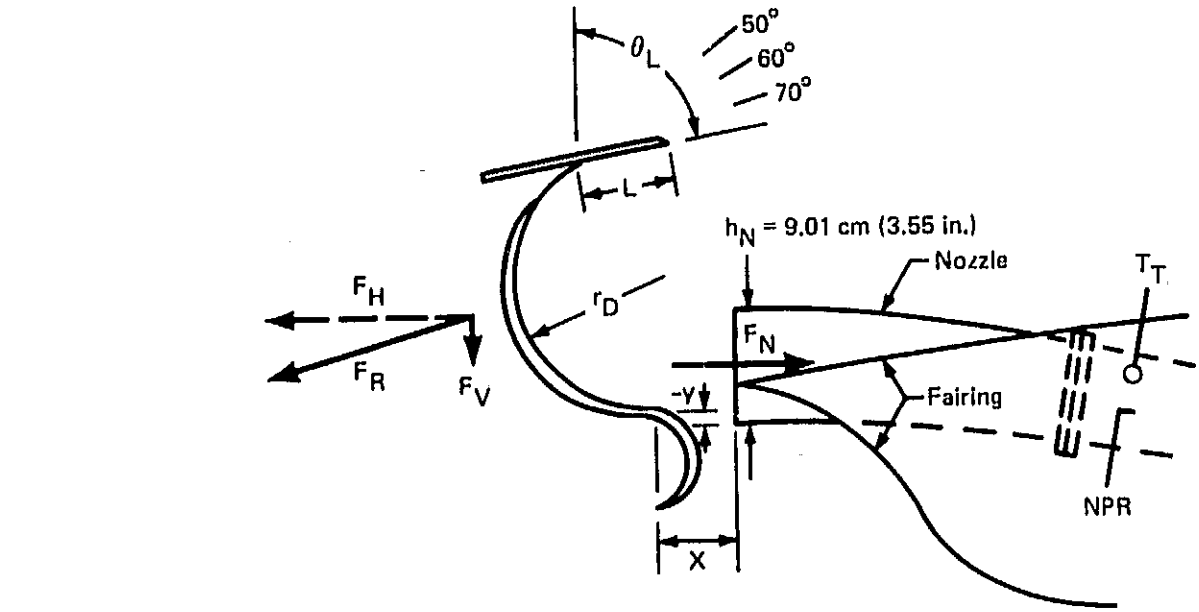

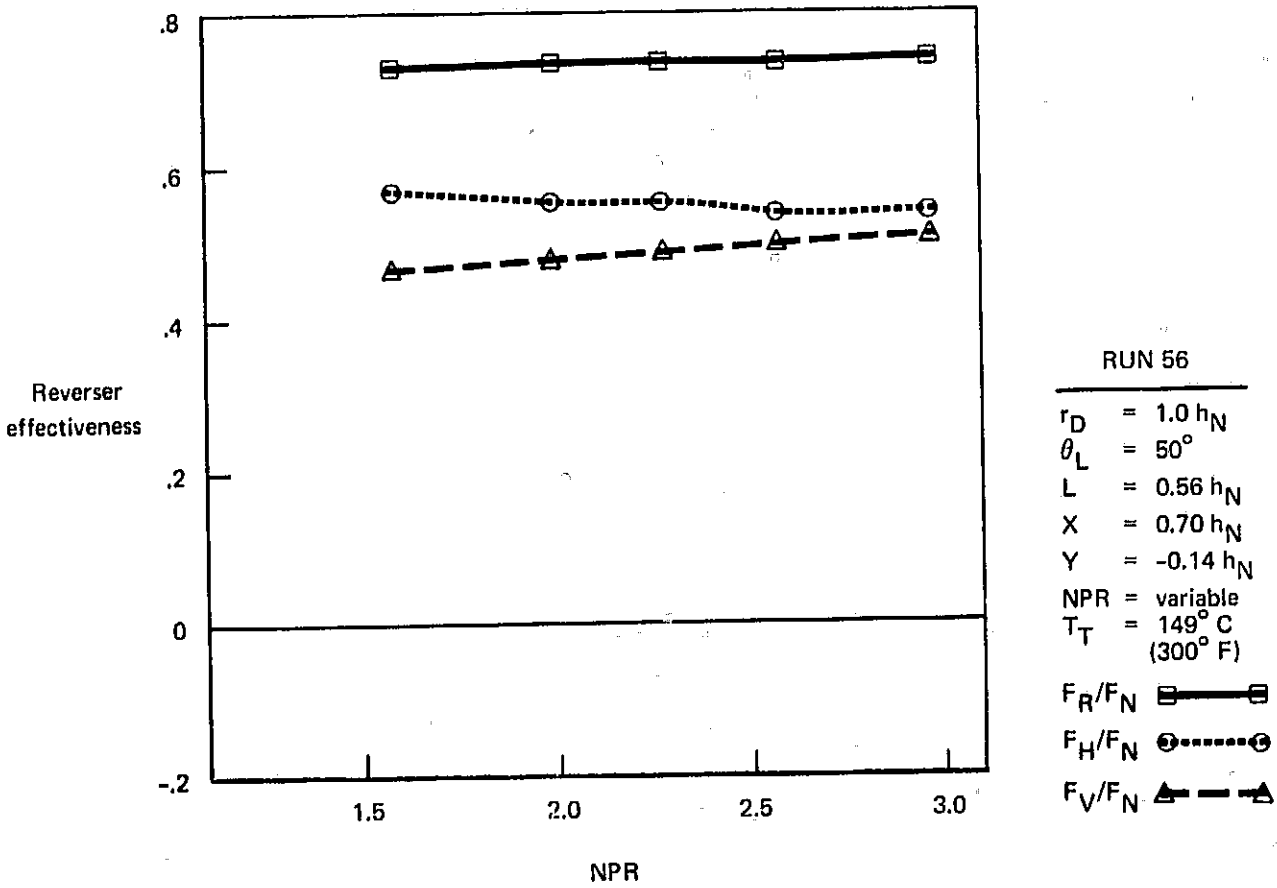

FIGURE 28.–SENSITIVITY OF NOZZLE PRESSURE RATIO ON REVERSER EFFECTIVENESS FOR A LIP ANGLE (θ_L) OF 50° ($r_D = 1.0\ h_N$)

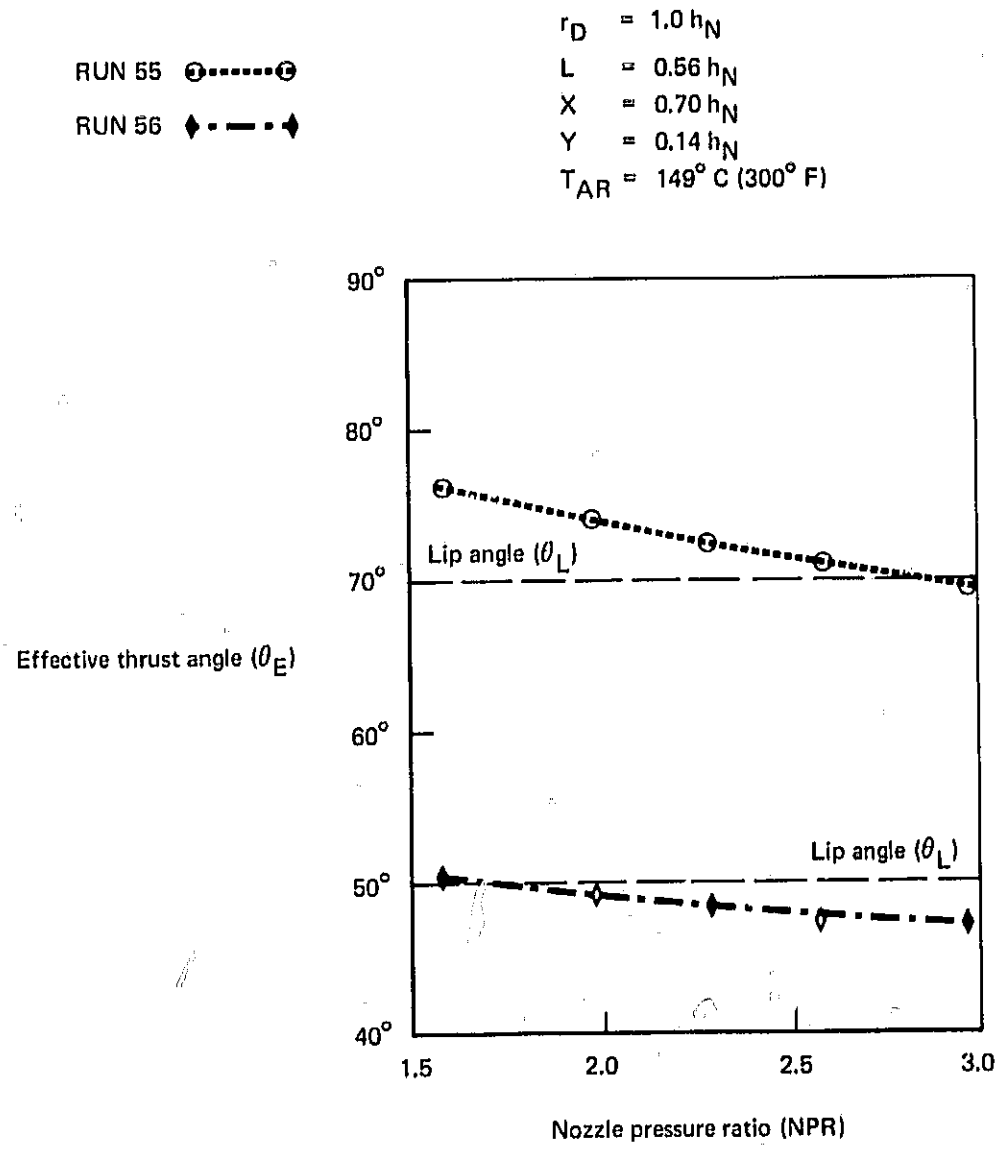

FIGURE 29.–EFFECTIVE REVERSER THRUST ANGLE (θ_E) COMPARED WITH THE GEOMETRIC LIP ANGLE (θ_L) OF 70°, 50° ($r_D = 1.0\ h_N$).

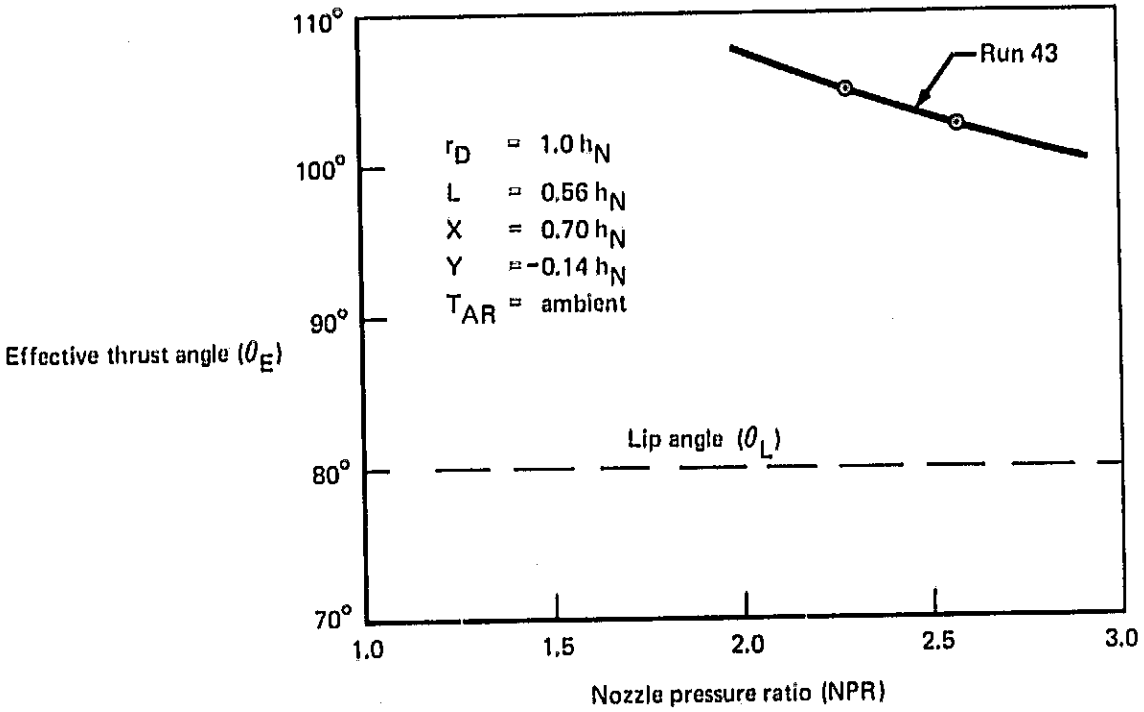

FIGURE 30.—EFFECTIVE REVERSE THRUST ANGLE (θ_E) COMPARED WITH THE GEOMETRIC LIP ANGLE (θ_L) OF 80° (r_D = 1.0 h_N)

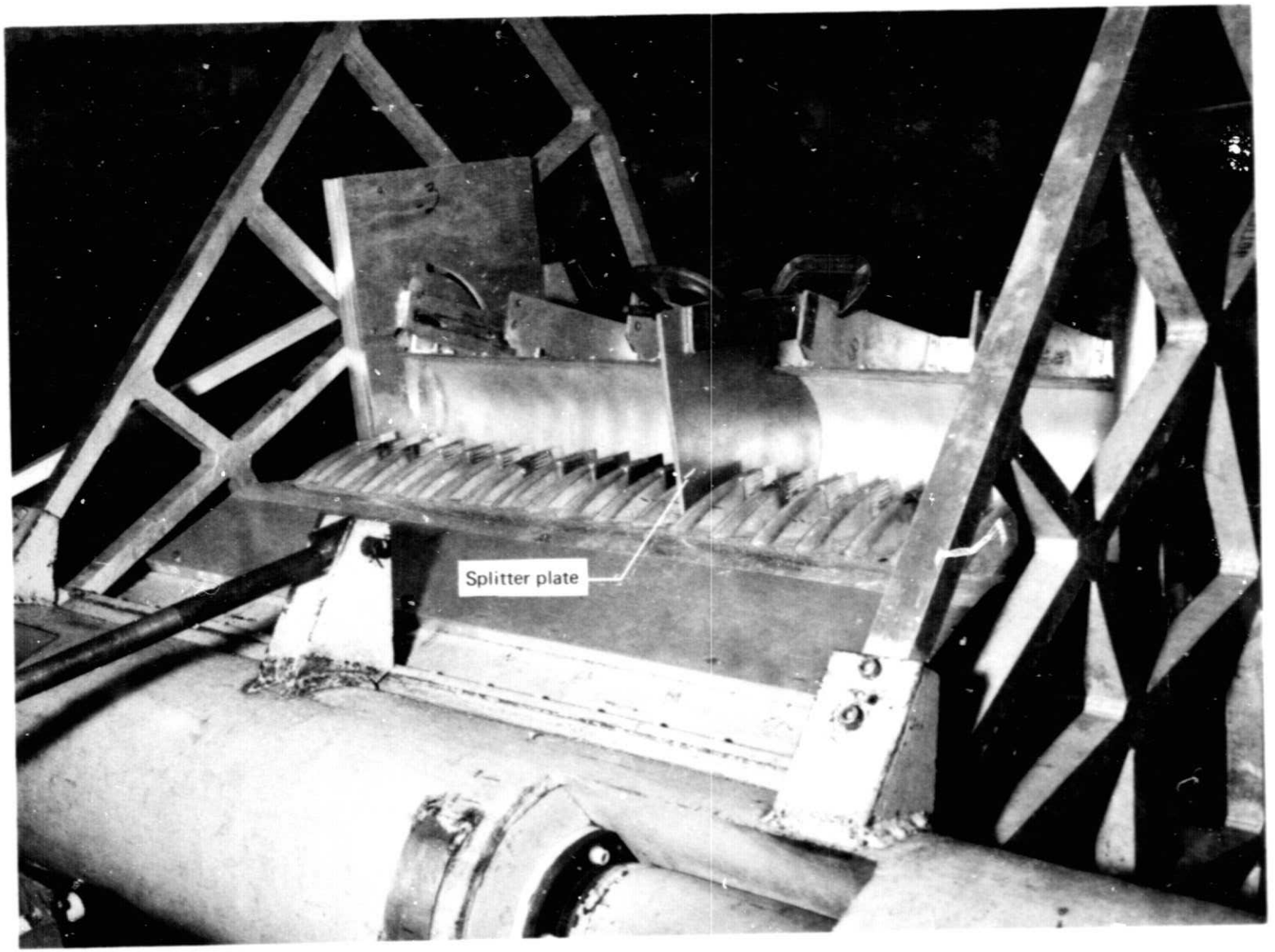

FIGURE 31.–THRUST REVERSER MODEL WITH SPLITTER PLATE INSTALLATION

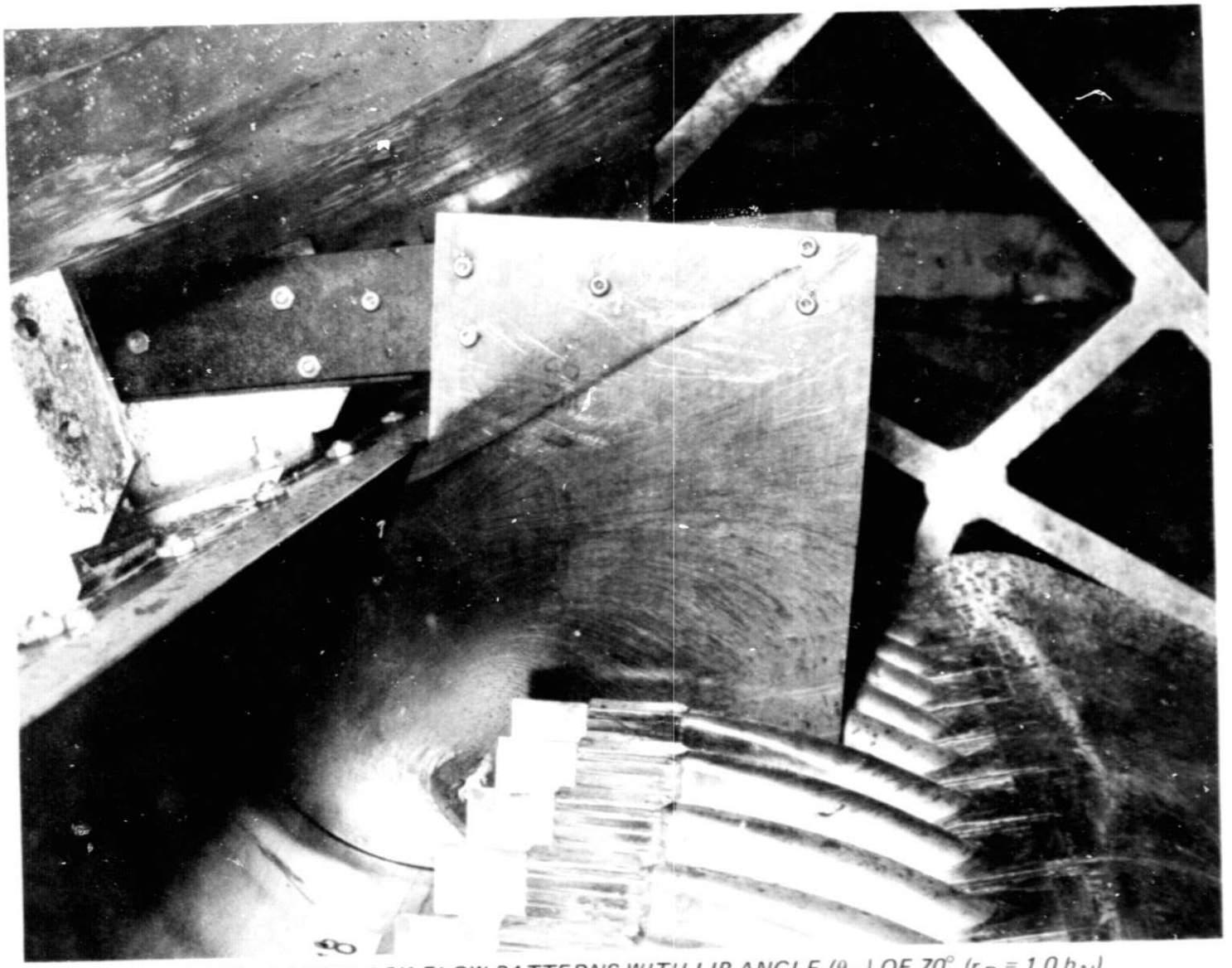

FIGURE 32.—LAMPBLACK FLOW PATTERNS WITH LIP ANGLE (θ_L) OF 70° ($r_D = 1.0\, h_N$), SIDE VIEW

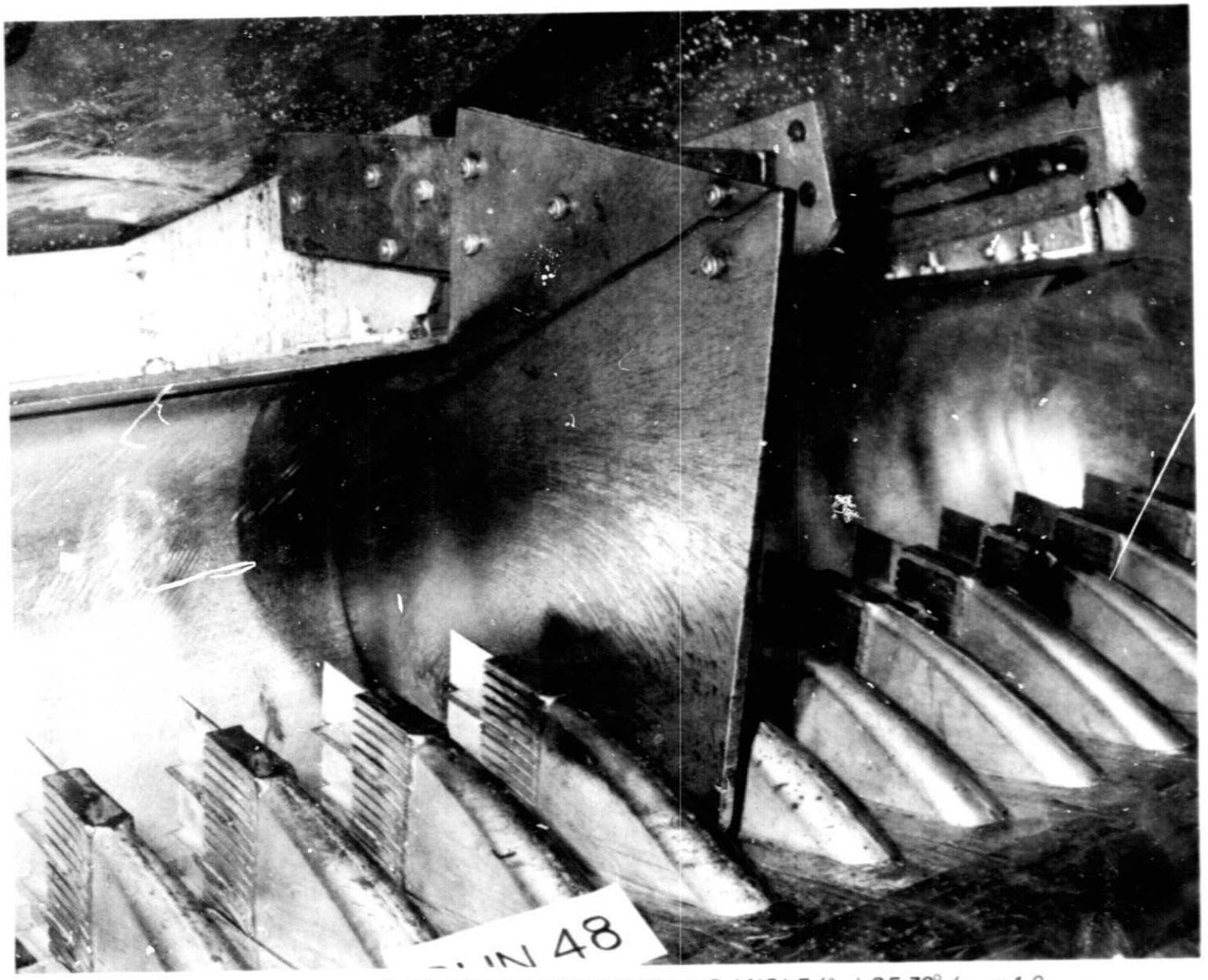

FIGURE 33.—LAMPBLACK FLOW PATTERNS WITH LIP ANGLE (θ_L) OF 70° (r_D = 1.0 IN), 3/4 FRONT VIEW

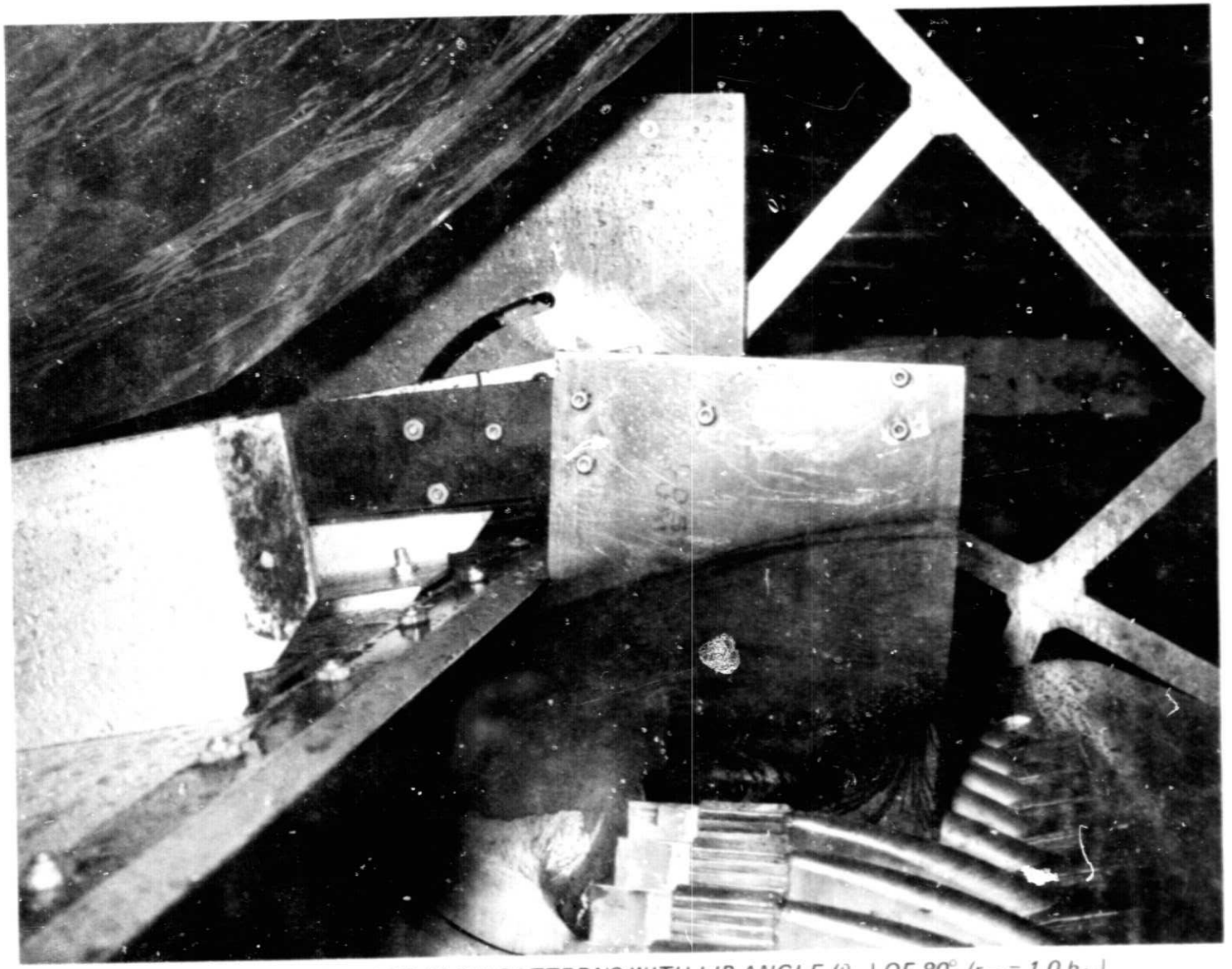

FIGURE 34.—LAMPBLACK FLOW PATTERNS WITH LIP ANGLE (θ_L) OF 80° ($r_D = 1.0\ h_N$)

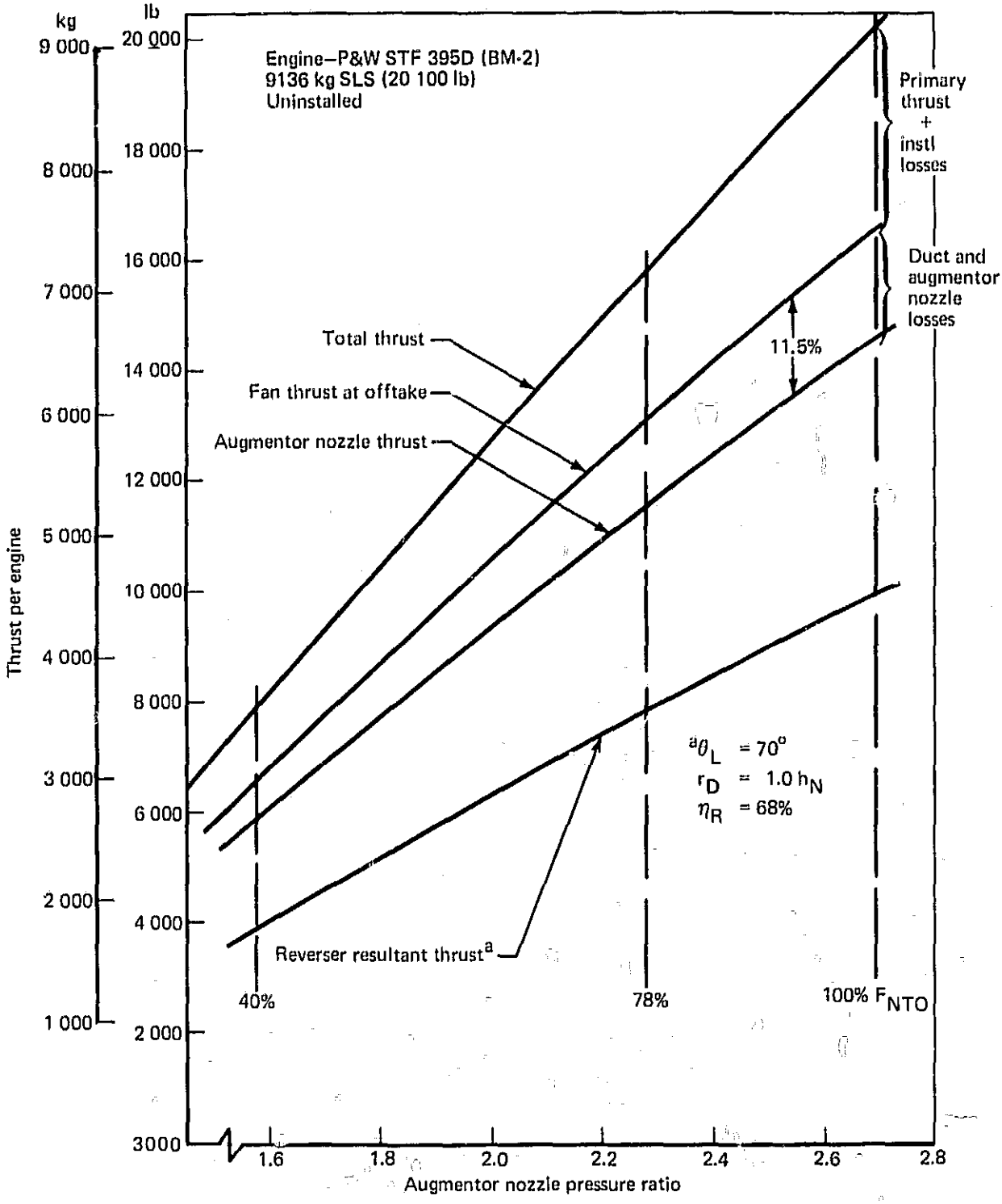

FIGURE 35.–BREAKDOWN OF THE AVAILABLE THRUST LEVELS FROM THE ENGINE STATION TO THE THRUST REVERSER

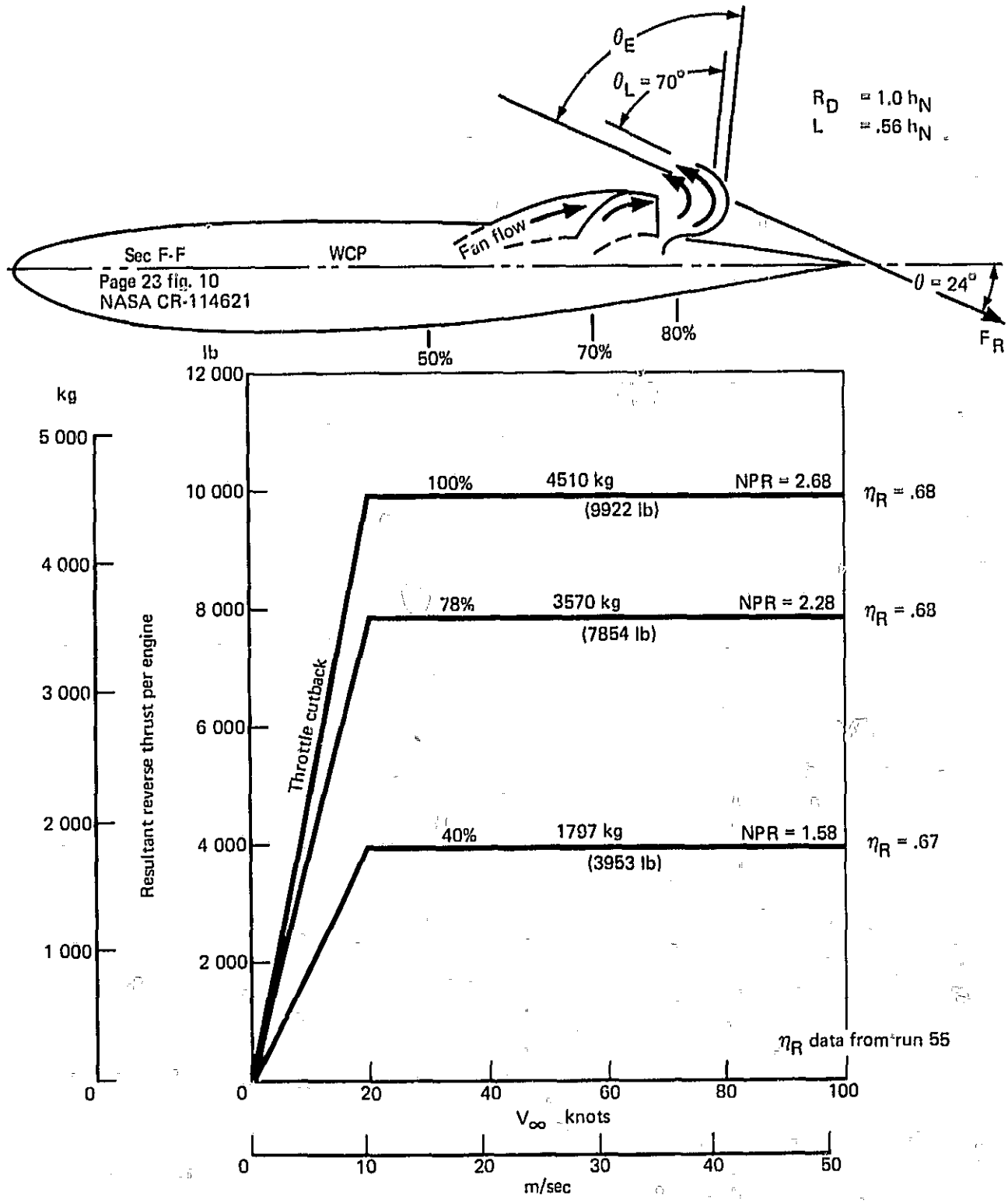

FIGURE 36.–AVAILABLE RESULTANT REVERSER THRUST AT THREE ENGINE POWER SETTINGS

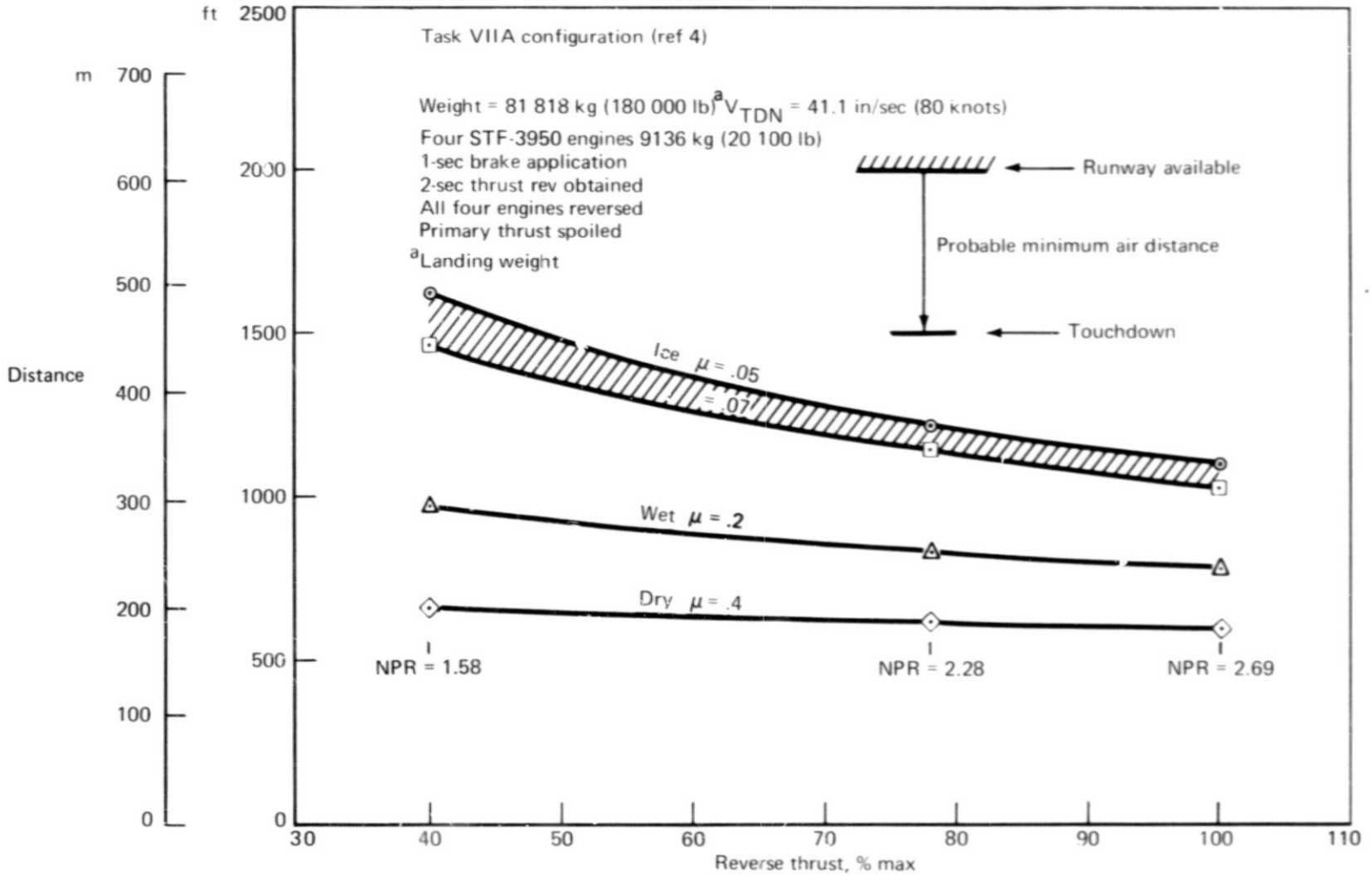

FIGURE 37.–EFFECT OF ENGINE POWER SETTING ON AUGMENTOR WING AIRPLANE STOPPING DISTANCE FOR DRY, WET, AND ICY RUNWAYS

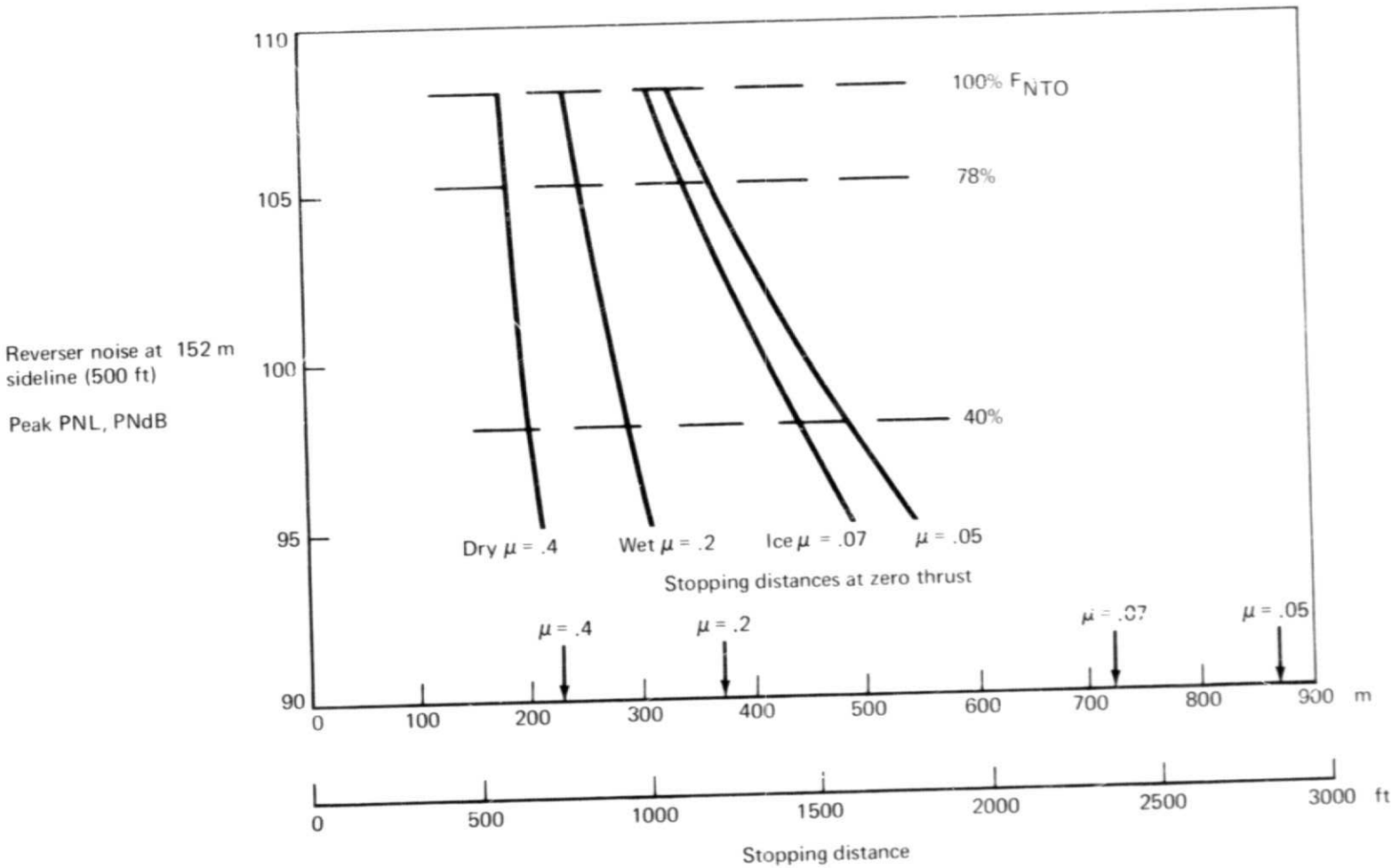

FIGURE 38.–RELATION OF ENGINE POWER SETTING AND THRUST REVERSER NOISE TO AIRPLANE STOPPING DISTANCE FOR DRY, WET, AND ICY RUNWAYS

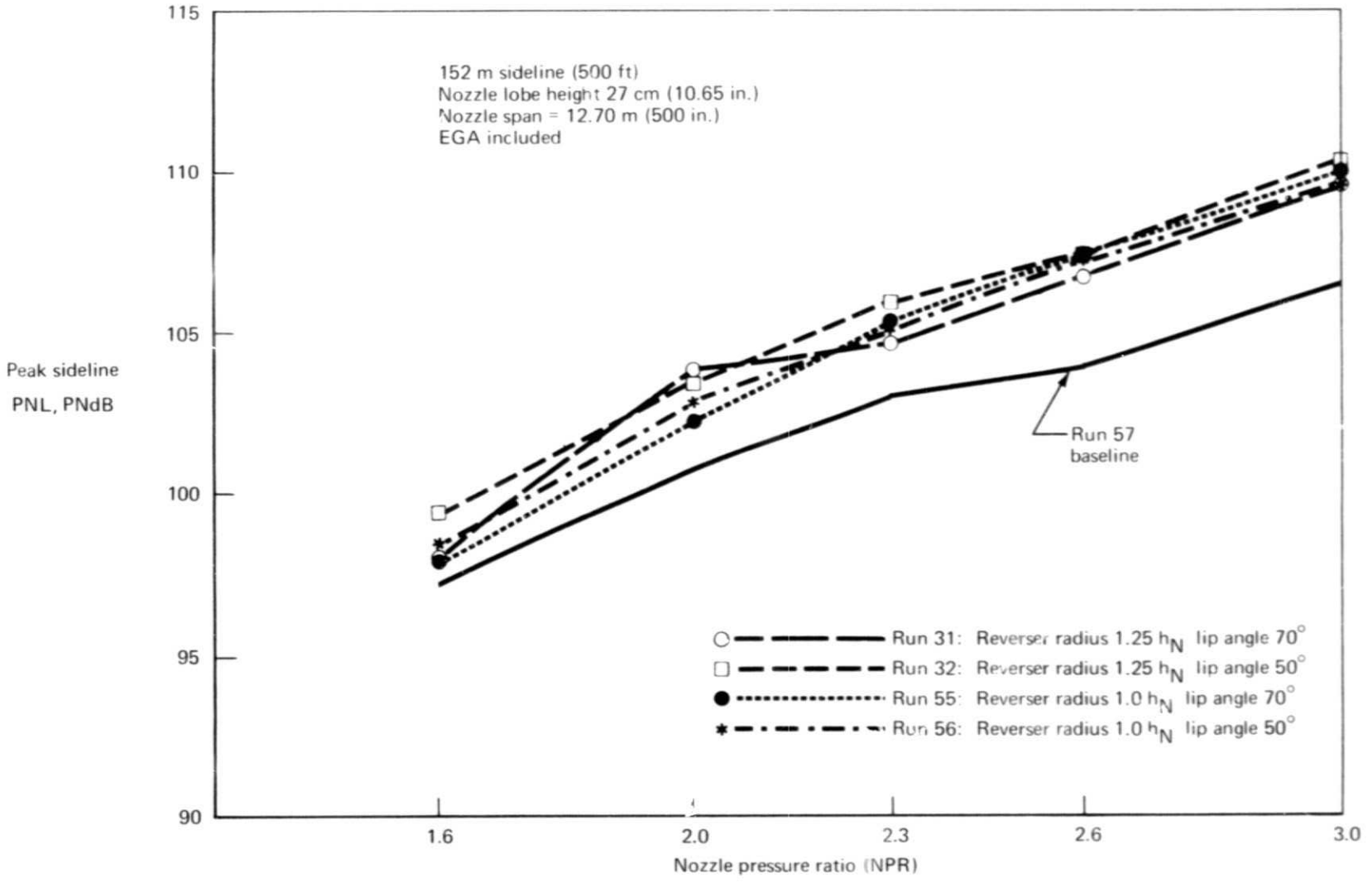

FIGURE 39.–EFFECT OF AUGMENTOR NOZZLE PRESSURE RATIO AND REVERSER DEFLECTOR LIP ANGLE ON PEAK PNL NOISE LEVELS AT 152 M SIDELINE (500 FT) WITH EGA

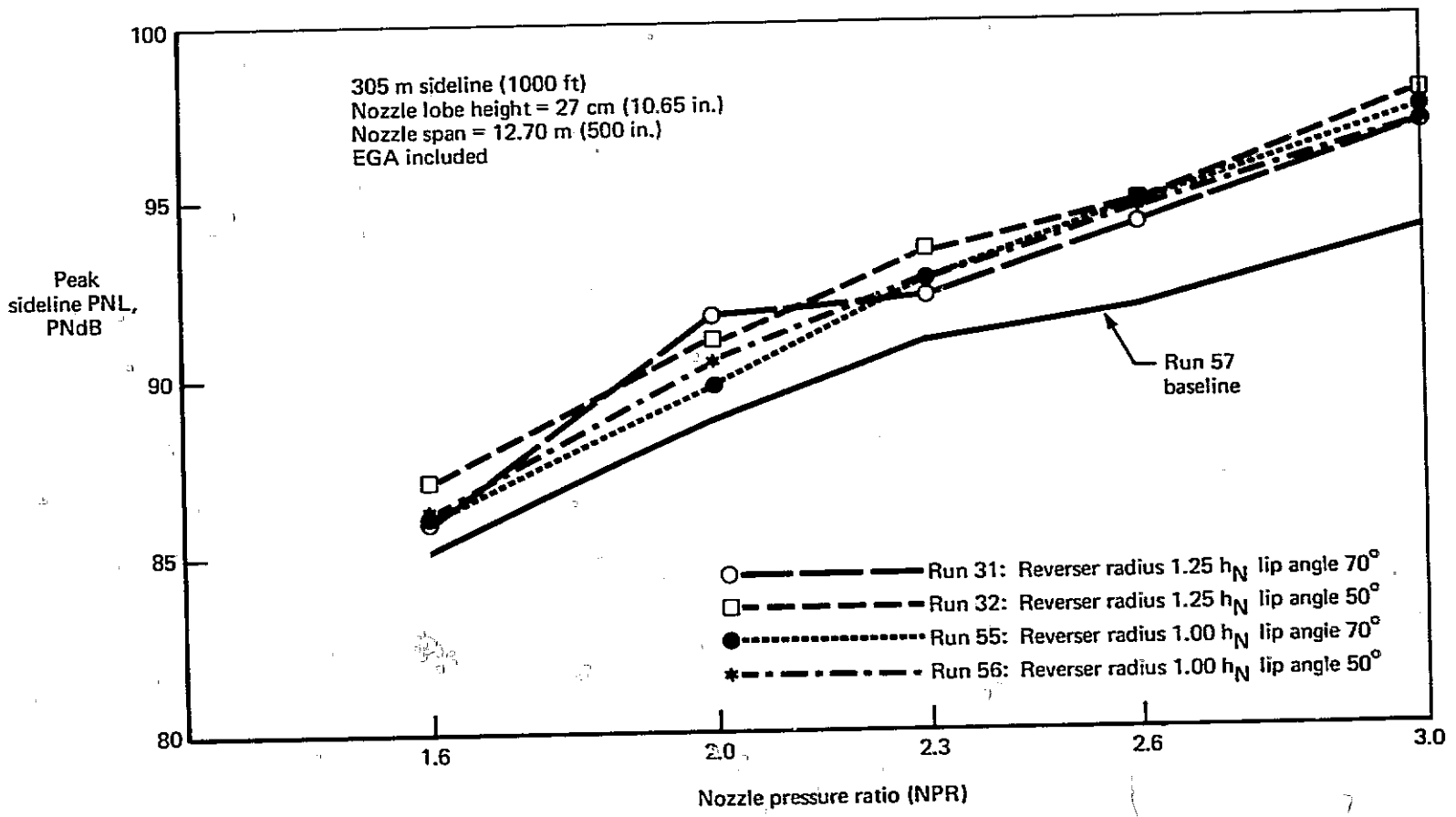

FIGURE 40.—THE EFFECT OF AUGMENTOR NOZZLE PRESSURE RATIO AND REVERSER DEFLECTOR LIP ANGLE ON PEAK PNL NOISE LEVELS AT 305 M SIDELINE (1000 FT) WITH EGA

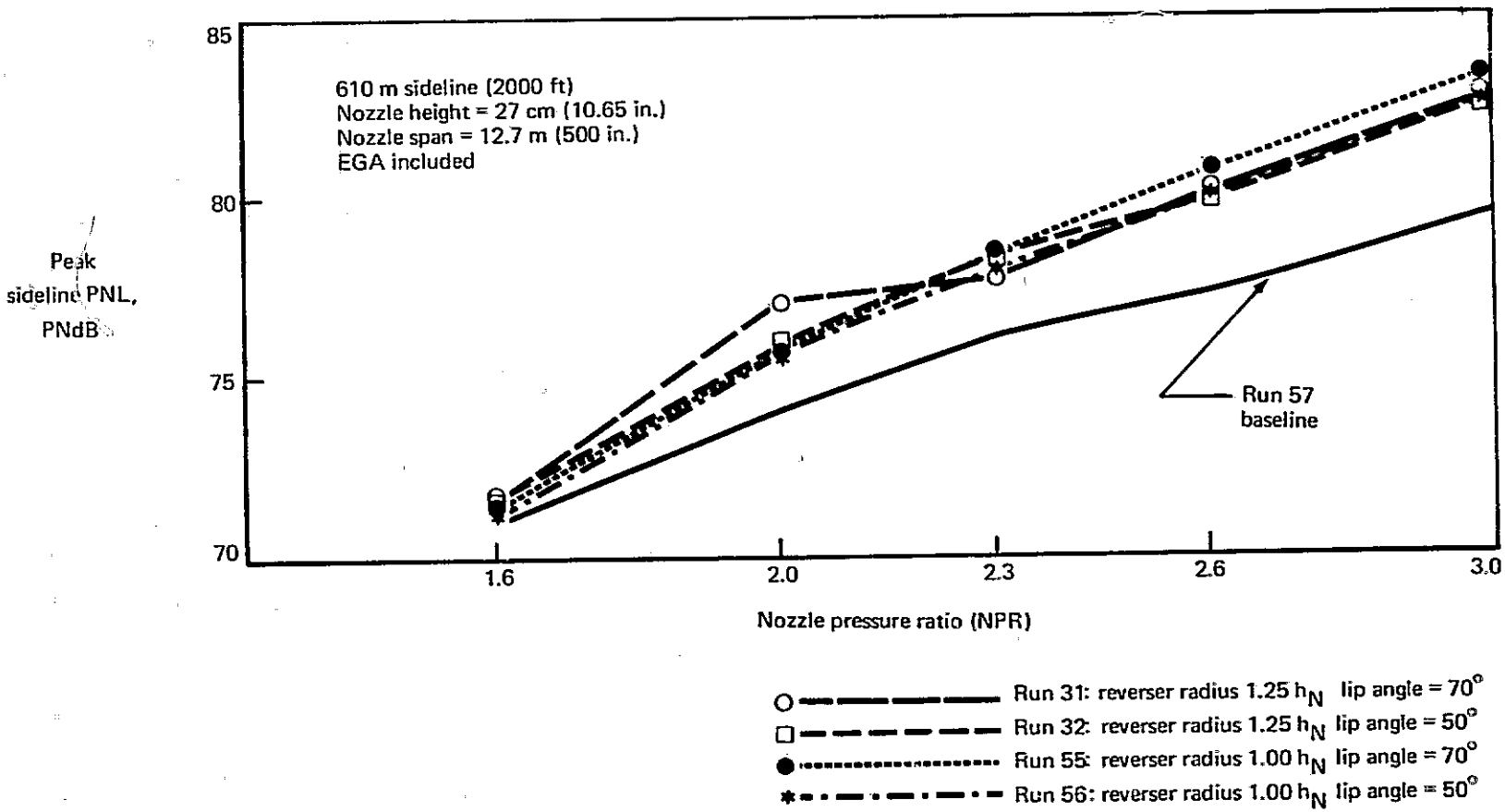

FIGURE 41.—THE EFFECT OF AUGMENTOR NOZZLE PRESSURE RATIO AND REVERSER DEFLECTOR LIP ANGLE ON PEAK PNL NOISE LEVELS AT 610 M SIDELINE (2000 FT) WITH EGA

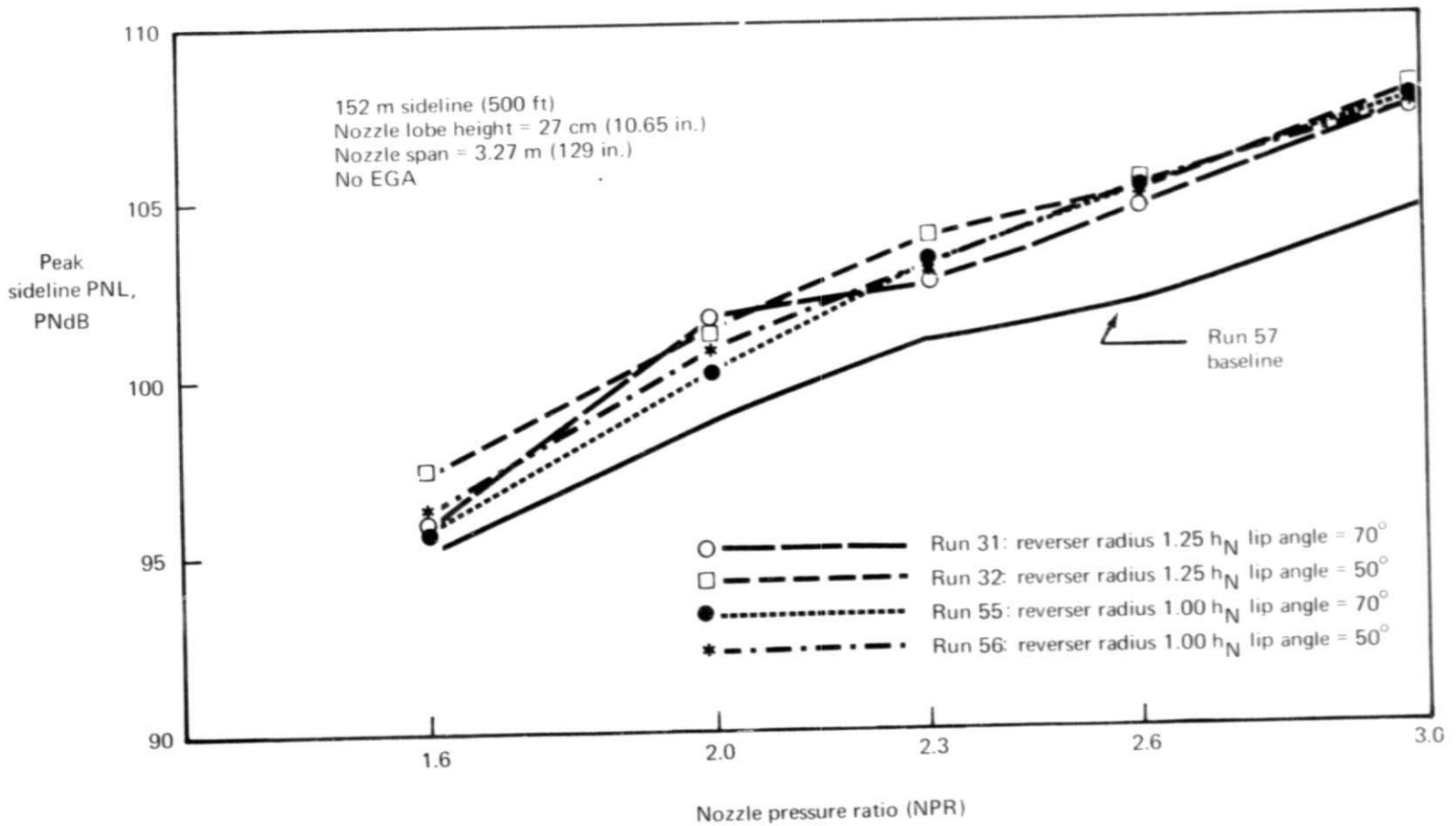

FIGURE 42.–EFFECT OF AUGMENTOR NOZZLE PRESSURE RATIO AND REVERSER DEFLECTOR LIP ANGLE ON PEAK PNL NOISE LEVELS AT 152 M SIDELINE (500 FT) WITHOUT EGA

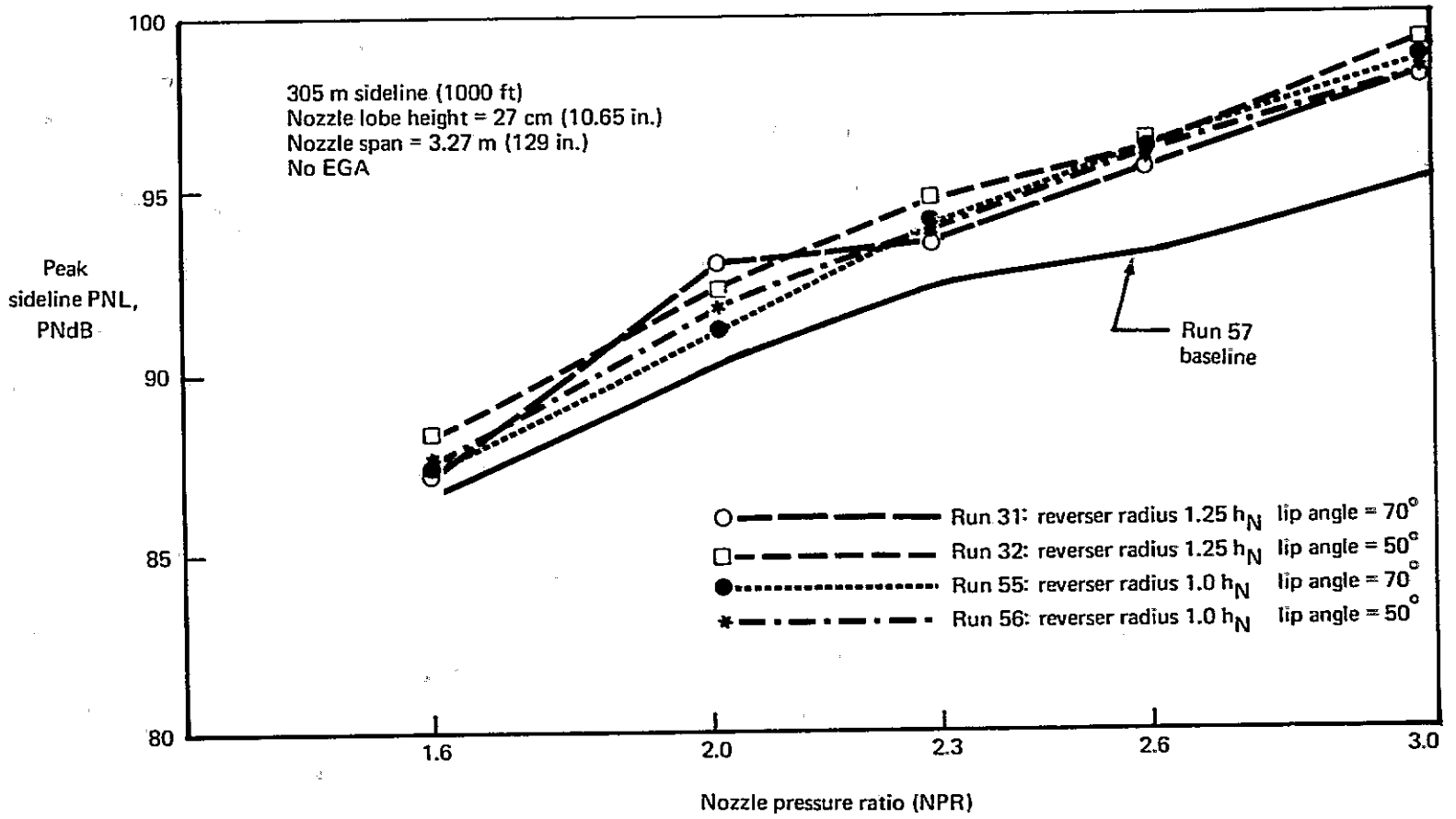

FIGURE 43.—EFFECT OF AUGMENTOR NOZZLE PRESSURE RATIO AND REVERSER DEFLECTOR LIP ANGLE ON PEAK PNL NOISE LEVEL AT 305 M SIDELINE (1000 FT) WITHOUT EGA

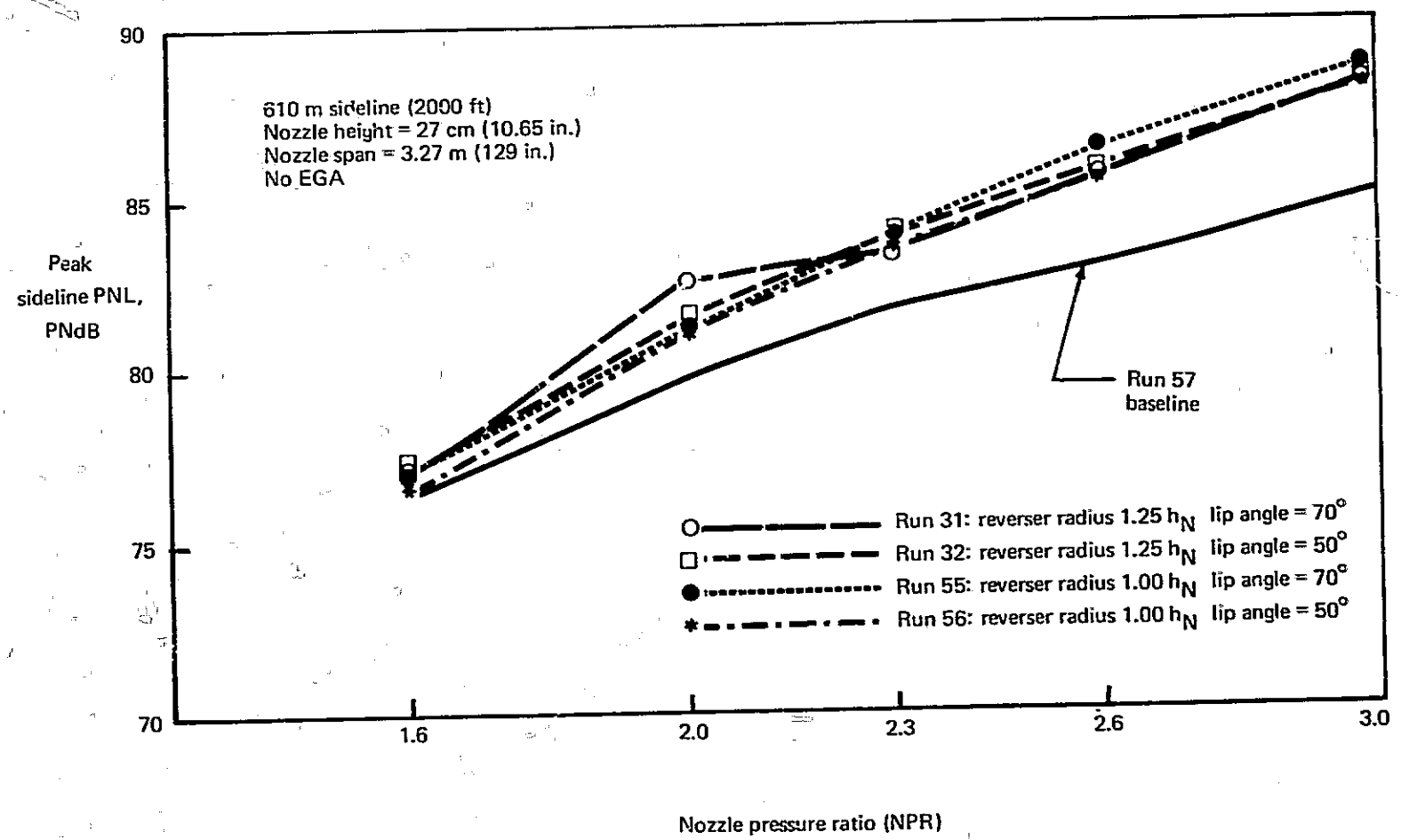

FIGURE 44.—EFFECT OF AUGMENTOR NOZZLE PRESSURE RATIO AND REVERSER DEFLECTOR LIP ANGLE ON PEAK PNL NOISE LEVELS AT 610 M SIDELINE (2000 FT) WITHOUT EGA

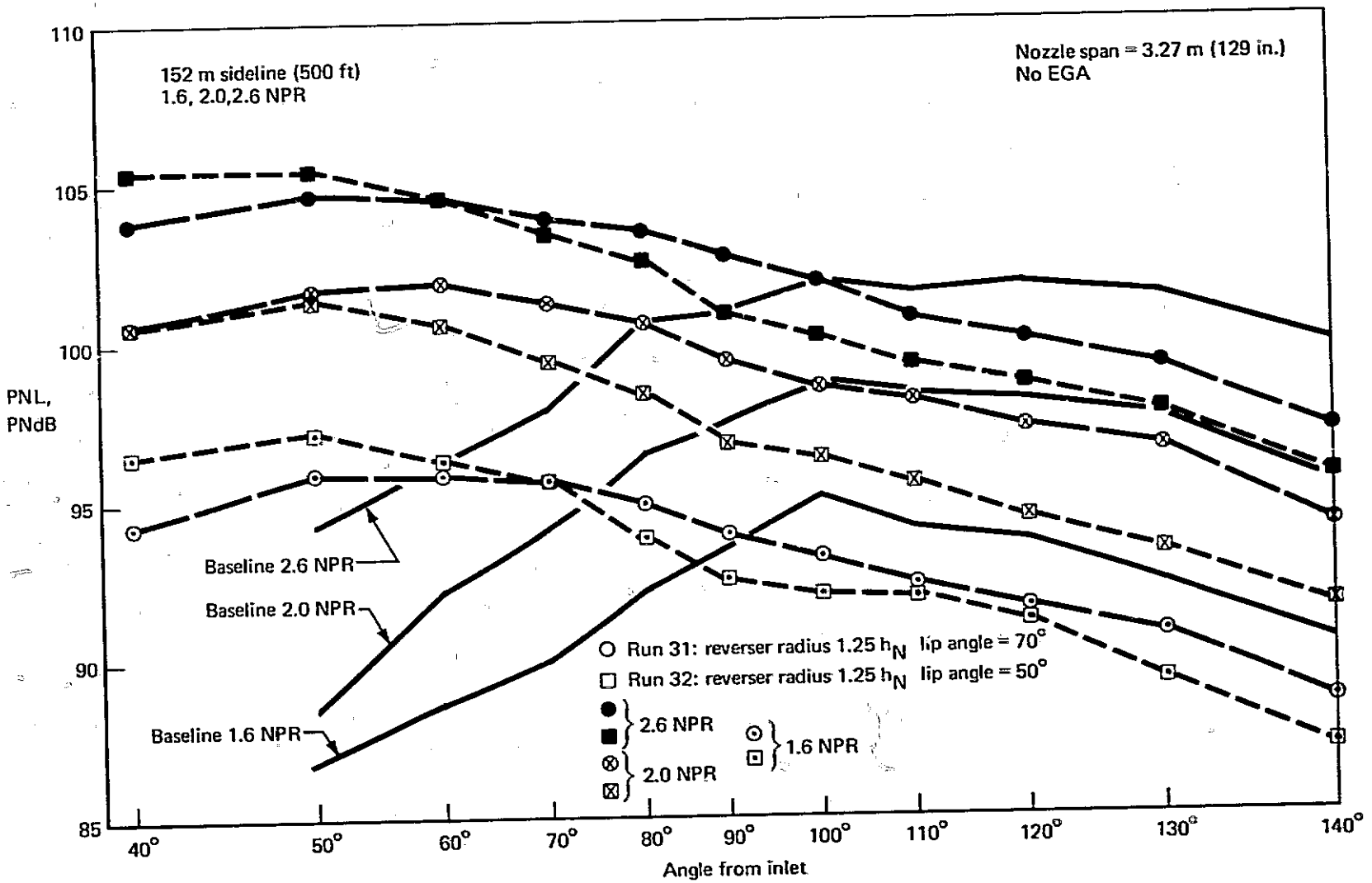

FIGURE 45.–PNL VS MICROPHONE ANGLE, 152 M SIDELINE (500 FT), $r_D = 1.25\ h_N$, NPR = 1.6, 2.0, 2.6

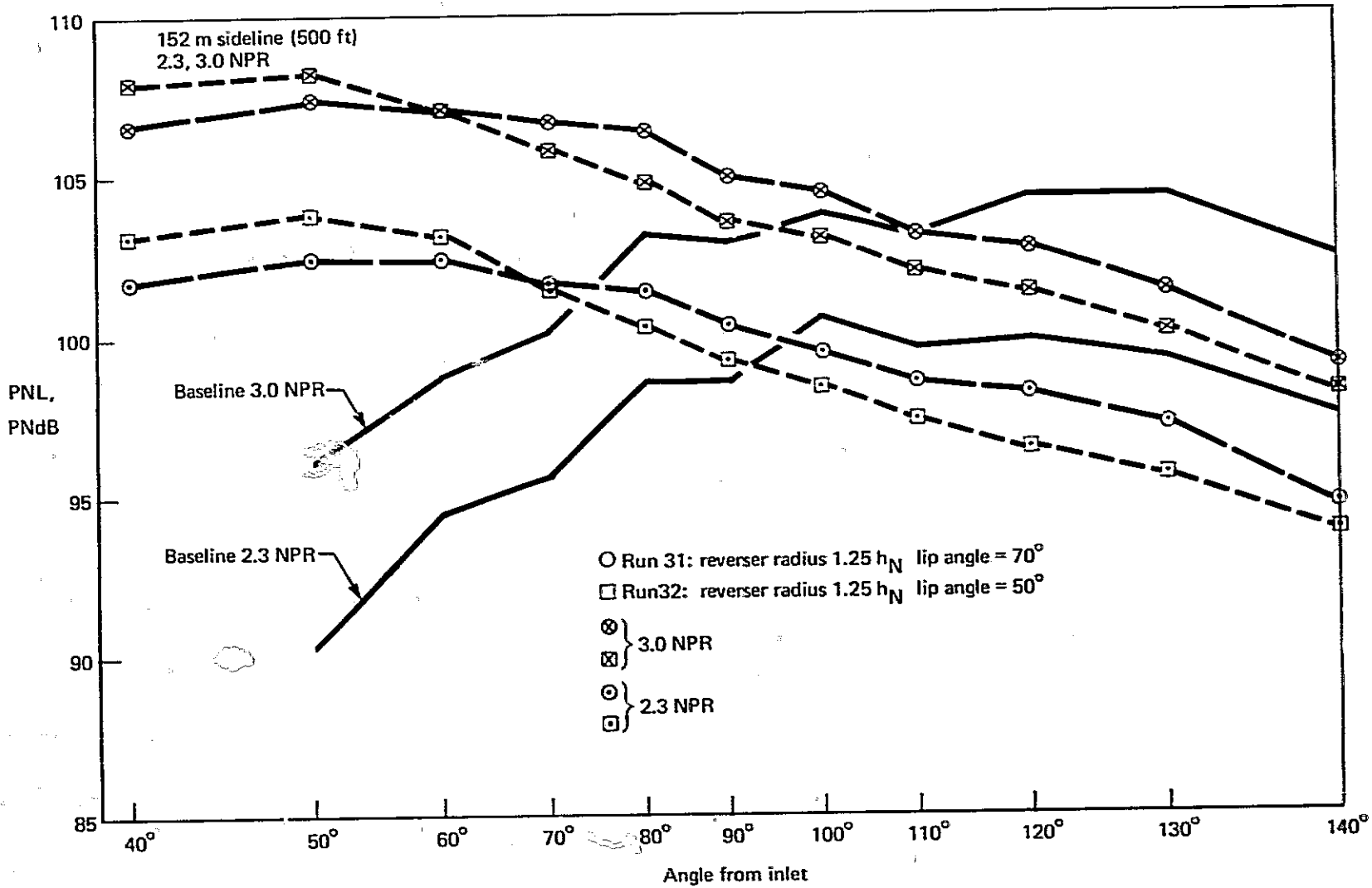

FIGURE 46.—PNL VS MICROPHONE ANGLE, 152 M SIDELINE (500 FT), $r_D = 1.25\ h_N$, NPR = 2.3, 3.0

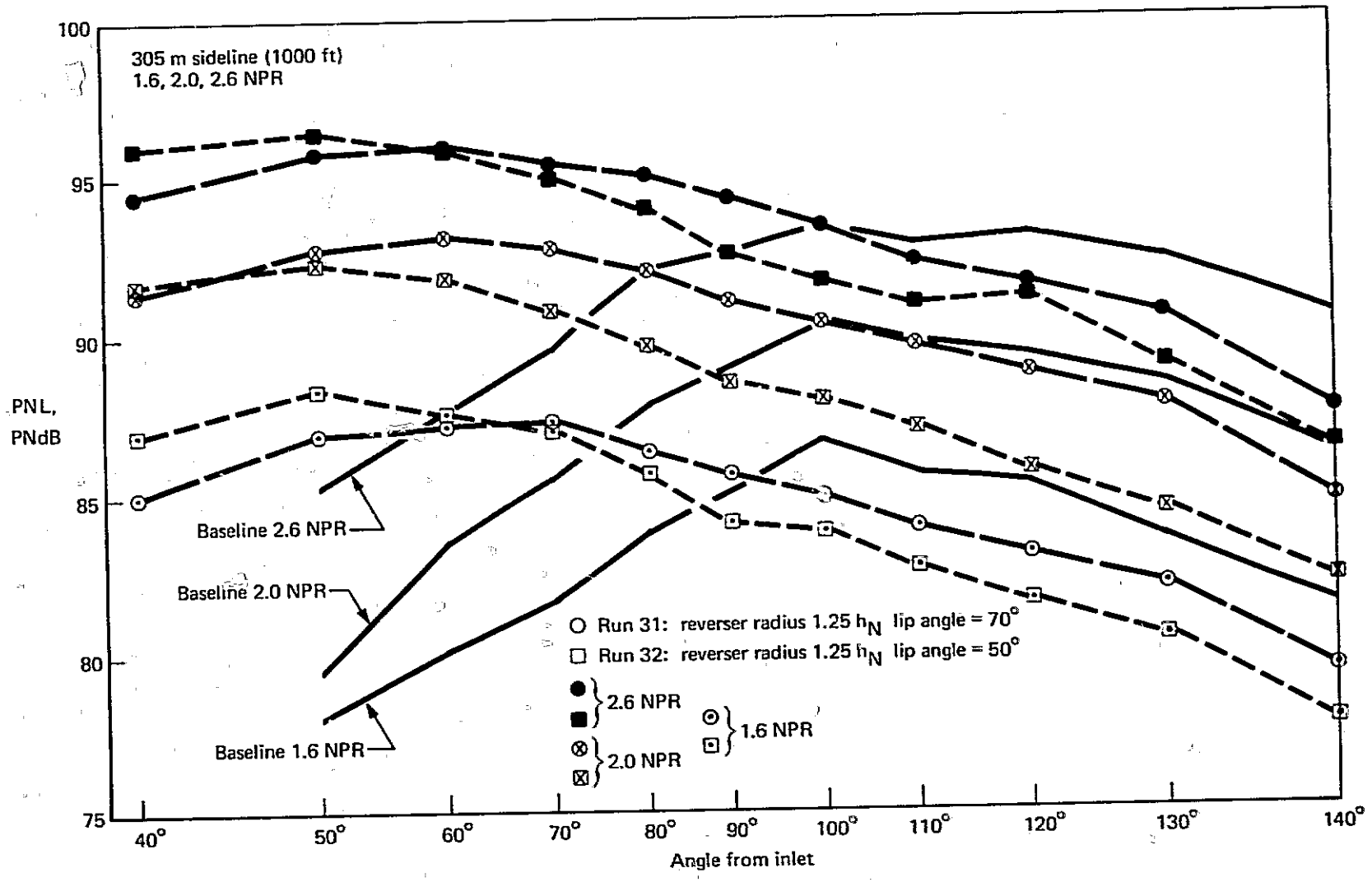

FIGURE 47.—PNL VS MICROPHONE ANGLE, 305 M SIDELINE (1000 FT), $r_D = 1.25\ h_N$, NPR = 1.6, 2.0, 2.6

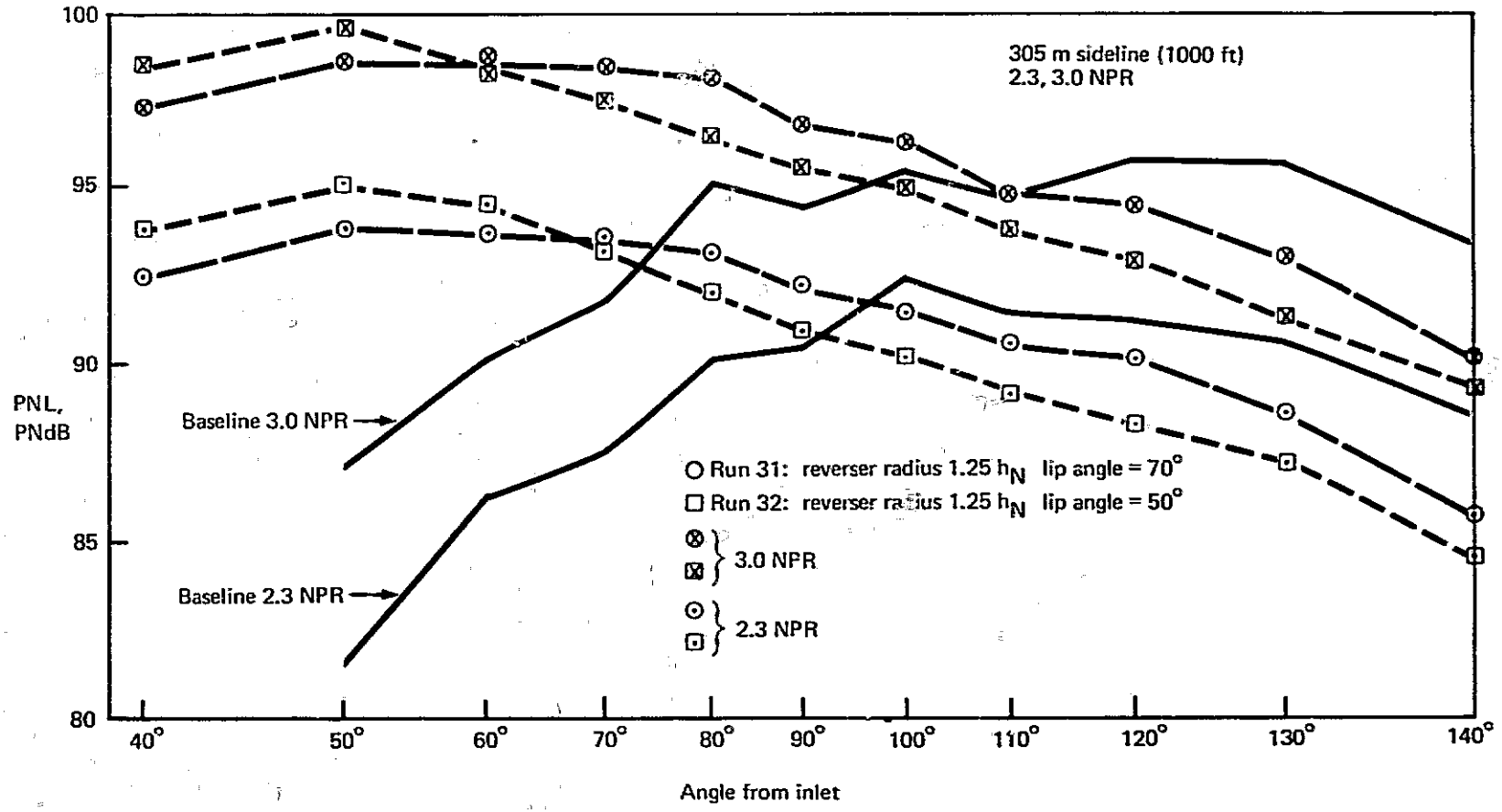

FIGURE 48.—PNL VS MICROPHONE ANGLE, 305 M SIDELINE (1000 FT), $r_D = 1.25\ h_N$, NPR = 2.3, 3.0

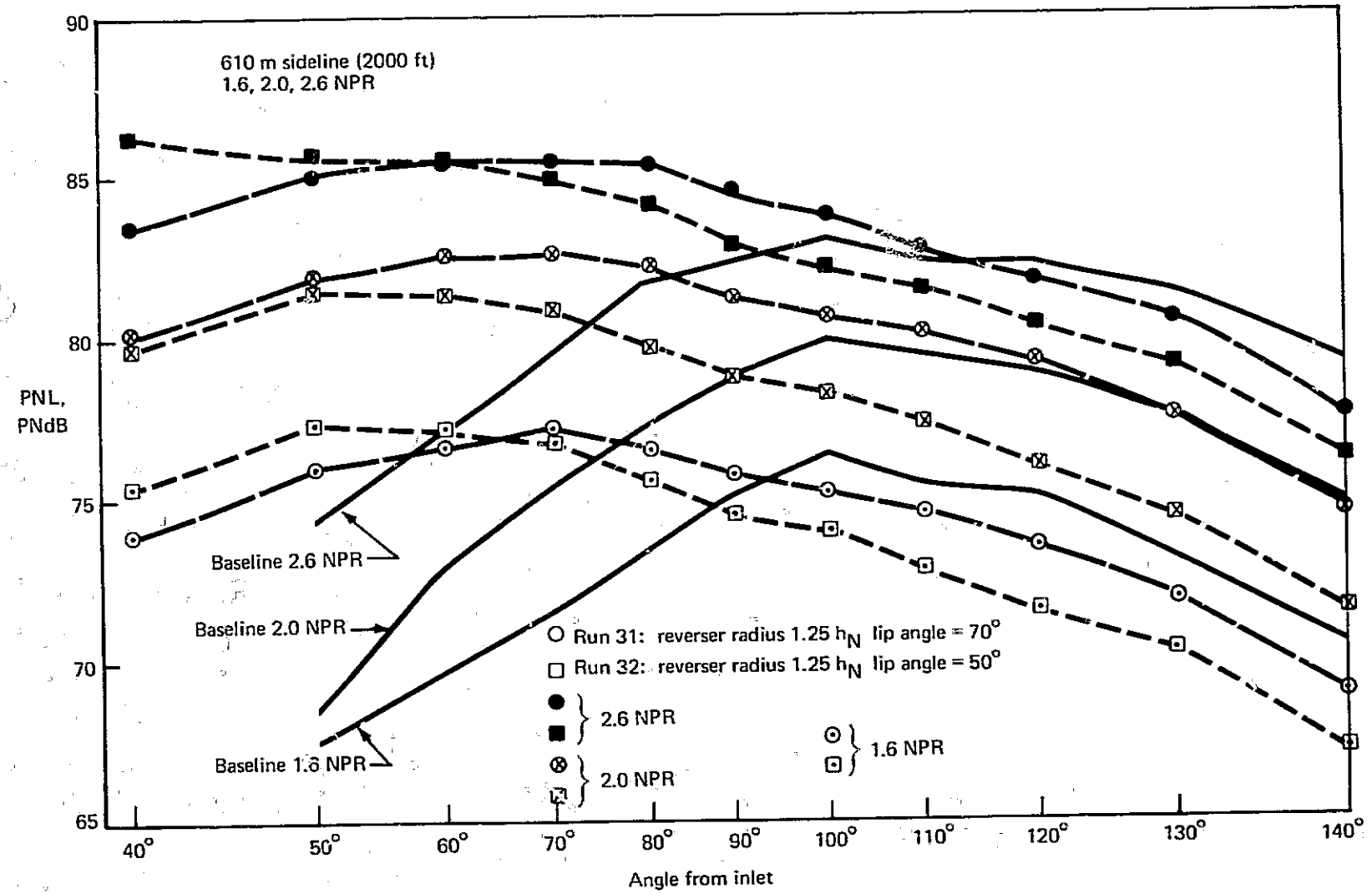

FIGURE 49.–PNL VS MICROPHONE ANGLE, 610 M SIDELINE (2000 FT), $r_D = 1.25\ h_N$, NPR = 1.6, 2.0, 2.6

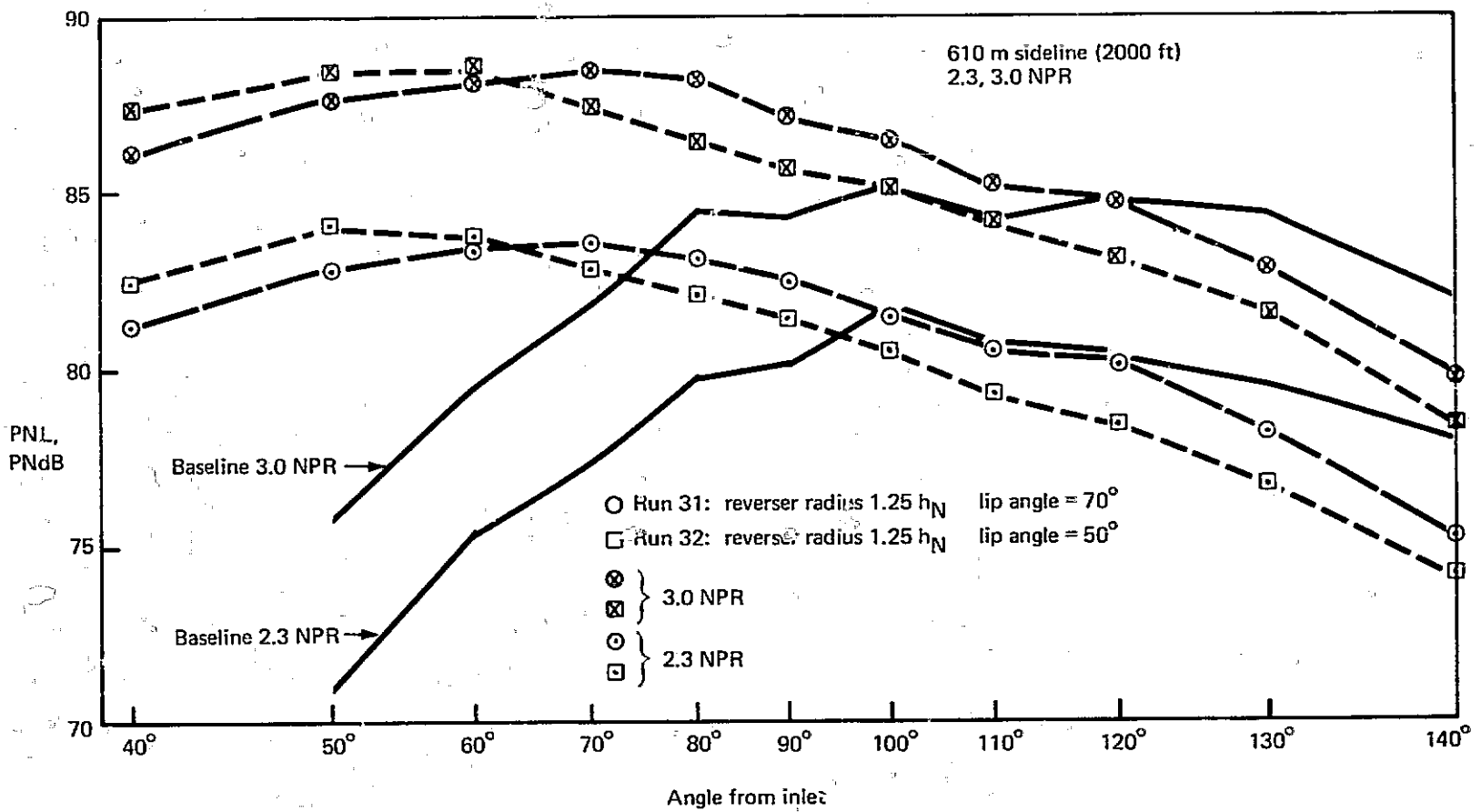

FIGURE 50.—PNL VS MICROPHONE ANGLE, 610 M SIDELINE (2000 FT), $r_D = 1.25\ h_N$, NPR = 2.3, 3.0

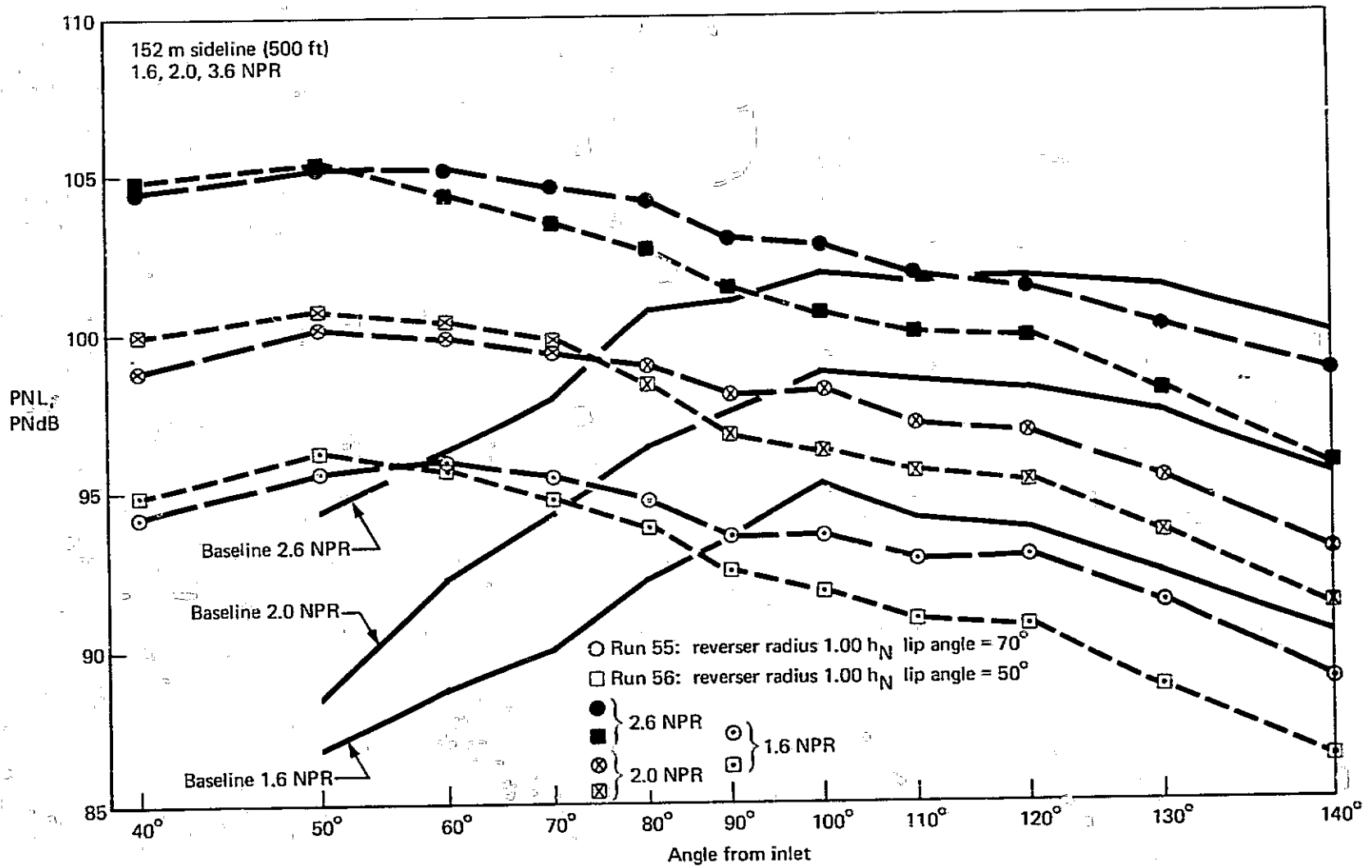

FIGURE 51.—PNL VS MICROPHONE ANGLE, 152 M SIDELINE (500 FT), $r_D = 1.0\ h_N$, NPR = 1.6, 2.0, 2.6

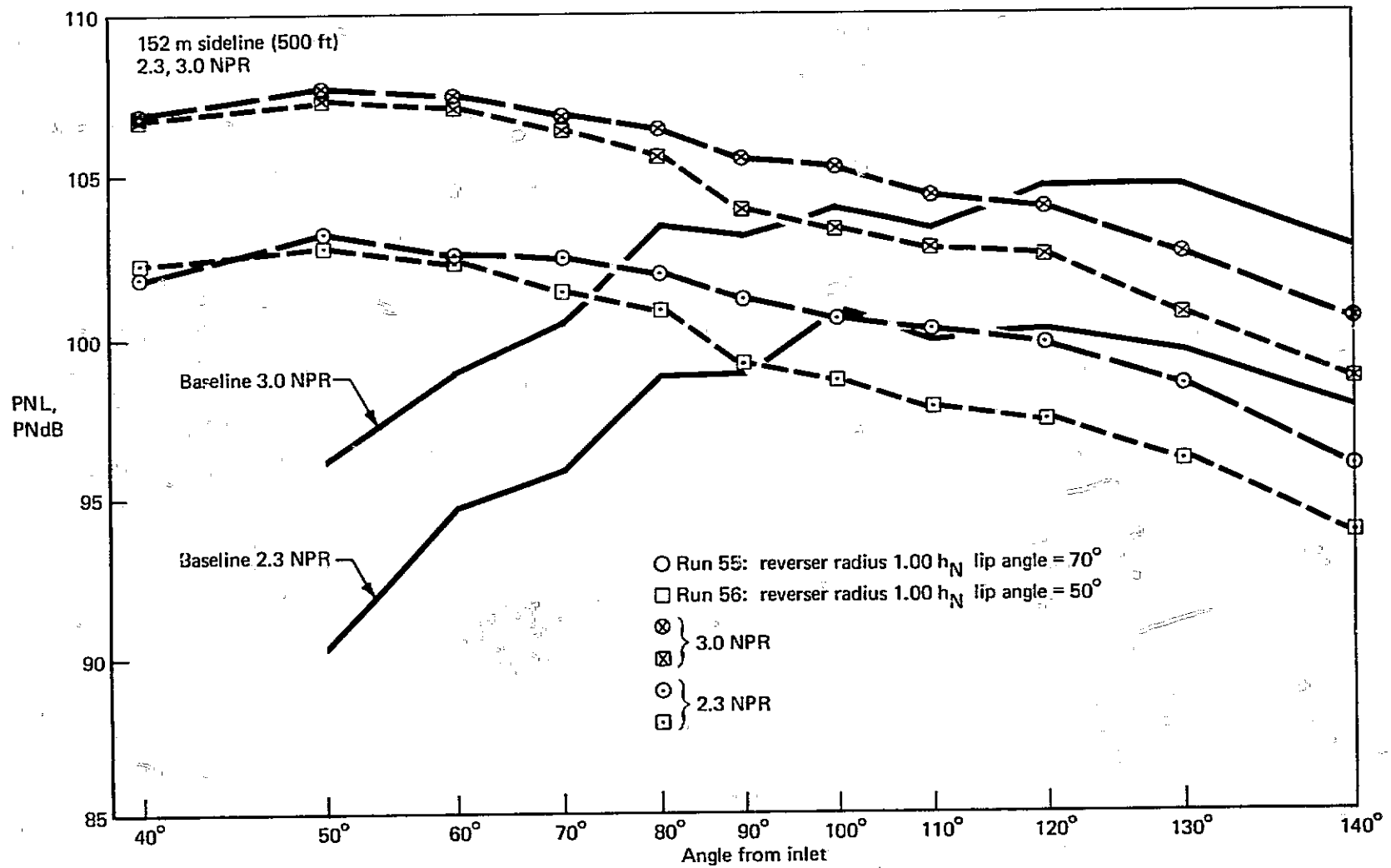

FIGURE 52.–PNL VS MICROPHONE ANGLE, 152 M SIDELINE (500 FT), $r_D = 1.0\ h_N$, NPR = 2.3, 3.0

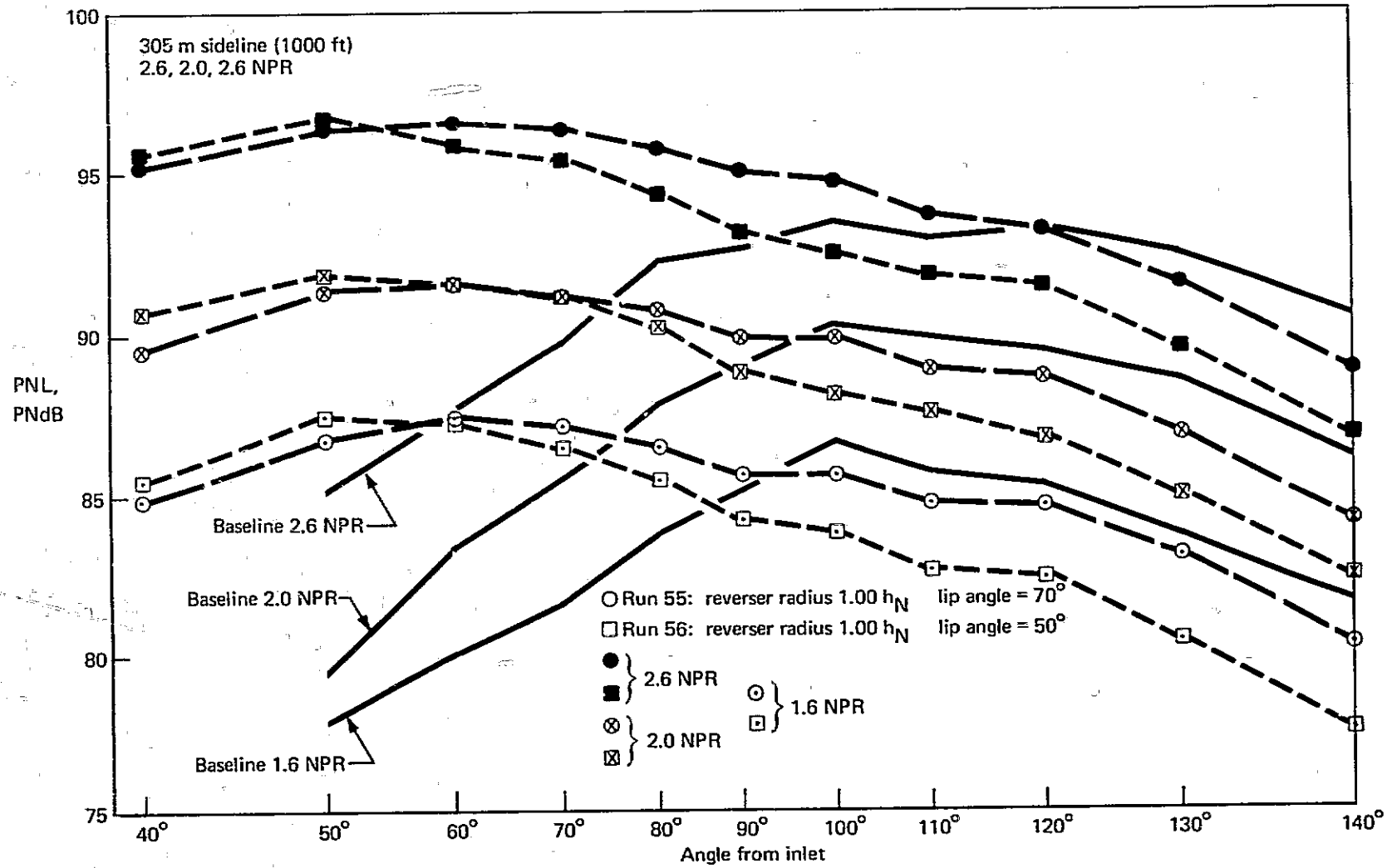

FIGURE 53.–PNL VS MICROPHONE ANGLE, 305 M SIDELINE (1000 FT), $r_D = 1.0\ h_N$, NPR = 1.6, 2.0, 2.6

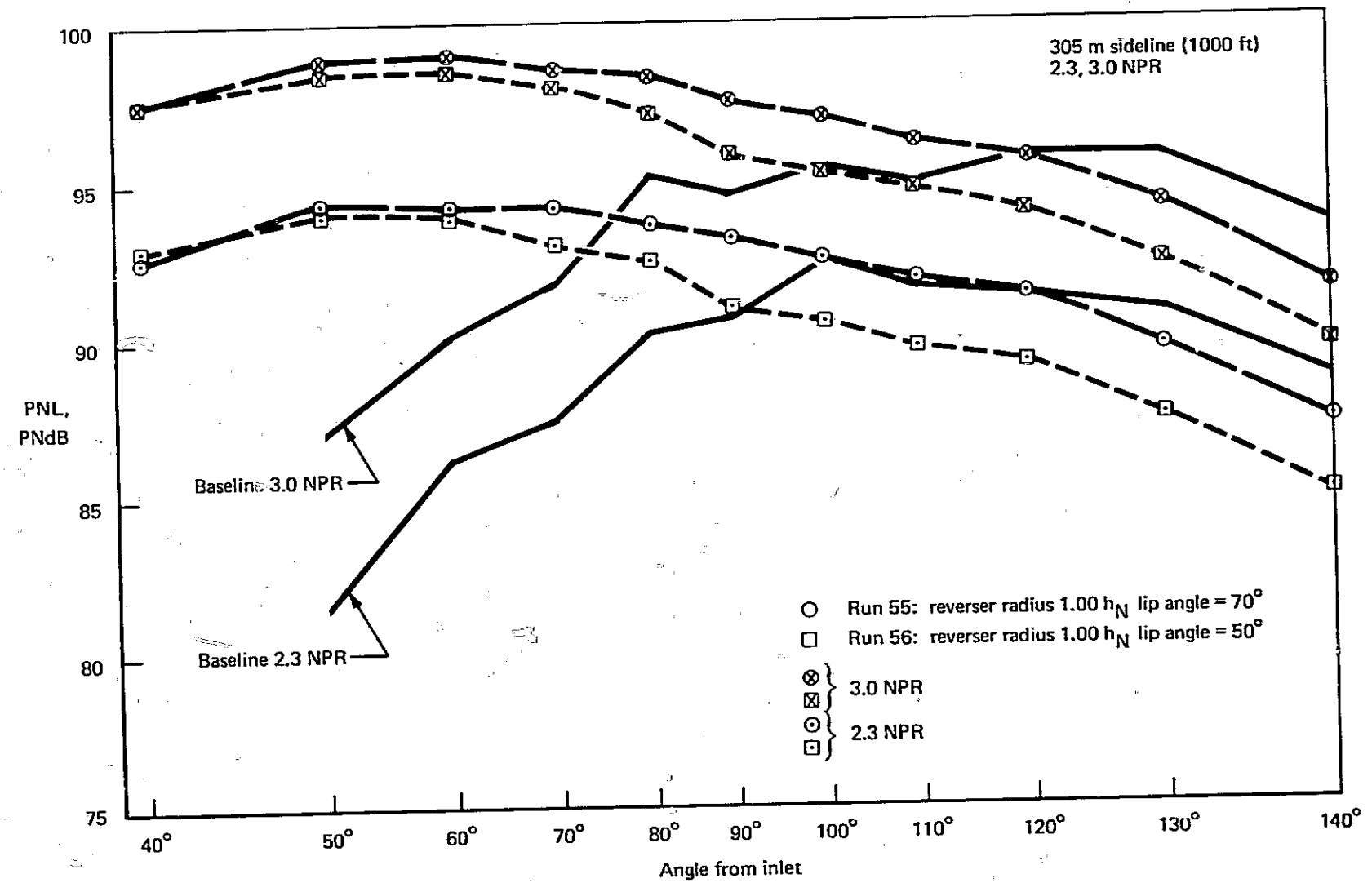

FIGURE 54.—PNL VS MICROPHONE ANGLE, 305 M SIDELINE (1000 FT), $r_D = 1.0\ h_N$, NPR = 2.3, 3.0

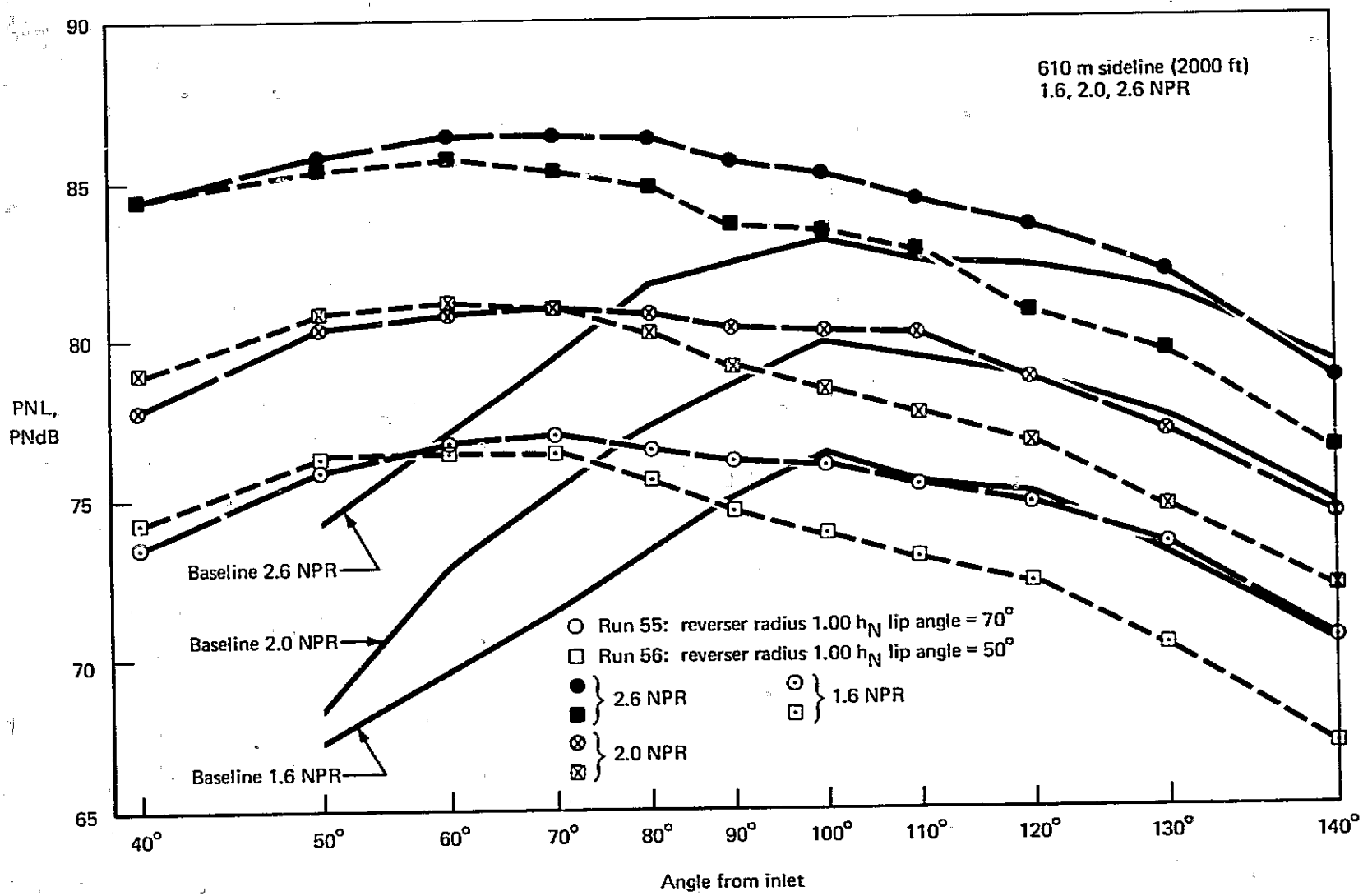

FIGURE 55.—PNL VS MICROPHONE ANGLE, 610 M SIDELINE (2000 FT), $r_D = 1.0\ h_N$, NPR = 1.6, 2.0, 2.6

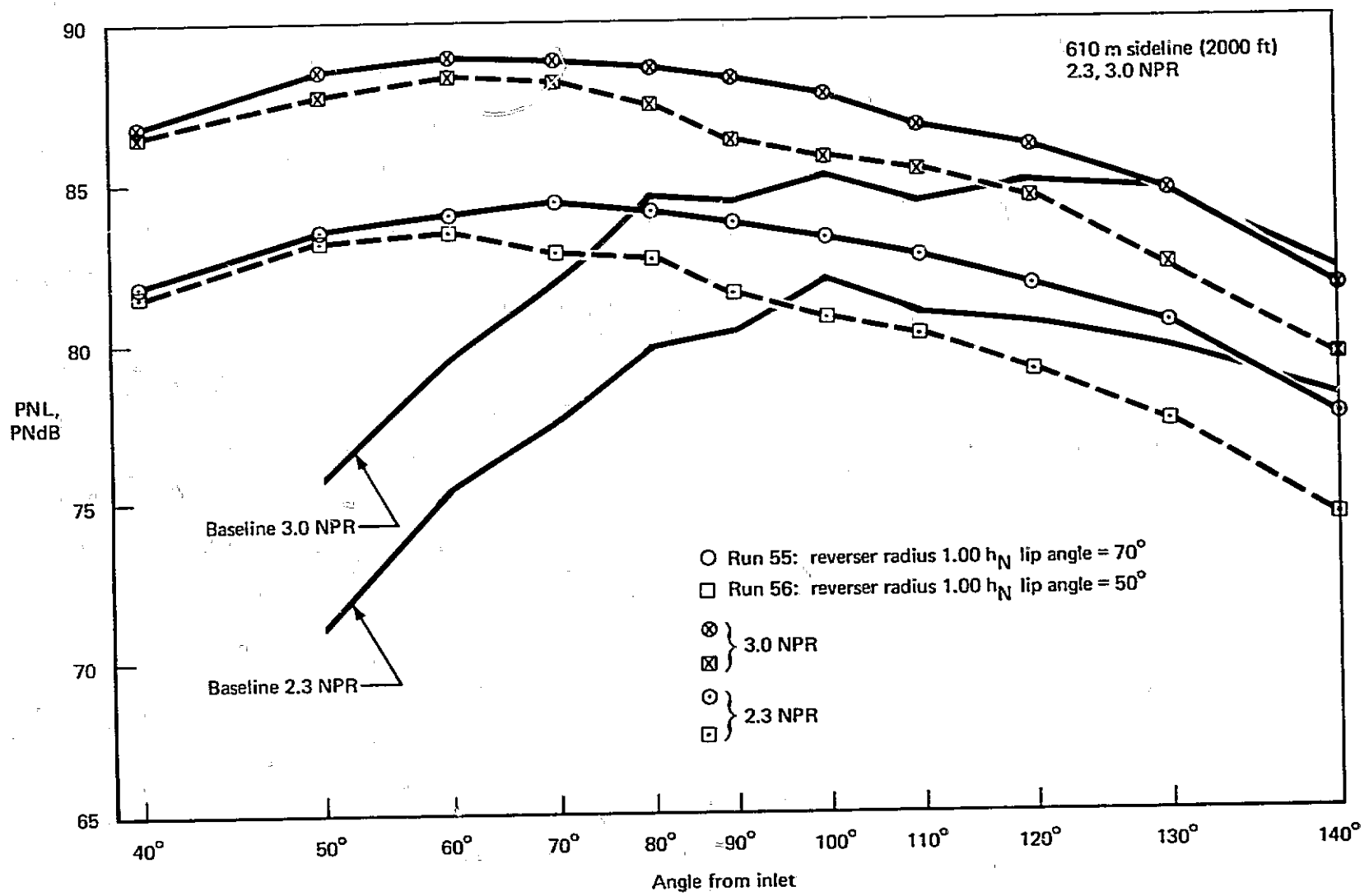

FIGURE 56.—PNL VS MICROPHONE ANGLE, 610 M SIDELINE (2000 FT), $r_D = 1.0\ h_N$, NPR = 2.3, 3.0

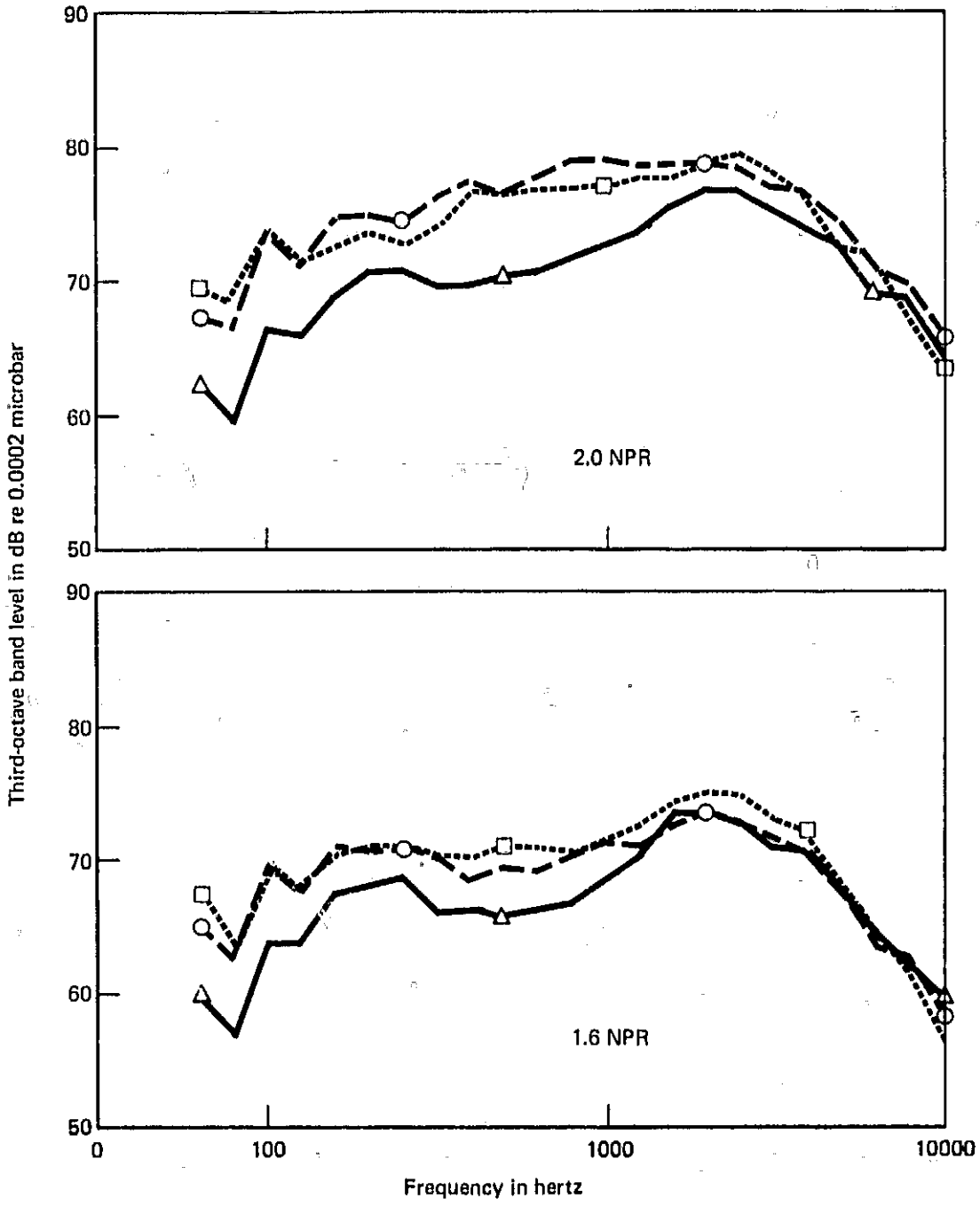

FIGURE 57.—ONE-THIRD OCTAVE BAND SPECTRA, $r_D = 1.25\ h_N$, NPR = 1.6, 2.0

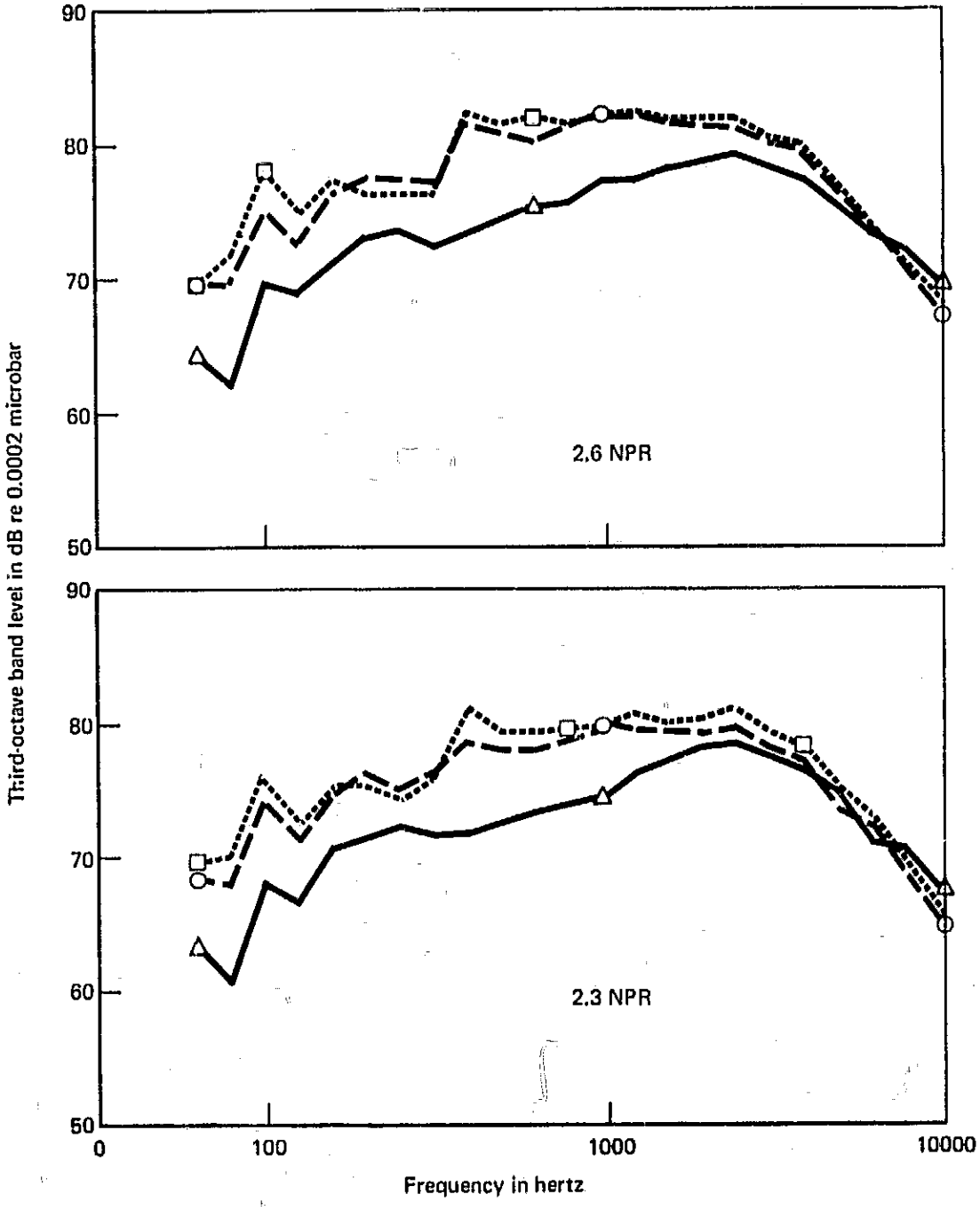

FIGURE 58.–ONE-THIRD OCTAVE BAND SPECTRA, $r_D = 1.25\ h_N$, NPR = 2.3, 2.6

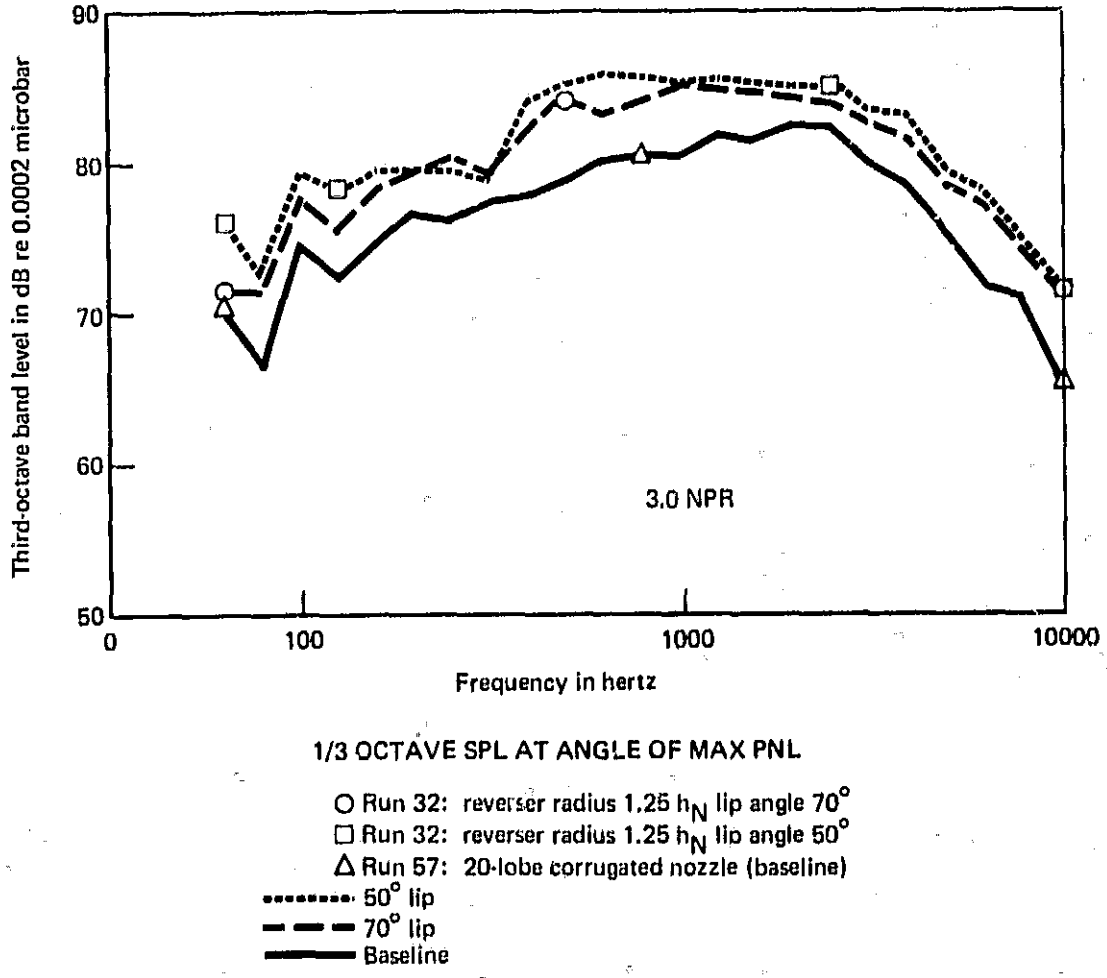

FIGURE 59.—ONE-THIRD OCTAVE BAND SPECTRA, $r_D = 1.25\,h_N$, NPR = 3.0

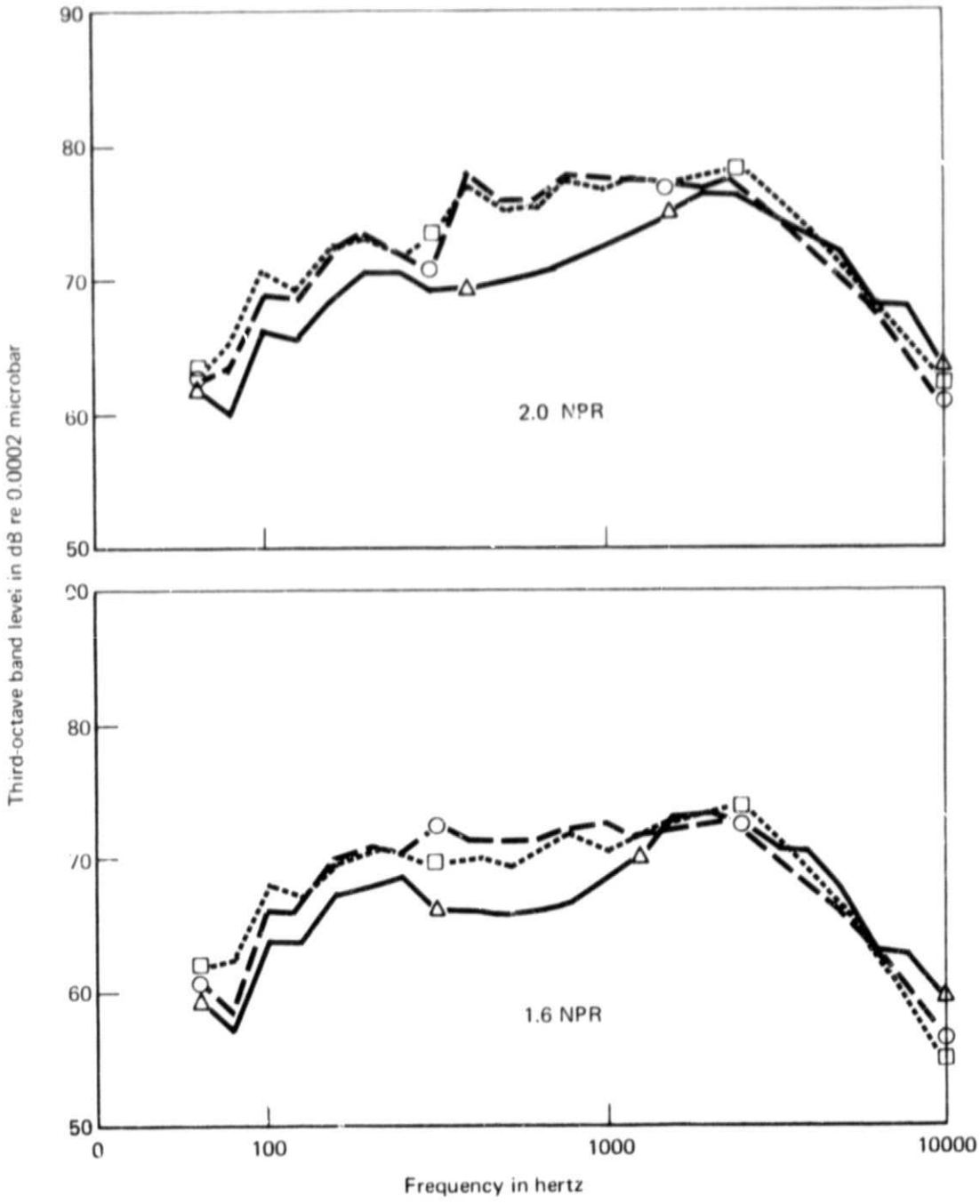

FIGURE 60.—ONE-THIRD OCTAVE BAND SPECTRA, $r_D = 1.0\ h_N$, NPR = 1.6, 2.0

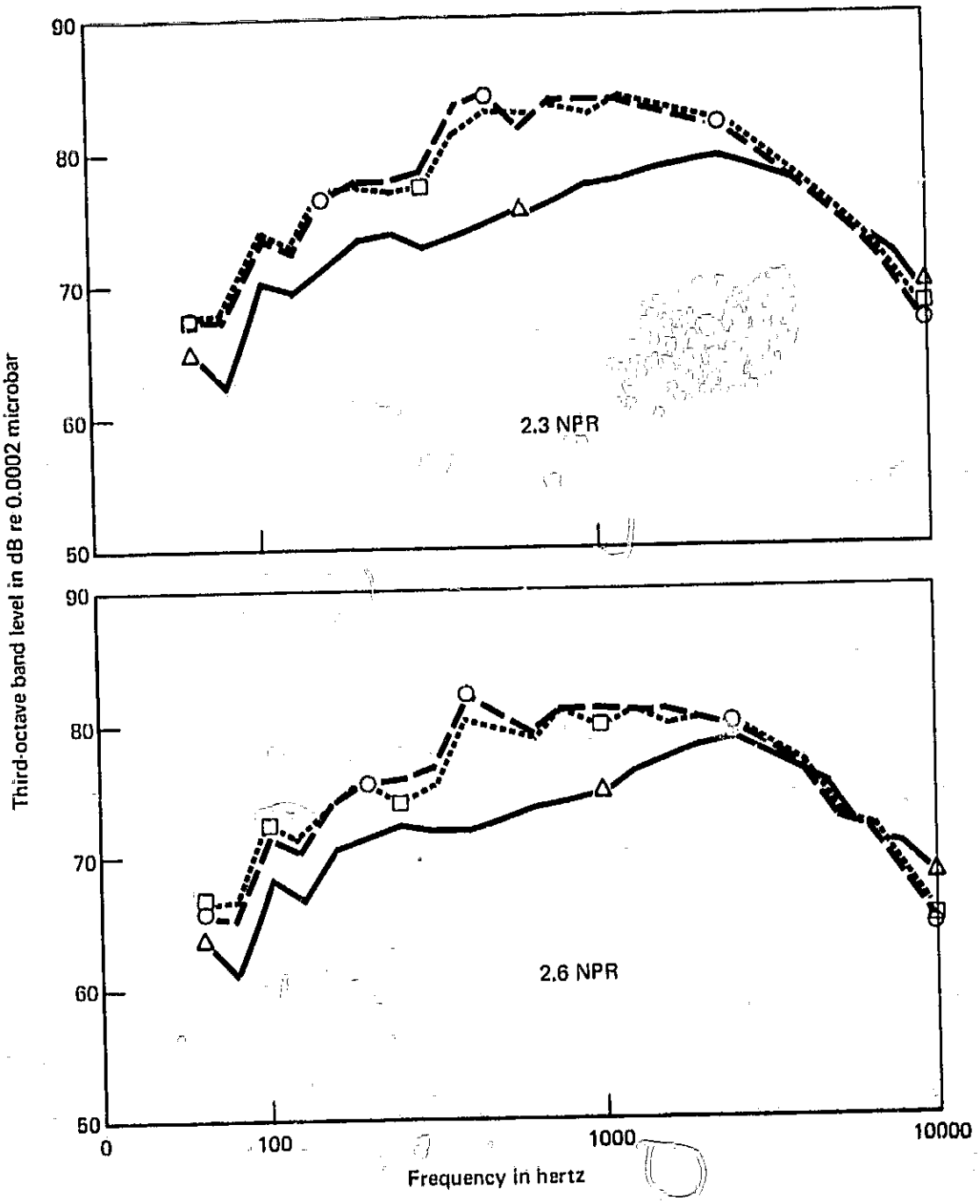

FIGURE 61.—ONE-THIRD OCTAVE BAND SPECTRA, $r_D = 1.0\ h_N$, NPR = 2.3, 2.6

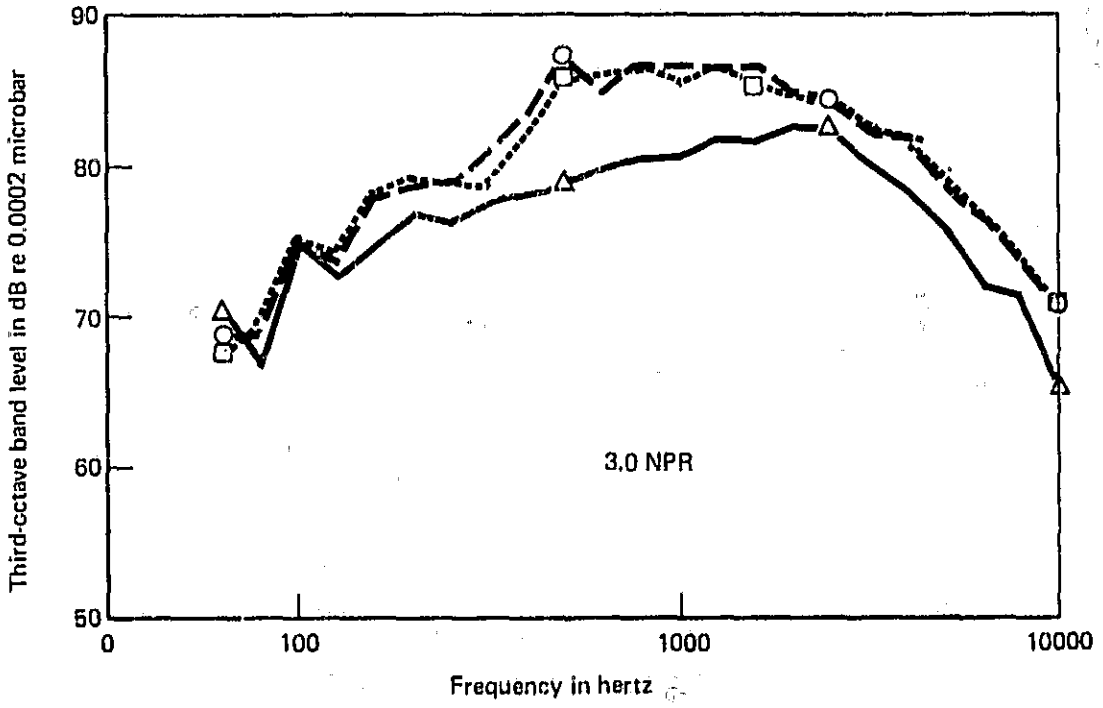

FIGURE 62.--ONE-THIRD OCTAVE BAND SPECTRA, $r_D = 1.0\ h_N$, NPR = 3.0